GRADUATE AERONAUTICAL LABORATORIES

CALIFORNIA INSTITUTE OF TECHNOLOGY

INTERACTION OF CHEMISTRY, TURBULENCE, AND SHOCK WAVES IN HYPERVELOCITY FLOW

G. V. Candler*, P. E. Dimotakis, H. G. Hornung, A. Leonard,
D. I. Meiron, B. V. McKoy, D. I. Pullin and B. Sturtevant

*University of Minnesota

Annual Progress Report

Firestone Flight Sciences Laboratory

Guggenheim Aeronautical Laboratory

Karman Laboratory of Fluid Mechanics and Jet Propulsion
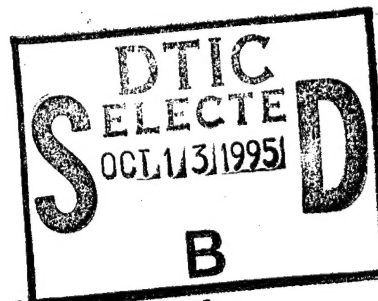
DTIC
SELECTED
OCT 13 1995
B

DTIC QUALITY INSPECTED 5

Pasadena

19951011 155

REPORT DOCUMENTATION PAGE

1. AGENCY USE ONLY (Leave blank)	2. REPORT DATE 1 September 1995	3. REPORT TYPE AND DATES COVERED Annual Progress Report

4. TITLE AND SUBTITLE
(U) Interaction of chemistry, turbulence, and shock waves in hypervelocity flow

5. FUNDING NUMBERS
PE - 61103D
PR - 3484
SA - AS
G - F49620-93-1-0338

6. AUTHOR(S)
G. Candler, P. Dimotakis, H. Hornung, A. Leonard,
D. Meiron, B. V. McKoy, D. Pullin, and B. Sturtevant
(compiled by H. Hornung)

7. PERFORMING ORGANIZATION NAME(S) AND ADDRESS(ES)
California Institute of Technology
1201 E. California Blvd.
Pasadena, CA 91125

8. PERFORMING ORGANIZATION REPORT NUMBER

9. SPONSORING/MONITORING AGENCY NAME(S) AND ADDRESS(ES)
AFOSR/NA
110 Duncan Avenue, Suite B115
Bolling AFB DC 20332-0001

10. SPONSORING/MONITORING AGENCY REPORT NUMBER

11. SUPPLEMENTARY NOTES

12a. DISTRIBUTION/AVAILABILITY STATEMENT
Approved for public release; distribution is unlimited

12b. DISTRIBUTION CODE

13. ABSTRACT (Maximum 200 words)

Significant progress was made during the second year of an interdisciplinary experimental, numerical and theoretical program to extend the state of knowledge and understanding of the effects of chemical reactions in hypervelocity flows. The program addressed key problems in aerothermochemistry that arise from interactions between the three strongly nonlinear effects: Compressibility; vorticity; and chemistry. Important new results included:

- Clear understanding of the two important parameters that define hypervelocity flow over spheres. Closed-form solution for stand-off distance.
- Completion of computation of hollow-core compressible vortex streets.
- First high-resolution interferograms of shock-shock interaction in hypervelocity flow. Detailed experimental and theoretical study shows that high-enthalpy real-gas effects do not further increase heat flux in type IV interaction. Interferograms establish flow quality in the hypervelocity shock tunnel T5.
- Upgrade of the Supersonic Shear Layer facility to higher Mach number. New results on supersonic shear layers and shear-layer/shock-wave interaction.
- Computational discovery of a flow field that is sensitive to vibration-dissociation coupling.
- Extension of the equilibrium flux method to a more robust, less dissipative form, and tests.
- Computation of collision cross section to electrons of low excited states of OH, NO, and CO_2.
- Establishment of Laser-Induced Thermal Acoustics as an accurate diagnostic for gas properties over large pressure ranges.

14. SUBJECT TERMS chemical reaction, shock wave, vorticity, hypervelocity, shock-vortex interaction, heat transfer gauges, laser scattering, laser-induced thermal acoustics, vibration-dissociation coupling

15. NUMBER OF PAGES 81

16. PRICE CODE

17. SECURITY CLASSIFICATION OF REPORT	18. SECURITY CLASSIFICATION OF THIS PAGE	19. SECURITY CLASSIFICATION OF ABSTRACT	20. LIMITATION OF ABSTRACT
Unclassified	Unclassified	Unclassified	UL

INTERACTION OF CHEMISTRY, TURBULENCE AND SHOCK WAVES IN HYPERVELOCITY FLOW

G. V. Candler*, P. E. Dimotakis, H. G. Hornung, A. Leonard,
D. I. Meiron, B. V. McKoy, D. I. Pullin and B. Sturtevant

California Institute of Technology
Pasadena, CA 91125
*University of Minnesota

23 August 1995

Annual Progress Report

EXECUTIVE SUMMARY

We report on the technical progress in the second year of an interdisciplinary experimental, numerical and theoretical program to extend the state of knowledge and understanding of the effects of chemical reactions in hypervelocity flows. The program combines unique experimental and computational facilities at Caltech to address the key problems in aerothermochemistry that arise from interactions between the three strongly nonlinear effects: Compressibility; vorticity; and chemistry. Fig. 1 presents an overview of the program.

Project / Investigator	I.1. Hornung	I.2. Hornung	I.3. Sturtevant	II.1. Meiron, Pullin	II.2. Sturtevant	III. Dimotakis	IV.1. Candler	IV.2. McKoy	IV.3. Pullin	V.2. Hornung
I.1. Transitional and Turbulent Boundary Layers		●	●		●	●	●			●
I.2. Nonequilibrium and Vorticity Downstream of Bow Shocks	●		●	●			●		●	●
I.3. Ablation With Chemical Reaction	●	●		●	●			●		●
II.1. Nonequilibrium Chemistry in Shock–Vortex Interaction		●	●		●	●	●	●	●	
II.2. Shock Wave Interactions in Hypervelocity Flow	●		●	●			●		●	●
III. Supersonic Shear–Layer Flows	●			●						●
IV.1. Measurement of Vibrational Nonequilibrium Reaction Rate	●	●		●	●			●	●	●
IV.2. Rates of Electron Driven Reactions in Hypersonic Flow			●	●			●		●	
IV.3. Nonequilibrium Leeward Shock–Vortex Aerodynamics		●		●	●		●	●		
V.2. DFWM for Composition and Temperature Measurement	●	●	●		●	●	●			

Fig. 1. Sub-projects, principal investigators, and main interactions.

The program has led to the following important new results (partial list):

- Clear understanding of the two important parameters that define hypervelocity flow over spheres. Closed-form solution for stand-off distance.
- Completion of computation of hollow-core compressible vortex streets.
- First high-resolution interferograms of shock-shock interaction in hypervelocity flow. Detailed experimental and theoretical study shows that high-enthalpy real-gas effects do not further increase heat flux in type IV interaction. Interferograms establish flow quality in T5.
- Upgrade of S^3L facility to higher Mach number. New results on supersonic shear layers and shear-layer/shock-wave interaction.
- Computational discovery of a flow field that is sensitive to vibration-dissociation coupling.
- Extension of the equilibrium flux method to a more robust, less dissipative form, and tests.
- Application of Schwinger multi-channel technique to computation of collision cross section to electrons of low excited states of OH, NO, and CO_2.
- Establishment of LITA as an accurate diagnostic for gas properties over large pressure ranges.

The research has again benefited extensively from close interaction within the program, including regular research conferences and seminars, and through extensive communication with outside groups through presentations at conferences and seminars, as well as through consultancies and industrial participation, see individual projects. The progress made corresponds to more than the half-way point according to our plans. The research has led to 3 Ph. D., 1 Ae. E. and 2 M. S. degrees and produced 8 new archival publications (+7 submitted) and 8 conference papers.

TABLE OF CONTENTS

INTRODUCTION

Background

This section and the following Statement of Work are identical to the corresponding sections in the first Annual Technical Report issued in May 1994, see Candler *et al.*, (1994). The repetition permits this second report to be read independently of the first one. For a complete picture of the progress made up to this half-way point in the course of this URI project, it is, however, necessary to consult both reports.

At the outset of this report it is pertinent to quote three of the opening paragraphs of the proposal that led to the current URI Grant:

"Transport to or from space, aero-assisted orbital transfer operations and other hypervelocity flight maneuvers necessarily occur at such high (near orbital) speeds, that the bow-shock heating of the components of air causes them to be dissociated, to react with each other, and, at particularly high speeds, to be ionized. Efficient air-breathing propulsion of such high-speed vehicles also requires supersonic combustion of the fuel. To a large degree, these applications have motivated the interest in the field of study that has been named aerothermochemistry by von Karman.

The character of the dynamics of reacting gases is changed relative to perfect-gas dynamics in two important ways: First, the equilibrium behavior is much more complicated, and second, characteristic times are introduced by the fact that the reactions proceed at finite rates. These two types of highly nonlinear gas imperfections, interacting with the classical nonlinear manifestations of gas-dynamics, namely shock waves and turbulence, produce many new flow structures and phenomena. Some of these are known and qualitatively understood, a few are quantitatively predictable by computation, all are of scientific, and most of practical importance to the operations listed above. The experimental data in this field are very limited, because of the difficulties associated with laboratory simulation. This constitutes the most important need in aerothermochemistry.

The proposed research work may be grouped under the following major headings:

> supersonic turbulent mixing and combustion
> effects of chemical reactions in external hypervelocity flows
> reaction rate models

The philosophy of this proposal is to concentrate interdisciplinary effort on particular problems in the first two categories. The main thrust of the proposed research is to use the two new facilities (T5 hypervelocity shock tunnel and S^3L Supersonic Shear-Layer Facility) for an experimental program to study and understand the effects introduced by chemical reactions. A parallel theoretical and computational effort will help design the experiments and test models and mechanisms of the gas behavior. The third category pervades the whole program and represents research in theoretical and computational chemistry and fluid dynamics, as well as comparison with experiment."

The program was then subdivided into the following four parts

I. Reaction-rate controlled shear flows
II. Shock-vorticity interactions
III Supersonic mixing and combustion
IV Chemistry in non-uniform flow,

all of which involve complicated and non-linear interaction between *vorticity, chemistry* and *compressibility.* By focusing the available facilities and expertise on the main problems in the field, sub-projects were determined as shown in Fig. 1 together with the PI's and the main interactions between them.

A brief outline of the objectives was then formulated in the following statement of work. The numbering of these sub-projects corresponds to that of the sections in this report under which the progress is described in more detail.

Statement of Work

I.1 Obtain qualitative information on the structure of transitional and turbulent boundary layers at high enthalpy. Determine the response of a laminar boundary layer to disturbances at the most strongly amplified frequency for the second mode instability. Perform T5 experiments on a sharp slender cone, using differential interferometry, laser-induced fluorescence and surface instruments.

I.2 Design experiments for testing the limits of binary scaling by making a numerical study of blunt body flows in nitrogen and air. Carry out T5 experiments on spheres using surface instrumentation, differential interferometry and degenerate four-wave mixing (DFWM). Extend the experiments to study the high-vorticity layer downstream of a bow shock associated with the large density rise caused by dissociation.

I.3 Determine the flux of reactive and inert species, and of heat and momentum to the surface of ablating bodies in hypervelocity flow. Carry out T5 experiments using sampling mass-spectrometric analysis and surface heat transfer and pressure measurements. Formulate analytical models of reactive effects on ablation.

II.1 Perform ultra-high resolution numerical experiments combined with nonlinear analysis and numerics to establish appropriate initial conditions to elucidate the generic mechanisms of shock-vortex interactions, namely, (1) interaction of a shock with a vorticity field in the presence of nonequilibrium chemistry, and (2) vorticity generation in shock focusing with chemistry.

II.2 Determine the effects of chemical relaxation on the shock-on-shock problem. Demonstrate the magnitude of nonequilibrium effects on shock impingement heating. Carry out experiments with a 2-dimensional model in T5, supported by local shock-polar analysis and numerical calculations of an ideal dissociating gas.

III Carry out S^3L experiments with chemically reacting and non-reacting flows, using schlieren, spectroscopy, Rayleigh scattering, chemical effects and new diagnostic methods, to gain understanding of the mechanisms of mixing when a shock interacts with a supersonic turbulent shear layer, and in the flow downstream of an expansion wave. Develop new related diagnostics and computational capabilities.

IV.1 Design and carry out an experiment in T5 to provide data to test chemical reaction models for flows with vibrational nonequilibrium. Use a previously developed computational technique to simulate the flow over proposed experimental configurations. Identify a configuration that exhibits significant effects of vibrational nonequilibrium on the reaction rates.

IV.2 Exploit computational methodologies and high-performance and cost-effective computing provided by highly parallel and scalable supercomputers to solve the complex equations which govern electron-molecule collision processes needed for robust modeling of the chemical and physical properties of hypervelocity flows.

IV.3 Demonstrate the effect of chemistry on the leeward shock-vortex separation region of hypervelocity flow about slender bodies using high-resolution CFD on the Intel Touchstone-Delta computer, combined with dimensional analysis and physical scaling.

V.2 Develop DFWM for measuring species concentration and temperature in hypervelocity flows. concentrate on NO-concentrations because of their importance in air flows. Buy the remaining equipment to complete the set of components, assemble the instrumentation, debug and apply it to T5 flows.

Current Status of Progress

In the following paragraphs, which mirror the statement of work, the progress in the subprojects is summarized.

I.1 The experimental results of the previous reporting period were further analyzed, prepared and submitted for archival publication. The experiments and equipment for sheet visualization of the cone boundary layer and for disturbance excitation at the second-mode frequency have been prepared. The new experiments will benefit from a data acquisition upgrade that was implemented for an industrial user, giving much higher data density. An existing chemically-reacting boundary layer code has been implemented.

I.2 Analysis of the results led to a well rounded and clear understanding of the two important parameters that define high-enthalpy flow over spheres in complex gas mixtures such as air and carbon dioxide, defining the limits of binary scaling and giving a closed-form expression for the shock stand-off distance. In preparation for the next phase, a conical nozzle for T5 was designed, built and partially calibrated. This provides the capability to operate satisfactorily with many different gases over the whole enthalpy range of T5. A novel visualization technique similar to the smoke wire method was demonstrated and is being further developed.

I.3 This subproject was scheduled to start at the end of the second year, *i.e.*, now. In the proposal, we pointed out that it was predicated on our ability to raise funds from other sources to build a mass spectrometer. To date, we have not been able to raise these funds.

II.1 Computation of hollow-core compressible vortex streets was completed and submitted for publication. Initial results from extensive computations of a shock with a contact discontinuity indicate that the early vorticity generation is not sgnificantly influenced by dissociative reactions. Analytic work led to an estimate for the vorticity generation by the shock/contact-surface interaction and a technique for computing similarity solutions for shock/contact interactions with and without chemistry.

II.2 The completion of the holographic interferometer and the quality of the heat flux gauges developed in the previous reporting period came to fruition in producing the first high-quality and detailed data on shock-shock interaction in hypervelocity flow. Results have demonstrated that existing predictions of stagnation-point density at high enthalpy, owing to the effects of dissociation, are *not* realized. Time-resolved heat flux measurements confirmed this observation and agreed accurately with previous experiments in the low-enthalpy range. This shows that real-gas effects *do not* further increase the large heat flux induced by shock impingement. A theoretical model was developed for the influence of thermochemistry on the jet shock system of the type IV interaction, using the ideal dissociating gas approximation. This leads to the conclusion that peak heating arises from a balance of the jet shock strengths, and that this balance *reduces* the influence of thermochemistry on the flow. The new instrumentation developed for this project enabled critical assessment of the flow quality in T5. High-resolution interferograms of the flow over blunt bodies agree with established theory within the experimental uncertainty. The new instrumentation has also greatly benefitted other projects within this URI program as well as industrial users of T5.

III The (S^3L) combustion facility was further upgraded to permit operation at higher Mach number, and experiments on supersonic shear layers as well as on shear-layer/shock-wave interaction to be completed. Progress has been made on the development of a robust, unsplit, shock-capturing numerical simulation method for one- and multi-dimensional chemically reacting flows and detonations. In the Image Correlation Velocimetry project, the final stages have been reached of the design and fabrication effort for the development of new CCD-imaging technology to permit recording of image pairs with small time separations (down to 1 μs).

IV.1 The work in the previous reporting period showed that the flow over a sphere was not suitable for testing the vibration-dissociation coupling models, because it is relatively insensitive to them. A computational search led to the discovery of a phenomenon that is very sensitive to the coupling model, and to the design of an experiment to test such models. The configuration is a double-wedge model, in which the shock on the second wedge is detached, so that a shock-shock interaction results that is very similar to the Type IV interaction studied under II.2, but with a wall-bounded supersonic jet. One of the models for the T5 experiments has been designed and is being built. This experiment will also benefit significntly from the data acquisition upgrade.

IV.2 Computations on the Intel Paragon at speeds typically between 3 and 10 GFLOPS have made it possible to apply the Schwinger multichannel method to achieve the determination of electron collision cross sections for three processes: 1. Near-threshold excitation of the lowest excited state of OH ($A^2\Sigma^+$). This is important in the dissociation of water vapor. 2. Impact excitation of the $A^2\Sigma^+$ state of NO, which is responsible for the γ-band emission from the bow shock of blunt body flows. 3. Impact excitation of five electronically excited states of CO_2. No experimental data exist in any of these cases.

IV.3 The equilibrium flux method was modified to make use of Osher intermediate states. The new scheme (EFMO) retains the robustness of the EFM scheme in capturing strong shocks, while substantially reducing its numerical diffusivity for good boundary layer resolution. EFMO was incorporated in a fully implicit version of the viscous 3-D code PGP3D. This code was tested extensively in flow over a cone at zero and finite incidence. The ideal dissociating gas model

has been incorporated into both the implicit and the explicit versions of PGP3D and is being tested.

V.2 This year, LITA has been transformed from a promising technique into an accurate and well-understood tool for the study of gas properties. This transformation has been accomplished through improvements in LITA signal modeling and a successful series of LITA experiments. The experiments demonstrate the accuracy of the improved model and the ability to extract accurate values of the sound speed and thermal diffusivity from LITA signals. The experiments also demonstrate the ability to obtain LITA signals in gases over a wide pressure range ($\sim$3 Pa–14 MPa at room temperature) and in challenging environments, e.g., CO_2 near its liquid-vapor critical point, and in flowing, turbulent gases.

A total of 7 higher degrees were earned. 8 papers were published or accepted for publication in the archival literature, and 7 have been submitted. 9 papers were published as conference papers or in proceedings. The work has resulted in a large number of presentations at various seminars, meetings and conferences. Details of these are given in the subsections.

Interactions

The interaction between the principal investigators and their research groups within the project followed the diagram in Fig. 1. very closely. Much of this interaction is forced by joint use of facilities or instrumentation, sharing of technical personnel, or through discussions that arise at almost weekly interactions in the Fluid Mechanics Research Conference at GALCIT. Interaction between the separate Aerothermodynamics URI's benefited from the meeting held at Calspan, Buffalo in 1994. Advantage was taken by several PI's of attendance at conferences (AIAA, 19thISSW) and meetings at AEDC to interact with other groups nationally and internationally.

Significant industrial participation in the research has begun through the work of MetroLaser in the T5 laboratory. T5 tests for the European Space Agency and Japanese companies have also been continued. A further major international interraction is the upcoming 20th International Symposium on Shock Waves organized to take place at Caltech 23-27 July 1995. Some 420 participants are expected to attend. Major funding for this conference comes from AFOSR.

Layout

The following chapters present the main results of the work in more detail, in the order shown above. Each subproject then lists the personnel, publications, degrees earned, and interactions separately. A few of the subprojects had received preliminary funding before the URI funding began, so that they are at a more mature stage than others.

Reference

Candler, G. V., Dimotakis, P. E., Hornung, H. G., Leonard, A., Meiron, D. I., McKoy, B. V., Pullin, D. I., and Sturtevant, B. 1994 "Interaction of Chemistry, Turbulence, and Shock Waves in Hypervelocity Flow," AFOSR Annual Technical Report F49620–93–1–0338 (GALCIT Report FM 94–2).

<div align="center">

CHAPTER I

REACTION-RATE CONTROLLED SHEAR FLOW

</div>

I.1 TRANSITIONAL AND TURBULENT BOUNDARY LAYERS

<div align="center">

Objectives and Status of Research

</div>

The objective of this experimental investigation is to obtain qualitative information on the structure of transitional and turbulent boundary layers at high enthalpy, and to determine the response of the laminar boundary layer to disturbances at the most strongly amplified frequency for the second mode instability. The experiments use surface heat transfer measurements on a slender, sharp cone and optical flow visualization to detect effects of chemical reactions on the heat transfer, transition location, and structure of the flow field.

The exploratory experiments conducted during the previous reporting period demonstrated a clear stabilizing effect of high-enthalpy real-gas effects that increases with decreasing dissociation energy, and found that the instability under the conditions tested occurred via the Tollmien-Schlichting mode. During the last year, most of the work concentrated on the preparation of the planned stability experiment, the implementation of boundary-layer software, and experiments at higher enthalpy, up to 29 MJ/kg in the laminar regime with nitrogen. The gas-dynamical oscillator for disturbance generation proved to be awkward, and was rejected in favor of the more easily adjustable glow discharge technique. The oscillator for this excitation is completed. The design of the tangential-sheet visualization in the boundary layer is completed, and optical components are being assembled. The extension of the data acquisition system to more than 50 test section channels permits a significant improvement to be made to the data density of the measurements. The cone is being instrumented to accommodate 40 heat flux gauges instead of the 14 of the previous measurements.

I.1.1 Introduction

At sufficiently high Mach number, theoretical work by Mack and others has shown that instability to small disturbances in a constant-pressure boundary layer occurs via a mode that has a characteristic frequency far in excess of the Tollmien-Schlichting mode. Experiments in cold (perfect-gas) hypersonic flows confirm this prediction. Experiments in T5, obtained during the previous reporting period, showed that the transition mechanism occurs via the T-S mode. The frequency of the T-S mode in T5 flows is typically 150 kHz, while the second-mode frequency is typically 1 MHz. The latter frequency is probably absent from the noise spectrum of the facility, which may be the reason for the observed behavior. The experiments also showed that high-enthalpy real-gas effects stabilize the boundary layer, while theoretical results (Reed *et al.*, 1992) indicate that the *second mode* is destabilized by them. To clarify the questions surrounding these phenomena, a focussed stability experiment is required.

Laminar constant-pressure boundary layers can be accurately computed by boundary layer theory. The importance of the chemical activity in the high-enthalpy flows studied here must be incorporated in the boundary layer calculations. A well-established code for this purpose is the Boundary Layer Integral Matrix Procedure (BLIMP), which was obtained for our use in the URI project from Air Force Wright Aeronautical Laboratory. Comparisons of experimental results with computations are required to understand the influence of cheical reactions in the laminar boundary layer.

I.1.2 Disturbance excitation

High-frequency oscillations may be generated in a supersonic flow by gas-dynamical means, either by a cavity in a wall, or by a spiked blunt body. To obtain frequencies in the MHz range, the characteristic dimension of the blunt body or the cavity has to be typically 1 mm in a 5 km/s flow. A spiked blunt body of this size was tried in T5 consisting of a small blunt body (2 mm diameter) with a spike. While this method of excitation does provide high-frequency disturbances, it is not possible to adjust the frequency without replacing the body or adjusting cavity dimensions.

The method used by Kosinov et al.(1990) for boundary layer excitation, which employs a glow discharge oscillator, is more attractive from this point of view. In this technique a spark gap in a hole in the surface under the boundary layer and almost flush with the surface is excited from a power-amplified sine wave oscillator. Every time the spark gap causes breakdown, a pressure pulse is emitted. Kosinov found this to be a suitable excitation device. Our ten times higher frequency requires the power amplifier to be good up to 2 MHz. The circuit for the excitation device has been designed and built, and is being tested.

I.1.3 Computations and comparison with experiment

The BLIMP code solves the two-dimensional or axisymmetric boundary layer equations using a fourth-order Galerkin scheme and a Newton-Raphson iteration procedure in a grid requiring typically 30 points across the boundary layer. The gas is modeled as a mixture of perfect gases, with equilibrium, finite-rate or frozen chemistry. The chemical reactions are modeled with the Arrhenius equations.

The interest in using this code is for comparisons with the measured laminar boundary layer flows. The code also provides for incorporation of various turbulence models, for which the transition location is required as an input. While the comparisons shown below include computations with various turbulence models, it is clear that such models have a much lower level of scientific respectability than the laminar flow computations. Fig. I.1 shows results for the case of an intermediate enthalpy, intermediate pressure flow, where the chemistry may be expected to be frozen. It is clear from the results in the laminar range that the agreement is satisfactory there. The discrepancy between computation and the similarity solution may be explained by the difference in evaluating the specific heat ratio which could be remedied by correcting the difference. The differences between the different turbulence models show that, even in the perfect-gas range, such descriptions of turbulence are inadequate.

At higher specific reservoir enthalpy and pressure, where we might expect equilibrium behavior of the gas in the boundary layer, the BLIMP code was applied in equilibrium mode. The comparison is shown in Fig. I.2. In this flow the boundary layer remains laminar all the way to the end of the cone, because the Reynolds number is too low. A significant difference is evident here, in that the
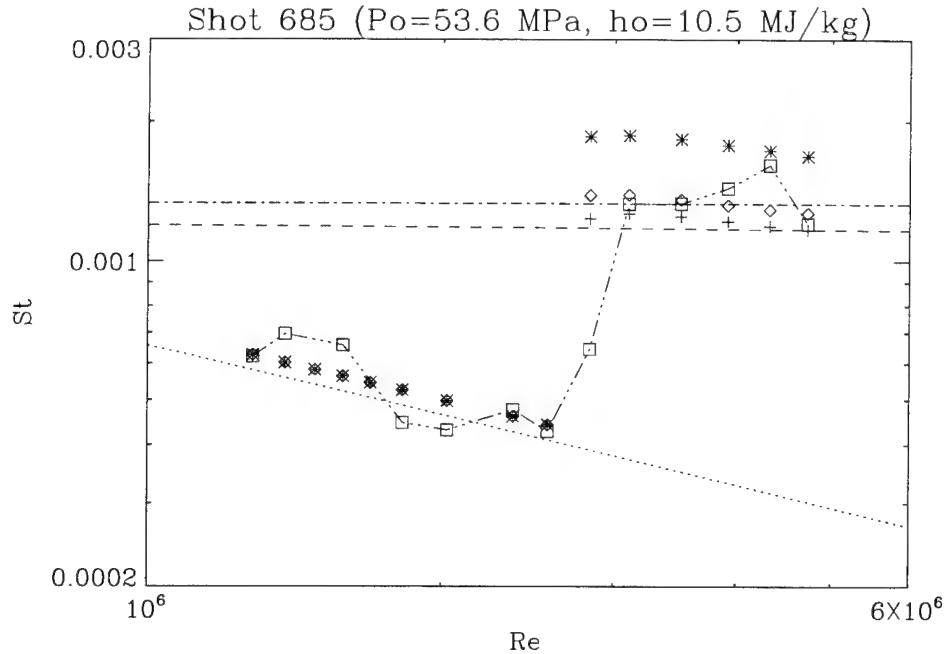
Fig. I.1. Comparison of BLIMP calculation with measurements of heat flux to the slender cone in the case of a medium-enthalpy condition in T5. Open squares are measured data. The other symbols represent results for the same conditions from BLIMP computation. The dotted line is the laminar boundary layer similarity solution. The discrepancy between the computation and similarity solution may be explained by the difference in evaluating the specific heat ratio. Dash-dot and dashed lines show application of the turbulence models of van Driest II and White and Christoph respectively. Asterisks, open diamonds and crosses show BLIMP computation with turbulence models of Kendall, Bushnell, and Cebeci-Smith respectively. In the turbulent layer computations the transition location was taken from the experimental results. The discrepancy among the turbulence models illustrates the inadequacy of representing turbulence so simply.

experiment shows a much larger increase of the heat flux between the frozen (see Fig. I.1) value and the high-enthalpy value than is predicted by the computations. Such differences may be expected to arise from the fact that the free stream in the facility is frozen at a slightly higher dissociation fraction than the equilibrium value, while the calculation has an equilibrium free stream at the same pressure and temperature as in the facility. However, the difference between the experimental and computed heat flux incrrease is much larger than can be explained by this cause. To be able to simulate the effect correctly, it is necessary to operate the code in non-equilibrium mode (presently being implemented).

References

Kosinov, A.D., Maslov, A.A. and Shevelkov, S.G., "Experiments on the Stability of Supersonic Laminar Boundary Layers," JFM, **19**, 1990

Mack, L.M., "Boundary-Layer Stability Theory," Internal Document No. 900-277, Rev. A, Jet Propulsion Laboratory, Pasadena, California, 1969.

Mack, L.M., "Boundary-Layer Stability Analysis for Sharp Cones at Zero Angle-of-Attack,"
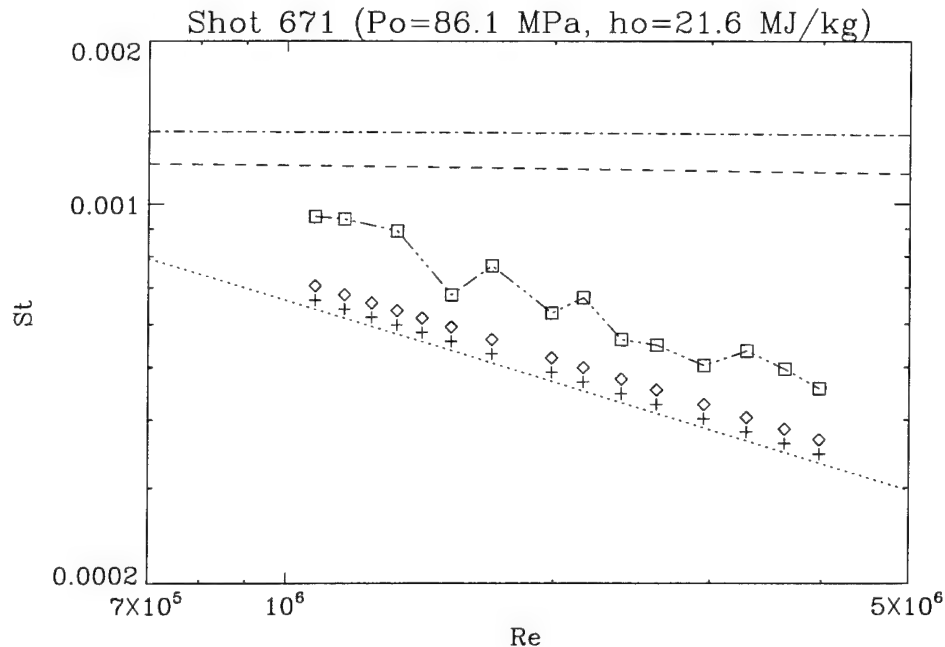
Fig. I.2. Comparison of frozen and equilibrium computations of the laminar-boundary-layer heat flux with a high-enthalpy experiment. The increase of the heat flux from recombination is much larger than predicted.

AFWAL-TR-86-3022, Wright Patterson AFB, Ohio, 1986

Reed, H.L., Stuckert, G.K. and Haynes, T.S., "Stability of Hypersonic Boundary-Layer Flows with Chemistry," AGARD 70th Fluid Dynamics Panel, Torino, Italy, 1992

Stetson, K.F. and Kimmel, R.L., "On Hypersonic Boundary Layer Stability," AIAA 30th Aerospace Sciences Meeting & Exhibit, Reno, NV, AIAA Paper 92-0737, 1992

Personnel associated with the research

1. Hans G. Hornung, Kelly Johnson Professor of Aeronautics, GALCIT Director.

2. Philippe Adam, Graduate Research Assistant.

3. Bahram Valiferdowsi, Staff Engineer.

Publications resulting from the research

1 Hornung H. G., Cummings E. B., Germain P., Sanderson S. R., Sturtevant B., and Wen C.-Y. (1994) "Recent results from hypervelocity research in T5," AIAA 94-2523, Colorado Springs.

2 Hornung, H.G., Wen, C.Y. and Germain, P., "Hypervelocity Flow Simulation,", 1994, in *Mechanics USA 1994*, ed. A. S. Kobayashi, Appl. Mech. Rev. **47** pp. S14-S19.

3 Germain, P. and Hornung, H. G. "The boundary layer on a sharp cone in hypervelocity flow" in *Shock Waves @ Marseille*, ed. R. Brun, L. Z. Dumitrescu, Springer Verlag, 1995, pp. 63-68.

4 Germain, P. and Hornung, H. G. "Transition on a slender cone in hypervelocity flow", submitted

to Phys. Fluids A.

Interactions

Presentations at conferences, see Publications, and at internal seminars and research conferences at Caltech. Invited speaker at DLR Göttingen, Germany, AIAA Colorado Springs and Reno, and IUTAM Symposium on laminar turbulent transition, Sendai, Japan. Seminar presentations at Princeton University, Mississippi State University. Discussions with R. Kimmel, AFWAL, J. R. Maus, AEDC, G. Anderson, NASA LaRC. Consultant to AEDC, (H. Hornung). Organization of International Symposium on Shock Waves, Pasadena, July 1995, 330 presentations.

I.2 NONEQUILIBRIUM AND VORTICITY DOWNSTREAM OF BOW SHOCKS

Objectives and Status of the Research

The objectives of this sub-project of the program are to design and execute a series of experiments as well as to perform numerical computations and theoretical analysis, in order to test the nature and limits of binary scaling, and to understand and extend the reaction-rate correlation for the shock-wave stand-off distance, in reacting blunt-body flows. In addition, the experiments are to be extended to investigate the high-vorticity layer downstream of the bow shock that is associated with the large density rise caused by dissociation. The objectives have been extended relative to those in the original proposal because of favorable developments during the reporting period.

The experimental and theoretical work on flow over spheres performed during the previous reporting period with differential interferometry and heat flux measurements in T5, as well as flow computations, were further analyzed. The result is a well rounded and clear understanding of the two important parameters that define high-enthalpy dissociating flows over spheres in complex gas mixtures such as occur in air or carbon dioxide flows. These lead to a complete view of the limits of binary scaling, and to a closed-form expression for the shock stand-off distance.

Preparations for the next stage of the project were included the design, manufacture and partial calibration of a conical nozzle for T5, and work on the development of a visualization technique similar to the smoke-wire method for use in high-enthalpy flows.

I.2.1 Correlation of results

The results obtained in the previous reporting period were further analyzed in order to obtain a clearer picture of the dependence of the flow field behind the bow shock on a sphere on two key parameters. The first of these is the reaction rate parameter $\widetilde{\Omega}$, the importance of which emerges from the following analysis of the flow along the stagnation streamline:

Consider the stagnation streamline along the symmetry axis between the shock and the stagnation point. The momentum and energy equations for inviscid adiabatic flow take the simple forms

$$dp + \rho u \, du = 0 = dh + u \, du$$

where p, ρ, u, and h are pressure, density, velocity and specific enthalpy respectively. Thus,

$$dp = \rho \, dh \ .$$

This equation does not mean that the entropy is constant along the stagnation streamline, but rather that the only entropy change that occurs is that associated with the chemical reaction:

$$T \, ds = \sum \hat{\mu}_i \, dc_i \ ,$$

where T, s are temperature and specific entropy, and the $\hat{\mu}_i$ and c_i are the chemical potentials and mass fractions of the constituents. Let the caloric equation of state be given in the form

$$h = h(p, \rho, c_i) \ .$$

Since the mass fractions must satisfy the identity

$$\sum_{i=1}^{n} c_i = 1 \ ,$$

the number of mass fractions that are independent is one less than the total number n of components present. It is usually convenient to choose c_1 as a dependent variable and the other c_i as independent variables. Thus,

$$dh = h_\rho d\rho + h_p dp + \sum_{i=2}^{n} h_{c_i} dc_i = h_\rho d\rho + \rho h_p dh + \sum_{i=2}^{n} h_{c_i} dc_i$$

where the subscripts denote partial differentiation. Solving for $d\rho$,

$$d\rho = \frac{1 - \rho h_p}{h_\rho} dh - \frac{1}{h_\rho} \sum_{i=2}^{n} h_{c_i} dc_i \ .$$

Note that the coefficient of dh is related to the frozen speed of sound a_f, and that dh may be replaced by $-udu$. Rewriting the first term on the right of this equation accordingly, it becomes

$$\frac{d\rho}{\rho} = -\frac{u^2}{a_f^2} \frac{du}{u} - \frac{1}{\rho h_\rho} \sum_{i=2}^{n} h_{c_i} dc_i \ ,$$

where

$$a_f^2 = \frac{-h_\rho}{h_p - 1/\rho} \ .$$

The frozen Mach number u/a_f after the normal shock is typically 0.2 or less. This means that, in the absence of dissociation, the density is practically constant along the stagnation streamline, and, with dissociation, the density change along the stagnation streamline is essentially controlled by the chemistry:

$$(d\rho)_s \simeq -\left(\frac{1}{h_\rho} \sum_{i=2}^{n} h_{c_i} dc_i \right)_s \ .$$

This approximation makes it possible to relate the average density on the stagnation streamline to the rate at which energy is absorbed by the chemical reactions at the shock. This then appears to be the right quantity to incorporate in a new reaction rate parameter

$$\widetilde{\Omega} \equiv -\frac{d}{\rho_s u_\infty} \left(\frac{1}{h_\rho} \sum_{i=2}^{n} h_{c_i} \frac{dc_i}{dt} \right)_s \ .$$

For a given gas mixture,

$$\widetilde{\Omega} \sim \rho_s d \left(\sum_{i=2}^{n} h_{c_i} \frac{dc_i}{dt} \right)_s / (\rho_\infty u_\infty^3),$$

which has the physical significance of

$$\widetilde{\Omega} = \frac{\text{Energy absorption rate by chemistry}}{\text{Input rate of free stream kinetic energy}}.$$

The second important parameter is the density ratio across an equilibrium normal shock. By this parameter, the effects of the recombination rate are brought into the analysis (equilibrium is the balance of forward and reverse reactions.) This equilibrium density ratio depends mainly on the free stream total enthalpy.

The analysis permits a closed solution to be obtained for the shock stand-off distance in two regimes: Where the equilibrium density ratio does not influence the result, and where, therefore, binary scaling works,

$$\widetilde{\Delta} = \frac{1}{\widetilde{\Omega}} \left[-1 + \left(1 + 2L\widetilde{\Omega} \right)^{\frac{1}{2}} \right], \tag{1}$$

with $L = 0.41$ and $\widetilde{\Delta} = \Delta \rho_\infty / \rho_s d$. At $\widetilde{\Omega} = 0$, this goes to the correct limit L. This is valid when the density at the stagnation point, $\rho_b < \rho_e$.

When $\rho_b = \rho_e$, binary scaling breaks down, and the appropriate formula is

$$\widetilde{\Delta} = \frac{\rho_s}{\rho_e} \left[L + \frac{1}{2\widetilde{\Omega}} \left(\frac{\rho_e}{\rho_s} - 1 \right)^2 \right]. \tag{2}$$

Again, this may be seen to have the correct limiting value $L\rho_s/\rho_e$ when $\widetilde{\Omega} = \infty$.

Equations 1 and 2 are plotted in Fig. I.3. The curves of the two-parameter family of equation 2, valid for large $\widetilde{\Omega}$, are nearly tangent to the single curve of equation 1, valid for small $\widetilde{\Omega}$ at the transition point, which is different for different ρ_s/ρ_e.

The theory is in good agreement with experimental results obtained over large ranges of enthalpy in different gases, as well as with numerically computed flows (see Wen and Hornung, 1995).

I.2.2 Conical nozzle

One of the difficulties encountered during the experimental program was that the contoured nozzle of T5 is necessarily designed for one flow condition. The advantages of the free-piston reflected shock tunnel include the ease with which the specific reservoir enthalpy can be changed, so that the full range from perfect gas behavior to high-enthalpy real-gas behavior can be studied in the same facility, without changing the model or test section configuration. However, in order to make full use of this flexibility, the contoured nozzle has to be used in relatively far off-design conditions that lead to non-uniform exit-plane flow. This is not the case with a conical nozzle, since a radial expansion gives uniform flow on spherical surfaces centered on the source point of the flow, for any gas, whether reacting or perfect. (At the high densities and relatively small area ratios in use at T5, the nozzle wall boundary layer is not so important as in nozzles with area ratios in excess of 200.) The penalty one pays by using a conical nozzle is the associated xial gradient of the flow properties. In some applications, such as are to be studied in this project and in the project planned for the near future by Candler (see section IV.1), the longitudinal extent of the model is small, and the axial gradient makes only little difference. Also, the conical free stream can be included in computations of the flow, so that valid comparisons of measured and computed flow fields can be realized.
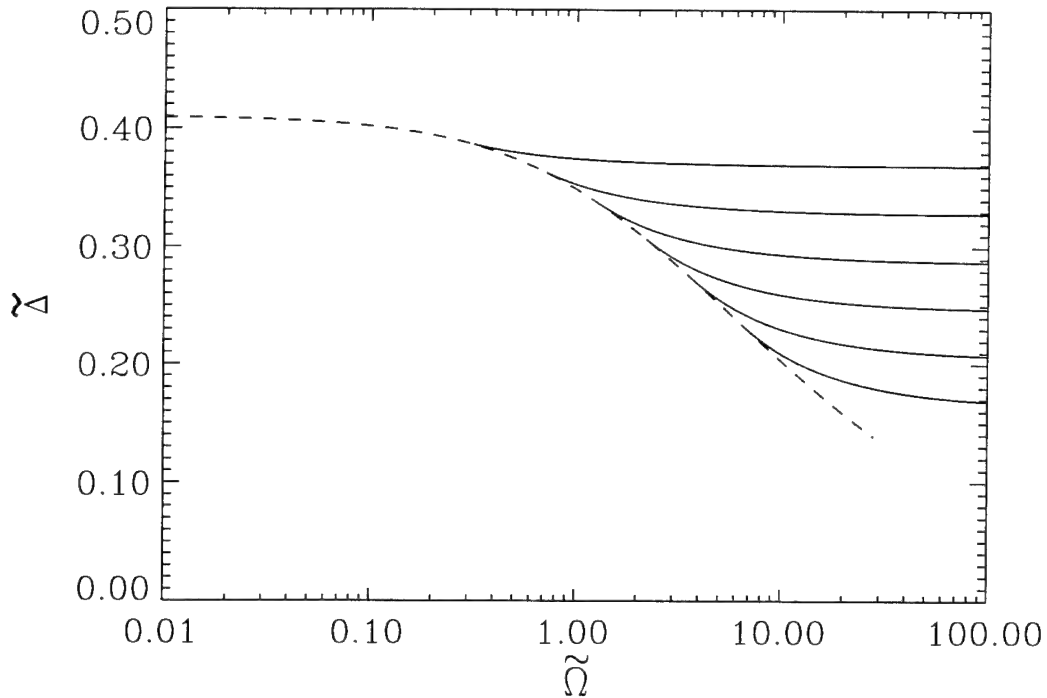
Fig. I.3. Plot of equations 1 (dashed line), and 2 (full lines) for $\rho_s/\rho_e = 0.4$, 0.5, 0.6, 0.7, 0.8 and 0.9.

The nozzle was designed in two parts so as to be fully interchangeable with the existing contoured nozzle. The divegence angle of the nozzle was chosen at 7 deg. which is a compromise between sufficient exit area at a fixed nozzle length and small axial gradients. It was necessary to make new molybdenum throat and nozzle inserts for this nozzle, because the contoured nozzle starts with a half angle of 14 deg.

A quick initial pitot calibration gave a flat distribution across the exit plane to within the error of the pitot-pressure measurement, as expected, and in contrast to the variation observed in the off-design use of the contoured nozzle (see Rousset, 1995).

I.2.3   Streak-line visualization

The thrust of the project during the next year will be the investigation of flow fields in which the vorticity generated by a curved bow shock plays a role. this will be particularly interesting in high-enthalpy flows, because the vorticity generated is proportional to the density ratio across the shock, and dissociating flows can give typically twice as high a density ratio as perfect diatomic gas flows, and because the shock curvature is also higher, which, for a given body, further increases the vorticity, and localizes it more.

This higher value and localization of the vorticity is likely to cause the high-vorticity layer to become unstable and form the kind of turbulent structures typical of a shear layer. To be able to see these, schlieren or interferometric techniques will often not be sensitive enough. Also, a streak-line visualization technique would be more suitable than one that is sensitive to density or

its gradient. For this reason an attempt was made to develop such a technique by analogy with the smoke-wire technique used in subsonic wind tunnels.

Building on our experience from the work in the previous reporting period, an exploratory investigation was conducted in T5, in which a wire, stretched across the nozzle exit was painted with a weak aqueous solution of salt. During the flow, the salt is ablated, and dissociates in the hot flow. The flow is then illuminated during the test with parallel light tuned to the wavelength of one of the D-lines of sodium. The sodium seeding in the flow absorbs the light, so that the parts which carry the sodium are opaque, and parts that are free of sodium are transparent.
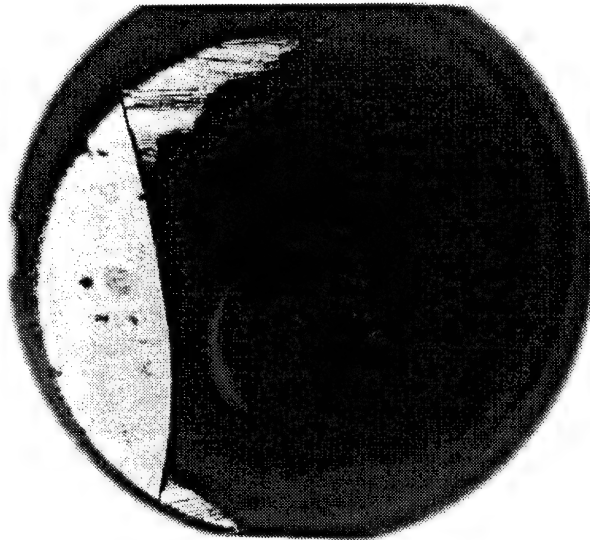

Fig. I.4. Photograph of the absorption of light by sodium seeding from a thin wire in a high-enthalpy flow in T5. Note the bending of the wire under the load of the drag force. The flow is opaque downstream of the wire. Note also the faint luminosity from the stagnation region of the model.

The exploratory investigation was successful inasmuch as it was possible to demonstrate that the introduction of the sodium by means of a wire works. It also showed that the sheet of sodium can be made opaque. This may be seen from Fig. I.4. It is now necessary to produce thin streak lines, and to determine the degree to which the wire affects the flow.

References

Rousset, B., 1995 "Calibration of the contoured nozzle of T5", Ae. E. thesis, California Institute of Technology.

Personnel associated with the research

1. Hans G. Hornung, Kelly Johnson Professor of Aeronautics, GALCIT Director.

2. Chih-Yung Wen, Graduate Research Assistant.

3. Patrick Lemieux, Graduate Research Assistant.

4. Bahram Valiferdowsi, Staff Engineer.

5. Bernard Rousset, Graduate Research Assistant.

Degrees earned during reporting period

Ae. E., Bernard Rousset, 1995.

Publications resulting from the research

1 Hornung H. G., Cummings E. B., Germain P., Sanderson S. R., Sturtevant B., and Wen C.-Y. 1994, "Recent results from hypervelocity research in T5," AIAA 94-2523, Colorado Springs.

2 Hornung, H. G., and Wen, C.-Y. 1995, "Nonequilibrium dissociating flow over spheres", AIAA 95-0091, Reno.

3 Wen, C.-Y. and Hornung, H. G. 1995, "Nonequilibrium dissociating flow over spheres", to be published in *J. Fluid Mech.*

4 Wen C.-Y. and Hornung, H. G. "Experiments on hypervelocity dissociating flow over spheres," in *Shock Waves @ Marseille*, ed R. Brun, L. Z. Dumitrescu, Springer Verlag, pp. 223-228.

5 Hornung, H.G., Wen, C.Y. and Germain, P. 1994 "Hypervelocity Flow Simulation," in *Mechanics USA 1994*, ed. A. S. Kobayashi, Appl. Mech. Rev. **47** pp. S14-S19.

Interactions

Presentations at conferences, see Publications, and at GALCIT Research Conferences. Invited speaker at DLR Göttingen, Germany, AIAA Colorado Springs and Reno. Seminar presentations at Princeton University, University of Minnesota, Mississippi State University. Discussions with G. Candler, Minnesota, and J. R. Maus, AEDC. Consultant to AEDC, (H. Hornung)

CHAPTER II
SHOCK-VORTICITY INTERACTION

II.1   NONEQUILIBRIUM CHEMISTRY IN SHOCK-VORTEX INTERACTION

Objectives and Status of Research

The objectives of this research are to elucidate the generic mechanisms controlling (1) interaction of a shock wave with a field of vorticity in the presence of nonequilibrium chemistry and (2) vorticity generation mechanisms in shock focusing with reaction chemistry. Progress continues on the computation of steady compressible vortex structures; the objective here is to use these solutions as special initial conditions for controlled numerical experiments on shock vorticity interaction. Work on the computation of hollow core compressible vortex streets has now been completed and submitted for publication. Work on compressible extensions of the Stuart vortices is now also nearing completion. Extensive computations of the interaction of a shock with a contact discontinuity which include dissociation chemistry are also in progress. Initial studies show that the initial vorticity generation due to the shock-contact interaction is not significantly affected by the dissociation chemistry. An analytic estimate of the deposition of vorticity by the shock has been derived by extending the shock-polars analysis of Samtaney and Zabusky (1994) to include the effects of chemistry. Work on the comparison of Whitham theory with numerical simulation continues. Finally a solution technique has been developed which allows the computation of similarity solutions for shock-contact interactions both with and without chemistry effects.

The next stage of this work will be the completion of the comparison of the results of Whitham theory with full numerical simulation. In addition work will begin on the use of the steady vortex configurations computed above as initial conditions for our flow simulation and the detailed study of the evolving vorticity both in the presence and absence of gas dissociation.

II.1.1 Steady Compressible Vortex Arrays

As discussed in our previous report part of our study of shock-vortex interactions progress concerns the computation of steady compressible vortex solutions. Our plan is to use these solutions as initial conditions and to then examine the shock-vortex interaction resulting from the interaction of an incipient shock with the vortex distribution both in the presence and in the absence of chemistry effects. Our work has concentrated on two models of steady compressible vortices. The first is an array of hollow core vortices, an extension of an approach initiated by Moore and Pullin (1987). This type of solution allows us to use hodograph techniques which make it possible to apply semi-analytic techniques to effect the solution. This work is now complete and the results have been submitted for publication. We have shown that for this particular compressible vortex array shock free transonic flow is possible for certain choices of the relevant parameters. We have also investigated the limit of an evacuated vortex core and find that we cannot obtain such solutions without the formation of limit lines indicating that shock free transonic flow may not be possible in this case.

The second model is obtained from a continuation of the analytical solutions of Stuart (1967) for a row of steady *incompressible vortices*, to finite M_∞. This reduces to the solution of coupled nonlinear equations for the density and stream-functions

$$\frac{2\hat{\rho}^2(\hat{\rho}^{\gamma-1}-1)}{\hat{q}_\infty^2(\gamma-1)} + \left(\frac{\partial\hat{\psi}}{\partial x}\right)^2 + \left(\frac{\partial\hat{\psi}}{\partial x}\right)^2 + \hat{\rho}_\infty\hat{\rho}^2 e^{-2\hat{\psi}/\hat{\rho}} = 0,$$

$$\frac{\partial}{\partial x}\left(\hat{\rho}^{-1}\frac{\partial\hat{\psi}}{\partial x}\right) + \frac{\partial}{\partial y}\left(\hat{\rho}^{-1}\frac{\partial\hat{\psi}}{\partial y}\right) - \hat{\rho}^{-1}e^{-2\hat{\psi}/\hat{\rho}} = 0,$$

where $\hat{\rho} = \rho/\rho_s$, $\hat{q} = q/c_s$, the subscripts "s" and "∞" refer to stagnation conditions and conditions at infinity respectively, and $\hat{\psi}$ is a non-dimensional stream-function. With suitable boundary conditions these equations can be solved by finite difference techniques to yield steady "*compressible Stuart vortex*" solutions of the Euler equations. These can then be used as initial conditions for the unsteady shock-vortex interaction codes. This work is now well along. We have again utilized both Rayleigh-Jantzen expansions as well numerical computation in order to provide independent checks on the results.

II.1.2 Numerical simulation of shock generated vorticity with chemistry

We have extended our calculations of shock generated vorticity to hypervelocity flow with chemistry effects included. We have investigated the Richtmyer-Meshkov instability in which a shock impinges upon a contact discontinuity for strong shocks i.e. for hypervelocity cases. To model the interaction of the flow with non-equilibrium chemical effects typical of high-enthalphy flows, the Lighthill-Freeman ideal dissociating gas model is employed. An interesting result of these investigations is that while dissociation causes significant changes in density and temperature, the growth of the perturbations reduces negligibly.

The governing equations of motion are the compressible Euler equations given below.

$$\mathbf{U}_t + \mathcal{F}_x(\mathbf{U}) + \mathcal{G}_y(\mathbf{U}) = \mathcal{S}(\mathbf{U}),$$

where

$$\mathbf{U} = \{\rho, u, v, E, \rho_1, \rho_1\alpha_1, \rho_2\alpha_2\}^T,$$
$$\mathcal{F}(\mathbf{U}) = \{\rho u, \rho u^2 + p, \rho uv, (E+p)u, \rho_1 u, \rho_1\alpha_1 u, \rho_2\alpha_2 u\}^T,$$
$$\mathcal{G}(\mathbf{U}) = \{\rho v, \rho uv, \rho v^2 + p, (E+p)v, \rho_1 v, \rho_1\alpha_1 v, \rho_2\alpha_2 v\}^T,$$
$$\mathcal{S}(\mathbf{U}) = \{Source\ terms\}^T.$$

The pressure, p is related to the total energy, E, by $p = (\gamma-1)(E - \frac{1}{2}\rho\mathbf{u}\cdot\mathbf{u})$.

The only allowable chemical reactions are the dissociation and recombination reactions for the diatomic species. Furthermore, it is assumed that the diatomic species are adequately modeled by the Lighthill Ideal Dissociating Gas model. The law of mass action for the IDG model may be written as:

$$\frac{\alpha_i^2}{1-\alpha_i} = \frac{\rho_{di}}{\rho_i}\exp\left(\frac{-\Theta_{di}}{T}\right),$$

where α_i is the mass fraction of the dissociated diatomic species, Θ_{di} is the disscociation temperature, ρ_{di} is the characteristic density and $i = 1$ if one dissociating diatomic gas is present in the domain or $i = 1, 2$ if there are two dissociating gases in the domain. Note that for the latter case, the gases undergo dissociation only and do not react with each other. For non-equilibrium cases the finite rate reactions proceed according to the Freeman model for an IDG gas and are given below:

$$\frac{d\alpha_i}{dt} = C_i(T, \alpha_i)\frac{\rho_i}{\rho_{di}}\left((1 - \alpha_i)\exp\left(\frac{-\theta_{di}}{T}\right) - \rho\alpha_i^2\right).$$

The function $C_i(T, \alpha_i)$ is given by

$$C_i(T, \alpha_i) = \frac{2C_{1i}T^{\eta_{1i}}\alpha_i + C_{2i}T^{\eta_{2i}}(1 - \alpha_i)}{W_i},$$

where W_i is the molar mass (molecular weight) of diatomic species i and C_{1i}, C_{2i}, η_{1i} and η_{2i} are constants that can be determined from experiment. The numerical method employed here is a second order accurate Equilibrium Flux Method. This technique now runs with high efficiency on a number of parallel architectures including the Intel Paragon. We have measured computational throughputs of roughly 3 Gigaflops when this algorithm is run on a 100 processor partition of this machine.

It is interesting to note that a second order Godunov method seems to be unsuitable for strong shock ($M \geq 10$) cases. EFM is more diffusive than Godunov type methods. However note that this feature of EFM, coupled with the fact that EFM does not require the calculation of the sound speed, is desirable.

The physical domain is a rectangular shock tube; x is the downstream direction and y and z are the transverse directions. The principal parameters are the speed of the incident shock, U_0, the properties of the gases across the interface and the product of the amplitude and wavenumber of the perturbation, $Ak = 2\pi A/\lambda$. To date we have considered the following gas combinations: H2-N2 (fast-slow) and N2-H2 (slow-fast). The initial unshocked gases were maintained at a pressure, $p_0 = p_b = 0.1atm$ and at a temperature of $T_0 = T_b = 298K$. At these temperatures only the diatomic species of the gases were present.

Some representative results are shown in the appended Figures. In Figure II.1 we show density contours for an interaction of a Mach 10 shock with an H2-N2 interface under frozen conditions. Figure II.2 shows the corresponding vorticity for this case. In Figures II.3 and II.4 we display the density and vorticity respectively for the same interaction but under equilibrium conditions.

II.1.3 Estimate of the initial vorticity using shock polars

It is well-known that for a perturbation of a fast-slow interface where the angle between the incident shock and the interface is constant and sufficiently small the Euler equations admit similarity solutions. In this particular case the solutions correspond to constant states which can be obtained using the method of shock polars. This technique has been used by Samtaney and Zabusky (1994)to compute initial vorticity deposition for shock initiated Richtmyer-Meshkov instability. We have extended these ideas to allow for dissociation. Our calculations indicate that significant departures from the frozen case occur at roughly Mach 6, as indicated in Figure II.5. However the change in the vortex sheet strength is small.
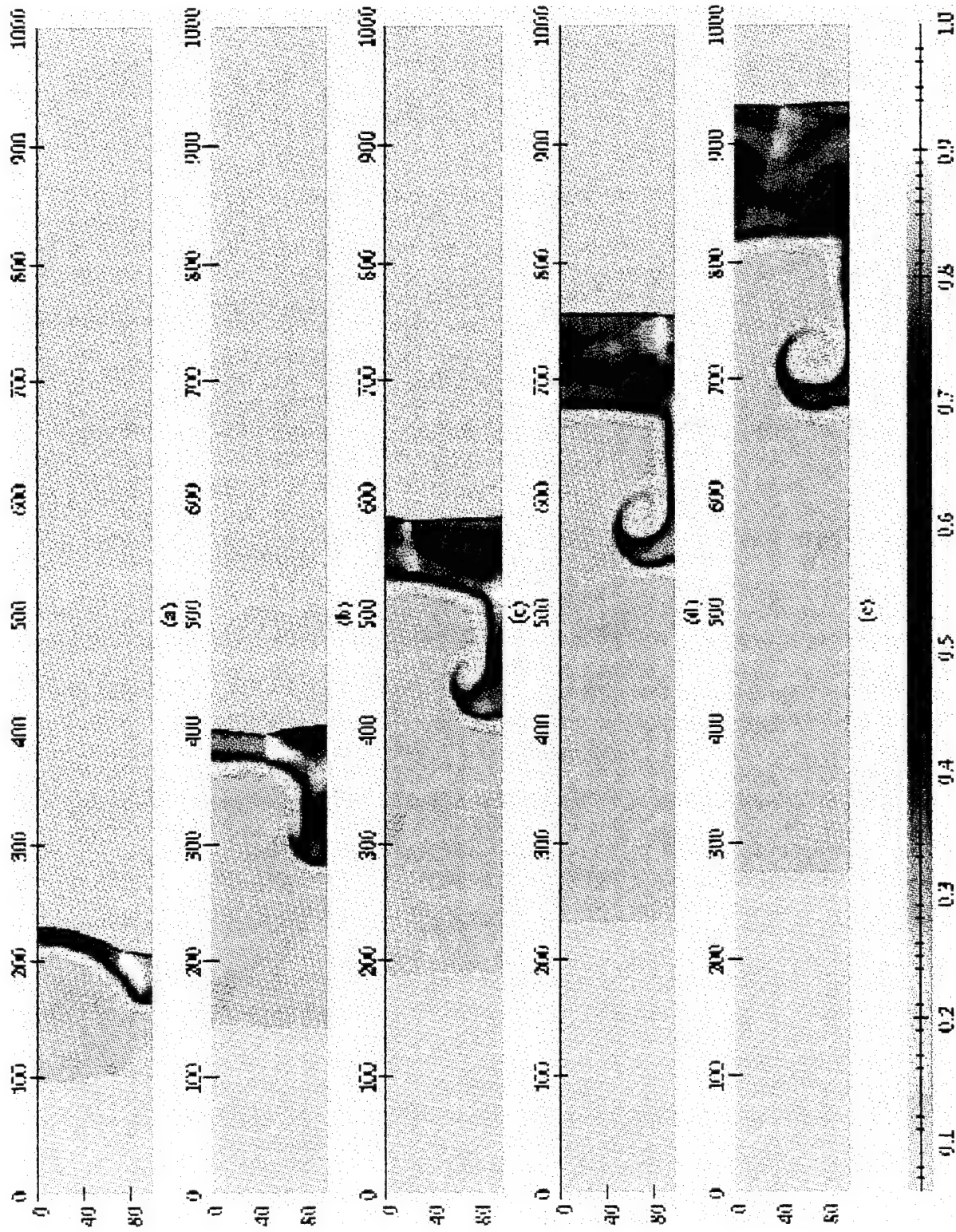
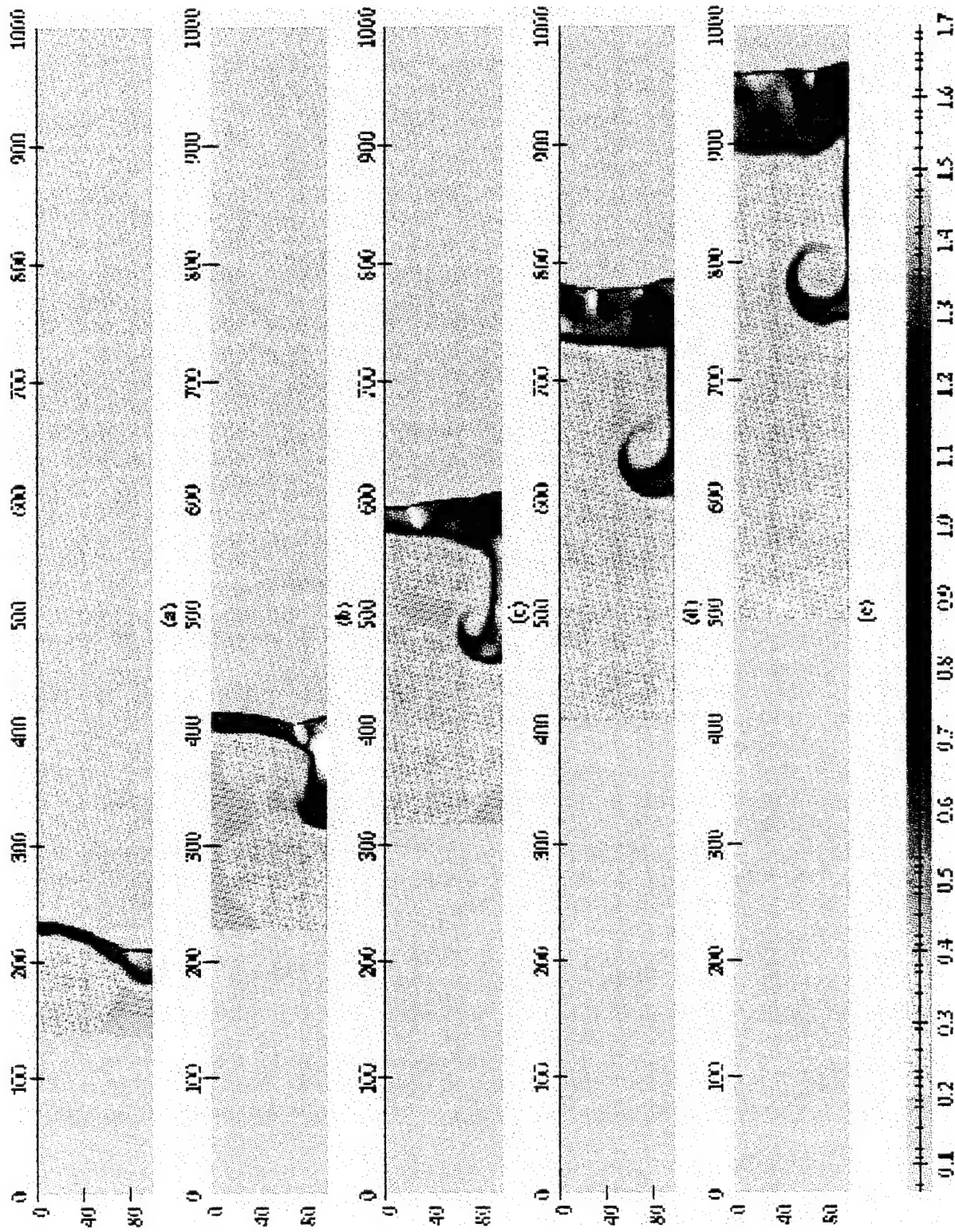Figure II.1: Density, H2-N2 Interface, M=10, A/L=0.1, Frozen

21

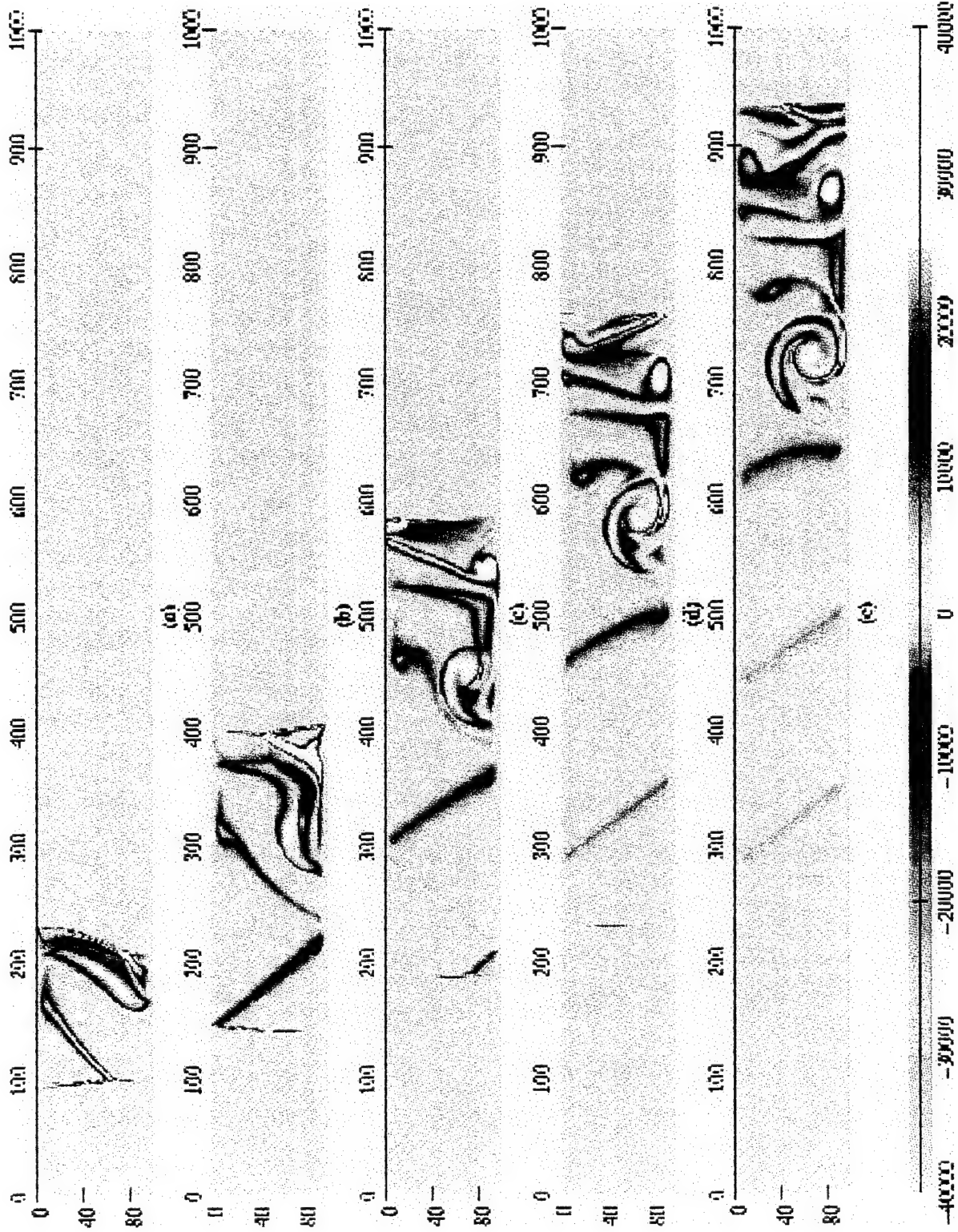Figure II.2: Density, H2-N2 Interface, M=10, A/L=0.1, Equilibrium

Figure II.3: Vorticity, H2-N2 Interface, M=10, A/L=0.1, Frozen
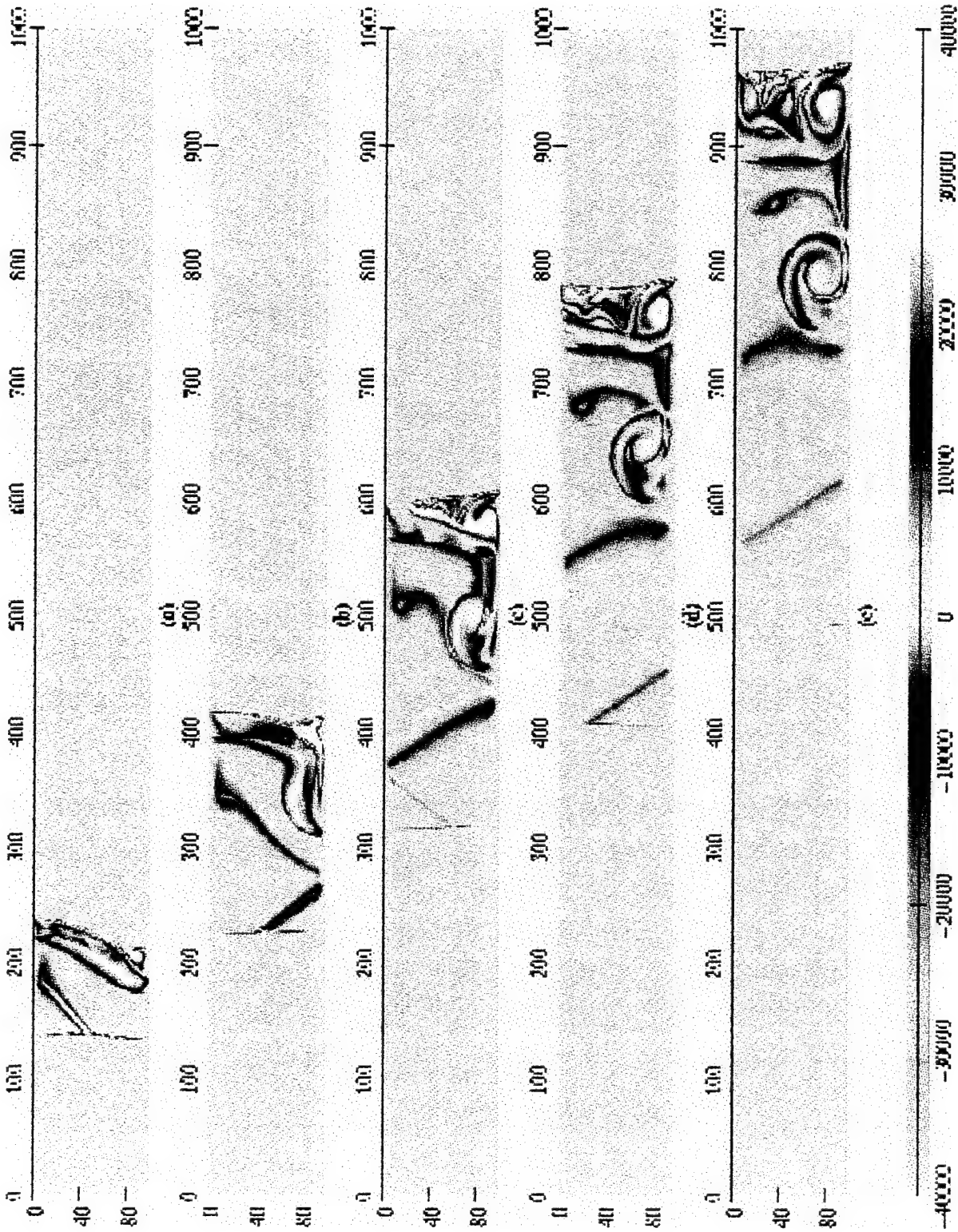
23

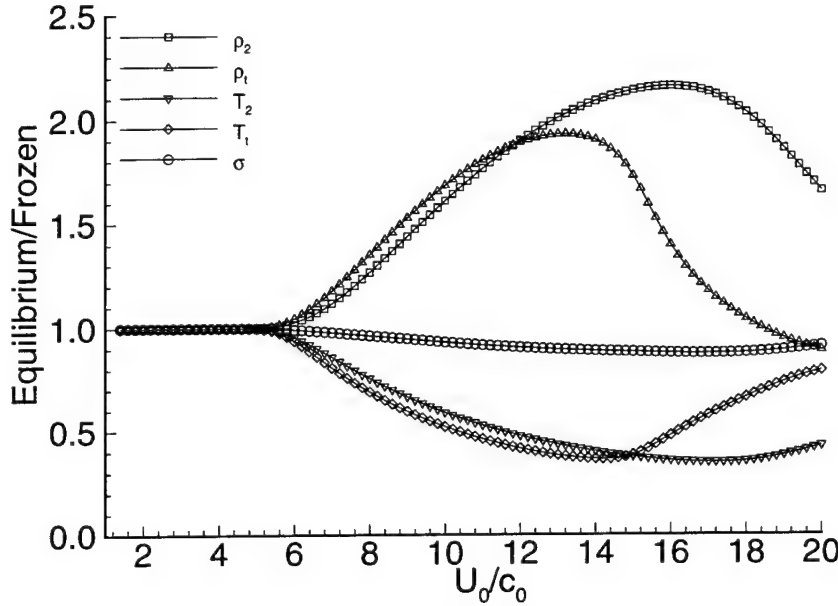Figure II.4: Vorticity, H2-N2 Interface, M=10, A/L=0.1, Equilibrium

Figure II.5. Local solution for a equilibrium dissociating flow normalized by the local solution for a frozen case. The interface is a sawtooth with angle 30^0. The gases are H_2-N_2. Here U_0, c_0 are the shock speed and the frozen speed of sound in the unshocked hydrogen, ρ_2, ρ_t are the densities behind the reflected and transmitted shock respectively. T_2, T_t are the temperatures behind the reflected and transmitted shock respectively, and σ is the strength of the vortex sheet.

It should be noted that this initial estimate of the vorticity is only accurate at early times. Subsequent interactions due to compression waves affect the circulation at the interface. In future work we will attempt to account for these interactions so as to obtain a more accurate estimate of the growth rate of the instability at later times.

II.1.4 Self-similar solutions of the compressible Euler equations

We have developed an iterative technique for computation of conically self-similar solutions of the two-dimensional unsteady Euler equations. The idea is to search for solutions to the Euler equations of the form

$$U(x, y, t) = \rho(\xi, \eta), u(\xi, \eta), v(\xi, \eta), E(\xi, \eta)$$

where

$$\xi = x/t \qquad \eta = y/t$$

Using this similarity transformation on the Euler equations leads to a system of nonlinear partial-differential equations

$$2\tilde{U} + \tilde{\mathcal{F}}_\xi + \tilde{\mathcal{G}}_\eta = 0$$

where

$$\tilde{\mathcal{F}} = \{\rho(u - \xi), \rho u(u - \xi) + p, \rho(u - \xi)v, E(u - \xi) + pu\}^T,$$

$$\tilde{\mathcal{G}} = \{\rho(v - \eta), \rho u(v - \eta), \rho v(v - \eta) + p, E(v - \eta) + pv\}^T,$$

which we solve by fixed point iteration. The technique may be applied to a fairly wide variety of two-dimensional flows which include the diffraction of a plane shock wave at a corner and the interaction of a plane shock with a density discontinuity in the presence of a wall. The similarity formulation includes flows with an arbitrary equation of state and is therefore directly applicable to hypervelocity flows with equilibrium disscociation/recombination chemistry of the type discussed above.

For the types of initial conditions we have considered (such as shocks incident on inclined contacts) similarity solutions exist and this technique allows us to compute them even when the subsequent temporal evolution may exhibit local instabilities of the Kelvin-Helmholtz type due to the formation of a contact discontinuity (vortex sheet). Another interesting aspect of this approach is that much sharper resolution of the flow discontinuities is obtained relative to temporal methods.

References

Moore, D.W., Pullin, D.I. 1987, The compressible vortex pair, *JFM,*, **185**, 188.

Stuart, J.T. 1967, On finite-amplitude oscillations in laminar mixing layers, *J.F.M* , **29**, 417.

Samtaney, R., Zabusky, N.J., 1994 Circulation deposition on shock-accelerated planar and curved density-stratified interfaces: Models and scaling laws *J. Fluid Mech.*, **269** 45.

Publications Resulting from Research

Ardalan, K., Meiron, D. I. and Pullin D. I., Steady compressible vortex flows: the hollow-core vortex array , sub judice, JFM.

Samtaney, R., Meiron, D. I. and Pullin, D. I. Hypervelocity Shock-Contact Interactions, Part 1: Richtmyer-Meshkov Instability , to be submitted, Physics of Fluids.

Samtaney, R., Meiron, D. I. and Pullin, D. I. Hypervelocity Shock-Contact Interactions, Part 2: Self-similar solutions of the compressible Euler equations., to be submitted, Physics of Fluids.

Personnel Associated with the Research

(1) Daniel I. Meiron, Professor of Applied Mathematics

(2) Dale I. Pullin, Professor of Aeronautics

(3) Dr. Ravi Samtaney, Senior Research Associate

(4) Mr. Kayvan Ardalan, graduate student. Thesis will entail study of the properties and stability of steady compressible vortex streets under a variety of boundary conditions.

Interactions

Invited talk at Rutgers by R. Samtaney. Visit at Lawrence Livermore Laboratory and discussions with K. Mikaelian and P. Miller. Presentations at GALCIT Research Conference.

II.2   SHOCK WAVE INTERACTIONS IN HYPERVELOCITY FLOW

Objectives and Status of Research

The objective of this experimental study is to determine the effects of chemical relaxation on the shock-on-shock problem, and, in particular, to quantitatively demonstrate the magnitude of nonequilibrium effects on shock impingement heating.

Holographic interferograms obtained for three different test conditions and a range of shock impingement locations have demonstrated that existing predictions of greatly increased stagnation density at high enthalpy, owing to the effects of dissociation, are not realized. Time resolved heat transfer measurements confirmed this observation and agreed accurately with existing low enthalpy experimental investigations. Thus, *we have shown that real gas effects do not further increase the large heat fluxes induced by shock impingement.*

The influence of thermochemistry on the jet shock system has been modeled using the ideal dissociating gas approximation. The central conclusion is that *peak heating arises from a balancing of the jet shock strengths and that this balance reduces the influence of thermochemistry on the flow.* Real gas effects were shown to be important at lower Mach numbers (< 7.5) and for impinging shock angles away from that which produces peak heating. The model accurately reproduces the experimentally observed heat transfer rates.

New instrumentation developed for this project has allowed critical assessment of the flow quality produced by the T5 facility. Measurements of the flow over blunt bodies without shock impingement agree with established theories within experimental uncertainty. This confirms the validity of the current data. This work is reported in full by Sanderson [9].

II.2.1   Introduction

The interaction of a weak oblique shock with the strong bow shock ahead of a blunt body in supersonic flow produces extreme heat transfer rates and surface pressures. Although the problem has been studied extensively in low enthalpy flows (Edney [3] [4]), the influence of high enthalpy real gas effects remains unknown. Edney [3] observed and classified six distinct interaction regimes that are known as types I–VI. Severe heating occurs for the type IV flow where the interaction causes the formation of a supersonic jet that impinges on the surface of the body. Local heat transfer rates and surface pressures, where the type IV jet meets the body, typically exceed the undisturbed stagnation point values by a factor of ten.

Shock loci techniques developed for the study of Mach reflection problems (Courant & Friedrichs [2]) give the solutions near the shock interaction points by mapping the problem into the pressure-flow deflection angle (p-δ) plane. This method of calculation allowed Edney [3] to study the variation of pressure at the jet impingement point for a perfect gas. The results of such a computation are shown in figure II.6 for typical values of the parameters. Using the stagnation point boundary layer solution of Cohen & Reshotko [1], Edney [3] correlated the heat transfer with the peak pressure and body diameter to jet width ratio, $D/\Delta x$, in the form,

$$\left(\frac{\dot{q}}{\dot{q}_0}\right)_{peak} \sim \sqrt{\left(\frac{p}{p_0}\right)_{peak} \frac{D}{\Delta x}}. \tag{1}$$

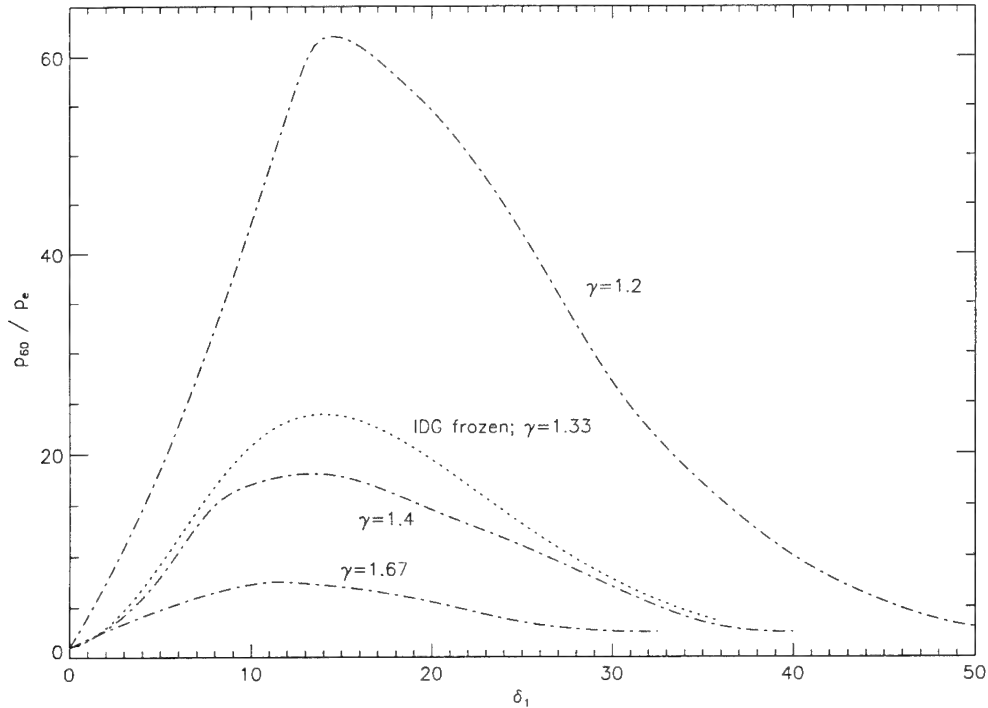Here the peak heat transfer rate and pressure are normalized with respect to the undisturbed

Figure II.6. Ratio of jet impingement pressure to undisturbed stagnation point pressure as a function of incident shock flow deflection angle, δ_1, and ratio of specific heats, γ (after Edney [3]; Figure 7-9). Free stream Mach number is $M_\infty = 10$.

stagnation point values. Given equation 1, figure II.6 indicates that reductions of the ratio of specific heats at high enthalpy should produce greatly increased heat transfer rates. The heat transfer intensification, $(\dot{q}/\dot{q}_0)_{peak}$, also increases strongly with Mach number. Although the ratio of specific heats is only a crude measure of the influence of equilibrium thermochemistry, the magnitude of the effect motivates the current experiments.

II.2.2   Scope of the current study

The objective of the present work was to determine the quantitative effects of thermochemistry on the shock impingement phenomenon. The current work consisted primarily of a series of experiments for both perfect and dissociating gases that utilized the capabilities the GALCIT T5 free piston shock tunnel. The flow topology was simplified by studying the nominally two dimensional flow about a cylinder with a coplanar impinging shock wave.

A significant preliminary objective of this project was to develop effective instrumentation for use in the hostile flow environment of hypervelocity shock tunnels. High resolution holographic interferometry was used to investigate changes in the flow structure as the location of the impinging shock wave was varied. Fast response heat transfer gauges were developed to provide time resolved measurements of the model surface temperature. The application of these developments to achieve the fluid mechanical goals of the project is reported in the following sections.

II.2.3 Description of experimental apparatus

The experimental arrangement is shown in figure II.7. High temperature and pressure gas was
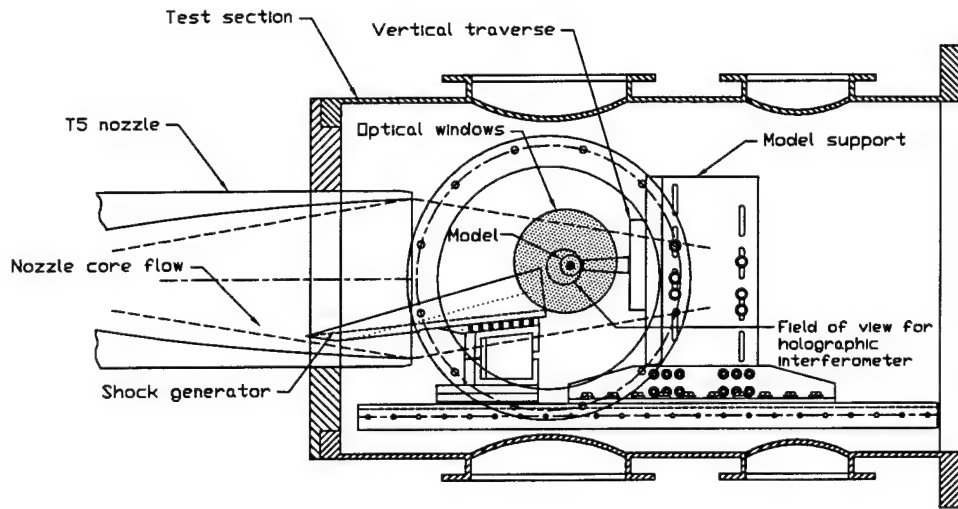

Figure II.7. Layout of apparatus in the test section of T5.

generated in the nozzle reservoir by the T5 hypervelocity shock tunnel. Free stream conditions are listed in table II.1. The cylindrical model (ϕ40 mm $\times$ 180 mm) was positioned in the free jet

Test condition		A	B	C
Nozzle reservoir conditions	Pressure (MPa)	14.6 $\pm$0.7	22.3 $\pm$1.3	28.3 $\pm$1.9
	Temperature (K)	3210	7550	8960
	Enthalpy (MJ/kg)	3.88	12.0	19.1
Test section conditions	Velocity (m/s)	2540	4450	5350
	Density (kg/m^3)	0.0218	0.0155	0.0157
	Pressure (kPa)	1.03	5.48	11.4
	N concentration (kg/mole)	9.9×10^{-5}	6.9×10^{-1}	3.65×10^{0}
	M_∞	9.9	6.3	5.3
	Re per mm	5500	1600	1350

Table II.1. SUMMARY OF THE FREE STREAM CONDITIONS. Results for condition B are not reported here.

test section through which the test gas exhausted into an evacuated dump tank. A large shock generator was partially inserted into the uniform nozzle core flow that extended upstream of the nozzle exit plane. Variations in the shock impingement flow field were investigated by vertically translating the model with respect to the exit of the shock generator. Optical access for holographic interferometry was available through windows that were mounted to flanges on the sides of the test section. Thermocouple gauges were used to record the surface temperature at 24 circumferential locations around the model forebody.

II.2.4   Experimental results

Figures II.8 & II.9 show holographic interferograms and heat transfer distributions obtained for the type IV interaction at low and high enthalpy respectively. The interferograms exhibit the characteristic features of the type IV flow. Two mutually inverted λ-shocks are observed along with a terminating strong shock and a region of elevated density behind it. Development of the holographic interferometer was successful in resolving the internal structure of the type IV jet. The circumferential locations of the maximum instantaneous heat fluxes, that are indicated in figures II.8 & II.9, coincide with the corresponding fringe shift maxima. The peak heat fluxes recorded during the entire sequence of shots at each test condition are listed in table II.2.

Test condition	A	C
Peak measured $\frac{q_{jet}}{q_{body}}$		
Instantaneous	15.2	8.0
100 μs averaged	13.5	6.0
Predicted $\frac{q_{jet}}{q_{body}}$		
Frozen	14.1	5.07
Nonequilibrium	-	4.37
Equilibrium	-	7.23

Table II.2. Comparison of measured and predicted heat transfer intensification for type IV flows with cylindrical model.

The conclusion of the experimental investigation was that the stagnation density and heat flux intensification decreased at high enthalpy. Care must be exercised in the interpretion of this trend since the Mach number of the flow in T5 decreased as the stagnation enthalpy was increased (Table II.1). The net result was that the influence of real gas effects was observed to be much less than that predicted by the variable γ model (Figure II.6).

In addition to these measurements of the influence of real gas effects, the high bandwidth of the heat flux gauges permitted examination of the temporal characteristics of the heat transfer signals. Sanderson [9] discusses observations of coherent unsteady fluctuations of the type IV jet that are consistent with oscillations observed in recent numerical simulations (Gaitonde [7], Zhong [10]).

II.2.5   Model of the influence of real gas effects

Modeling of the influence of real gas effects followed the pattern of the existing perfect gas model of the type IV field (Edney [3]). Thermochemical effects were investigated in four conceptual stages;

1. Normal shock solutions were obtained using the ideal dissociating gas model due to Lighthill [8].

2. Extension to oblique shock waves.

3. Mapping to the p-δ plane to obtain solutions for the λ-shock points.

4. Modeling of the impingement heating using the equilibrium reacting flow similarity solution of Fay & Riddell [5].
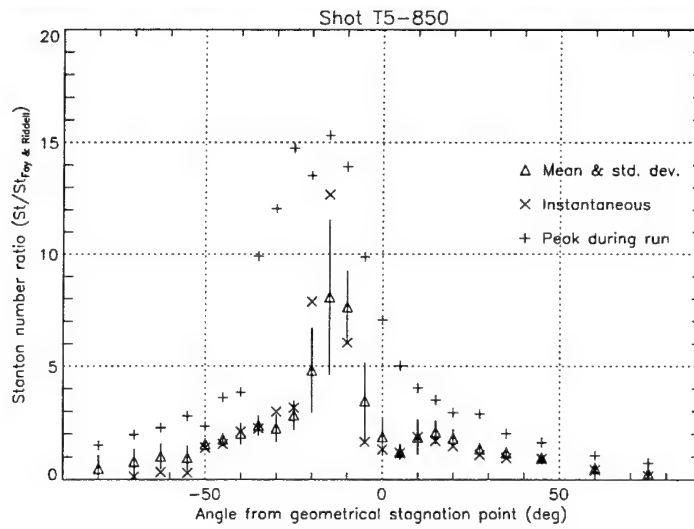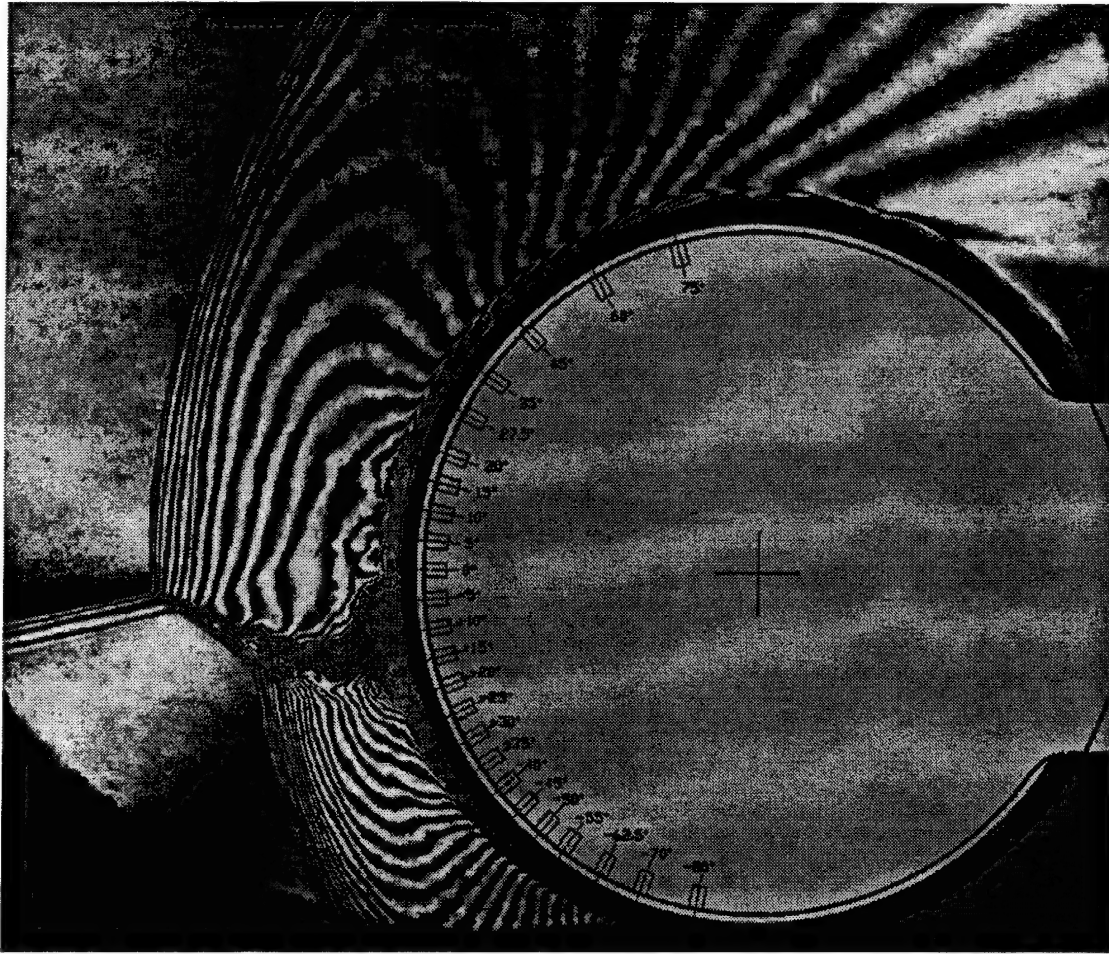
Figure II.8. Shot T5-850; condition A.

Sanderson [9] shows that the heat transfer intensification may be expressed in the form;

$$\frac{\dot{q}_{jet}}{\dot{q}_{body}} \sqrt{\frac{\Delta x}{D} \frac{\zeta_{1_{body}}^2 \zeta_{2_{body}}}{\zeta_{1_{jet}}^2 \zeta_{2_{jet}}}} = func(P_\infty, H_{0_\infty}, \hat{\rho}_d, \alpha_\infty, \beta_1). \tag{2}$$
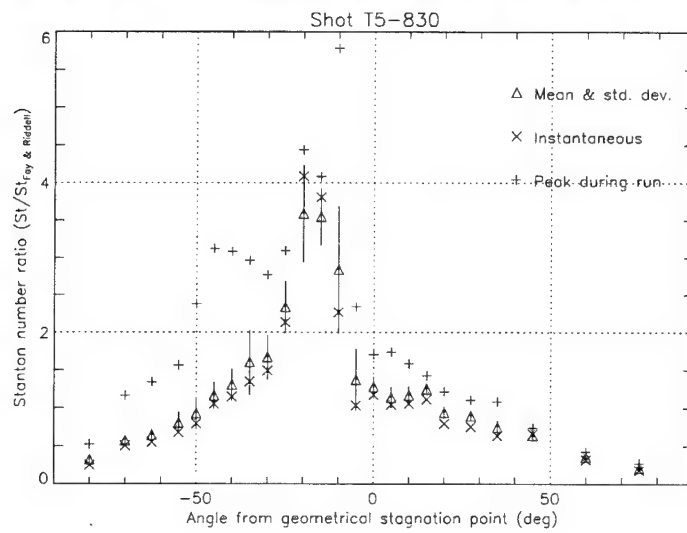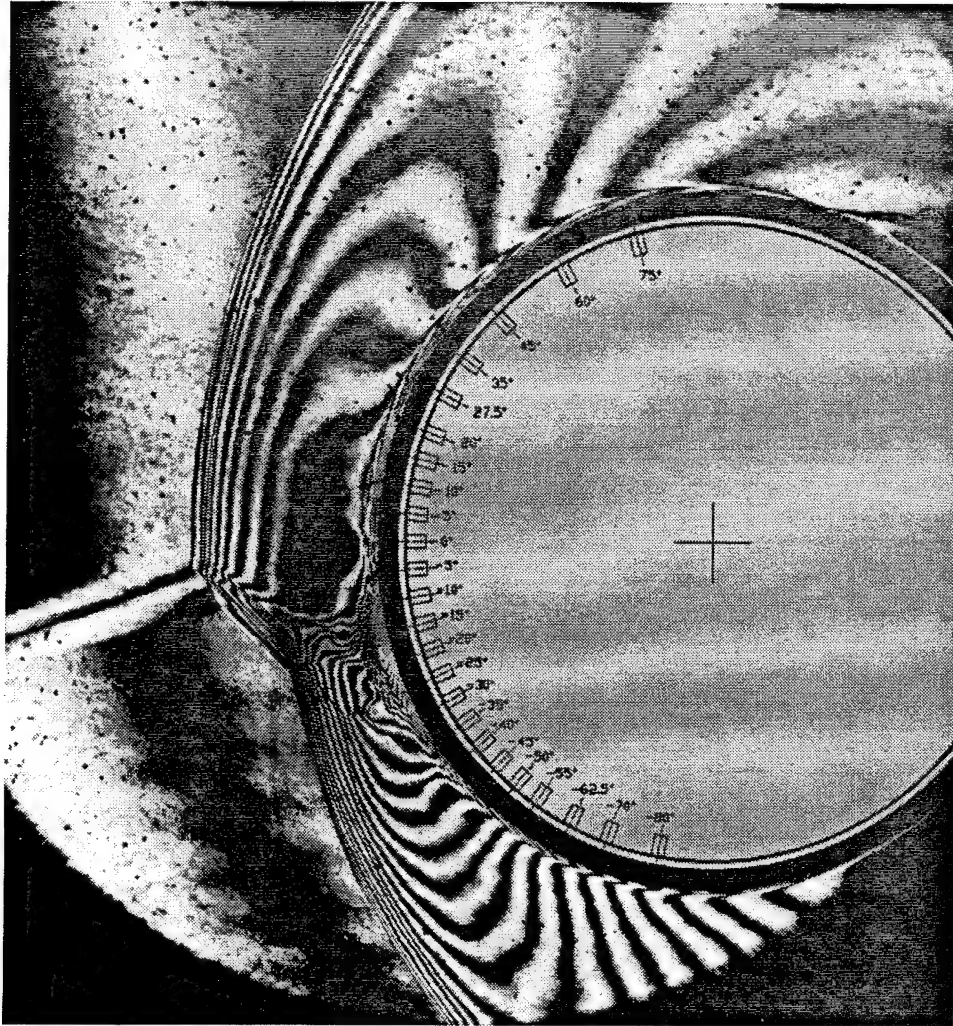
Figure II.9. Shot T5-830; condition C.

The parameters are $P_\infty = p_\infty/\rho_\infty u_\infty^2 \sim 1/M_\infty^2$, H_0 is the stagnation enthalpy normalized with respect to the dissociation energy of the gas, $\hat{\rho}_d$ is the equilibrium constant, α_∞ is the dissociated mass fraction of the free stream and β_1 is the angle of the impinging shock wave. Since this is a local solution the geometrical terms on the left hand side, that specialize the result for a particular configuration, remain indeterminate; where $\Delta x/D$ is the jet width to body diameter ratio. The various similarity coefficients, ζ, are determined from the similarity solution of Fay & Riddell [5] and the Newtonian solution for the velocity gradient at the outer edge of the boundary layer.

The behavior of the local solution 2 with stagnation enthalpy is illustrated in figure II.10 for typical values of the remaining parameters. Three solutions were obtained in order to investigate the influence of nonequilibrium thermochemistry;

1. The frozen solution that applies when the reaction rates are slow.

2. The equilibrium solution that applies when the reaction rates are fast.

3. A nonequilibrium approximation whereby the weak oblique waves at the λ-points are frozen and the strong bow shock and terminating jet shock reach equilibrium.

The validity of the approximate nonequilibrium solution was assessed by computing the reaction rates (Freeman [6]) immediately downstream of the translational discontinuities. Figure II.10 shows that equilibrium real gas effects increase the heat transfer intensification with respect to the frozen solution. This occurs because of increased density rise across the weak oblique jet shocks. In the
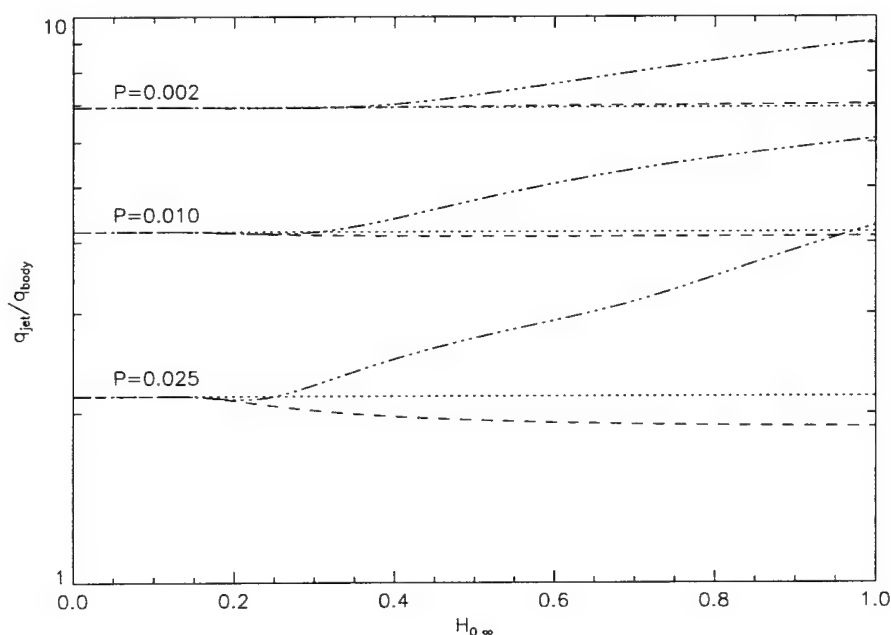
Figure II.10. Influence of dimensionless stagnation enthalpy, $H_{0\infty}$, Mach number, $\sim 1/P_\infty^{\frac{1}{2}}$ and reaction rate on type IV heat transfer intensification, $\frac{\dot{q}_{jet}}{\dot{q}_{body}}\frac{\Delta x}{D}\frac{\zeta_{1body}^2\zeta_{2body}}{\zeta_{1jet}^2\zeta_{2jet}}^{\frac{1}{2}}$. $\cdots\cdots$ curves are the frozen solutions. — $\cdots$ — curves are the equilibrium solutions. $---$ curves are the nonequilibrium approximate solutions. The parameters are $P_\infty = 0.002, 0.010, 0.025$, $\hat{\rho}_d = 1 \times 10^7$, $\alpha_\infty = 0$ and $\beta_1 = 16°$.

nonequilibrium approximation, where the jet shocks remain frozen, the heat transfer intensification decreases slightly with respect to the frozen solution. Within the scope of the approximation, non-monotonic behavior with the reaction rate is indicated. Further analysis (Sanderson [9]) demonstrates that peak heating conditions for a perfect gas minimise the influence of real gas effects for equilibrium flows and promote nonequilibrium effects by depressing the reaction rate in the supersonic jet.

Specific predictions of the model for the test conditions listed in table II.1 are compared with the experimental data in table II.2. The extent of chemical reactions at the low enthalpy condition A was negligble and so only the frozen solution is shown. Reaction rates for condition C were sufficiently high that departures from equilibrium were expected to be slight. The calculated values accurately reproduce the experimental heat transfer measurements.

References

[1] COHEN, C. B. & RESHOTKO, E. 1956 Similar solutions for the compressible laminar boundary layer with heat transfer and pressure gradient. NACA Report 1293.

[2] COURANT, R. & FRIEDRICHS, K. O. 1948 *Supersonic Flow and Shock Waves.* Interscience.

[3] EDNEY, B. E. 1968 Anomalous heat transfer and pressure distributions on blunt bodies at hypersonic speeds in the presence of an impinging shock. FFA Report 115.

[4] EDNEY, B. E. 1968 Effects of shock impingement on the heat transfer around blunt bodies. *AIAA J*, **6**(1), 15–21.

[5] FAY, J. A. & RIDDELL, F. R. 1958 Theory of stagnation point heat transfer in dissociated air. *Journal of the Aeronautical Sciences*, **25**(2), 73–85.

[6] FREEMAN, N. C. 1958 Non-equilibrium flow of an ideal dissociating gas. *JFM*, **4**, 407–425.

[7] GAITONDE, D. 1993 Calculations on unsteady type IV interaction at Mach 8. Wright Laboratory, WL-TR-93-3002.

[8] LIGHTHILL, M. J. 1957 Dynamics of a dissociating gas. Part I. Equilibrium flow. *JFM*, **2**, 1–32.

[9] SANDERSON, S. R. 1995 Shock wave interaction in hypervelocity flow. Ph.D. Thesis, California Institute of Technology.

[10] ZHONG, X. 1994 Application of essentially non-oscillatory schemes to unsteady hypersonic shock-shock interference heating problems. *AIAA J*, **32**(8), 1606–1616.

Publications Resulting from the Research

Sanderson, S. R. and Sturtevant, B. 1995 Shock wave interactions in hypervelocity flow, in "Shock Waves @ Marseille", *Proc. 19th Intl. Symp. Shock Waves*, Eds. R. Brun and L. Z. Dumitrescu, 69-74, Springer Verlag, Berlin.

Hornung, H. G., Cummings, E. B., Germain, P., Sanderson, S. R., Sturtevant, B. and Wen, C.-Y. 1994 Recent results from hypervelocity research in T5, Presented at 18th AIAA Aerospace Ground Testing Conference, 6/20-23, 1994, AIAA 94-2523, GALCIT, Colorado Springs, CO.

Sanderson, S. R. 1995 Shock wave interaction in hypervelocity flow. Ph.D. Thesis, California Institute of Technology.

Personnel Associated with the Research

1. B. Sturtevant, Professor of Aeronautics.

2. Simon R. Sanderson, Graduate Student.

3. Jean-Paul Davis, Graduate Student.

Degrees Earned

1. S. Sanderson, Ph.D., 1995

Interactions

1. Interacted with shock-on-shock calculations reported in Section IV.1.

2. Graduate student collaborated for two months with peer from HEG, Göttingen, Germany.

3. Organized 20th International Symposium on Shock Waves, Pasadena, July, 1995, at which 400 shock-wave specialists will meet.

CHAPTER III

SUPERSONIC SHEAR-FLOW MIXING AND COMBUSTION

Objectives and status of the research

The objective of this part of the research effort is to gain an understanding of mixing and combustion processes in supersonic and compressible shear flows, including the effects of shock-wave interactions with turbulent mixing regions. This part of the effort includes experimental investigations in supersonic mixing-layer flows, with supersonic/subsonic freestreams, as well as all-hyperbolic (supersonic/supersonic) freestreams, a numerical simulation effort of chemically-reacting flows and detonations, and the development of image correlation velocity-measurement techniques and instrumentation that would be applicable to both subsonic and supersonic flows.*

Progress during the reporting period has been made in all three areas, with a major upgrade of the Supersonic Shear Layer (S^3L) Combustion facility, to allow higher Mach number flows to be attained, and experiments on supersonic shear layers and shear-layer/shock-wave interactions completed; the development of a robust, unsplit, shock-capturing, numerical simulation method for the calculation of one- and multi-dimensional chemically-reacting flows and detonations; and further developments in Image Correlation Velocimetry. We are presently in the final phases of a design and fabrication effort to develop new CCD-imaging technology to permit the recording of a pair of images in quick succession (as close as $1\,\mu s$ apart). Several of the new CCD-imaging devices have tested favorably on the wafers recently returned to us from the silicon foundry.

In the next stage of this effort, direct measurements of mixing in all-hyperbolic shear layers will be undertaken, as well as the development of a modified test section for the S^3L facility to study wall-bounded mixing and combustion in supersonic flows; the numerical simulations of chemically-reacting flows and detonations will be extended to unsteady, two-dimensional flows; and the first trials of the new image-pair recording CCD's will be conducted in a laboratory environment.

II.2.1 Bi-supersonic shear-layer flows

As part of our continuing experimental investigations of the behavior of all-hyperbolic, fully-developed, turbulent, mixing-layer flows, we have studied two bi-supersonic flows, at low and moderate compressibility levels. An example of the low-compressibility flow (nominal nozzle-exit conditions: $M_1 = 1.5\,[N_2]$, $M_2 = 1.2\,[N_2]$) is shown in Fig. III.1. Evident in this schlieren flow visualization is a near-normal stationary compression shock in the bottom freestream, located slightly downstream of the nozzle-exit plane. The (oblique) Mach wave incident on the normal-wave front is seen to terminate there, as demanded by the downstream (shock-processed) subsonic flow. The flow is observed to be supersonic a short distance downstream of this wave. As indicated at this downstream location, an oblique Mach wave is refracted, from the top freestream, through the mixing layer, into the bottom freestream. Refractions of this type are only possible in all-hyperbolic (as measured in the Galilean reference frame of the wave) flow.
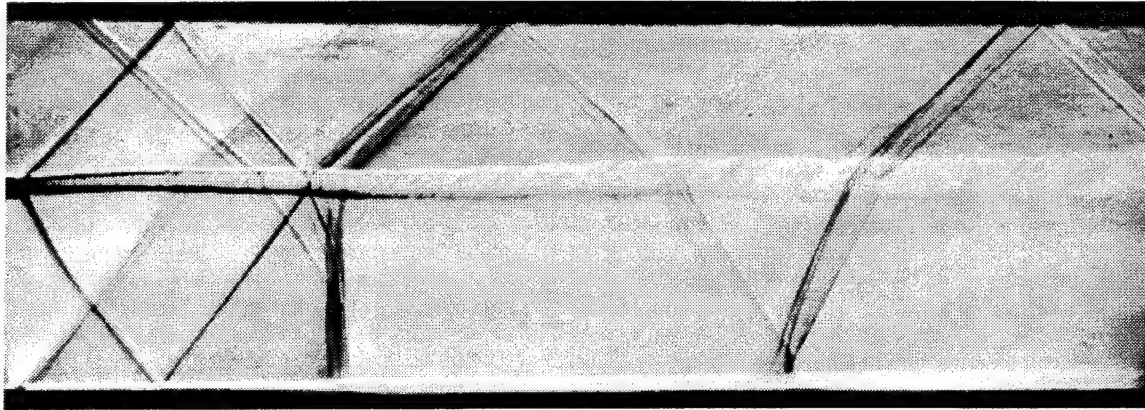

Fig. III.1. Schlieren (oblique knife edge) photograph of $M_1 = 1.5$ [N$_2$], $M_2 = 1.2$ [N$_2$] (nominal nozzle-exit conditions) mixing-layer flow.

The bottom freestream can be seen to be accelerated back to a supersonic state by an effective freestream area change produced by the displacement thicknesses of the mixing layer and the bottom-guidewall boundary layer, in addition to the weak curvature of the shear layer. This interaction, dubbed the "aerodynamic Laval nozzle", was also described in the discussion of a different mixing-layer flow in our previous Annual Technical Report (Candler *et al.* 1994). The significant influence even small changes in the effective freestream area has on these flows is noteworthy. This sensitivity is largely traceable to the the Mach-number/area relationship, *e.g.*, Fig. 5.2 of Liepmann & Roshko (1957), for quasi-one-dimensional flow in the transonic Mach number regime.

A second example of low-compressibility flow behavior is shown in Fig. III.2. The non-linear computer-control system for the Supersonic Shear Layer Facility (*cf.* Hall 1991), permits extremely precise control of the freestream stagnation pressures, allowing for considerable flexibility in setting particular test-section flow conditions. Exploiting this ability, a flow configuration was designed, at a slightly lower (5%) top-freestream stagnation pressure than the flow discussed above. This change in the top-freestream nozzle-exit condition significantly modifies the interaction between the two freestream flows and the fully-developed turbulent mixing layer. Notably, the normal shock observed in the previously-discussed (Fig. III.1) flow is now "unfolded" into a Mach reflection of the incident oblique shock from the bottom guidewall. Visualizations recorded in a set of runs of decreasing stagnation pressures exhibit a gradual shortening of the Mach stem, until regular reflection is attained.

These flow configurations, *i.e.*, two moderately-supersonic, acoustically-similar gas streams, provide us with an important diagnostic capability. In these flows, turbulence-generated density gradients are relatively weak in comparison to the wave-generated gradients. As observed in the schlieren photographs, *e.g.*, Fig. III.1, this discrepancy in the two types of gradients, in addition to the transmission of the waves through the mixing layer, provides an instantaneous visualization of the details of the wave-turbulence interactions. Given that many of the these waves are well-approximated as infinitesimal disturbances, these interactions can be viewed as passive measurements of the instantaneous, fully-developed turbulent Mach number field.

We have also investigated some bi-supersonic mixing-layer flows at moderate-compressibility conditions. A schlieren visualization of this $M_1 = 1.5$ [He], $M_2 = 1.2$ [N$_2$] (nominal nozzle-exit conditions) mixing-layer flow, is reproduced in Fig. III.3. The compressibility of this flow, as
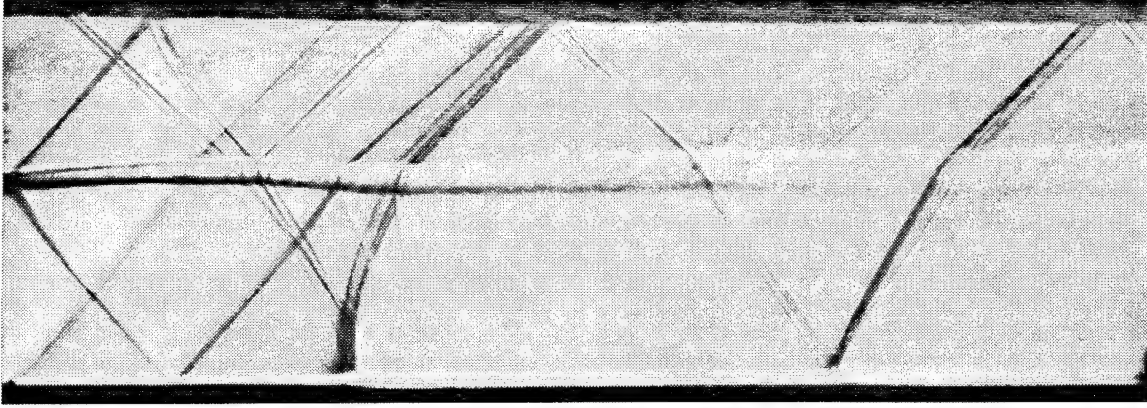
Fig. III.2. Schlieren (oblique knife edge) photograph of $M_1 = 1.5$ [N$_2$], $M_2 = 1.2$ [N$_2$] (nominal nozzle exit conditions) mixing-layer flow. Visualization recorded at a slightly lower top-freestream nozzle-exit stagnation pressure than that of the Fig. III.1 flow.

measured by the total convective Mach number,

$$M_c \equiv \frac{u_1 - u_2}{a_1 + a_2} \tag{1}$$

is $M_c \approx 0.7$, in contrast to the low-compressibility flows ($M_c \approx 0.1$) discussed above. A consequence of the increased compressibility level is the presence of two different pressure-wave systems in this flow: a lab-frame-stationary system generated by the imposition of the mixing-layer displacement thickness when the two freestream flows first interact (extreme left-hand side of Fig. III.3) and a traveling-wave system in the bottom freestream. Significantly, no such traveling wave system was observed in the low-compressibility flows.

As noted earlier, the stationary-wave refractions, through the mixing layer, observed in this flow are disallowed if one of the freestreams is elliptic, in the Galilean frame of the wave. These finite-strength wave-turbulence interactions do not appear to have a significant effect on the growth rate of the layer, consistent with the observations of Shau et al. (1993). The insensitivity of the mixing-layer growth rate to these wave-turbulence interactions, in this high-density-ratio, ($\rho_2/\rho_1 \approx 5$)-case, is interesting, considering the (net) baroclinic vorticity (circulation) that such refractive interactions can generate.

The system of traveling waves, present in the freestream flow, are of the same character as those observed originally by Lowson and Ollerhead (1968), Tam (1971), and Oertel (1979), in supersonic, turbulent, jet flows, and more recently by Hall et al. (1993), in a supersonic, mixing-layer flow. As discussed by these authors, these waves appear to be associated with large-scale turbulent structures, convecting supersonically with respect to (in this case) the bottom (low-speed) freestream. Defining convective Mach numbers of these features with respect to each of the freestreams, i.e.,

$$M_{c1} \equiv \frac{u_1 - u_c}{a_1} , \qquad M_{c2} \equiv \frac{u_c - u_2}{a_2} , \tag{2}$$

where u_c is the lab-frame convection velocity of these features, we deduce $M_{c1} \approx 0.2$ and $M_{c2} \approx 1.6$. This "fast-mode" convection velocity, as observed in a bi-supersonic mixing-layer flow, is at variance with the convection-velocity stream-selection rule proposed by Papamoschou (1989). Additional exceptions to this proposed rule are found in the experiments of Martens et al. (1994) as well as

in the Papamoschou data (1989).** These observations are at a lower M_c, however, than this case, where the effect of compressibility appears to be less significant, *i.e.*, $M_{c1} \approx M_{c2} \approx M_c$ for small M_{c1}, M_{c2}.
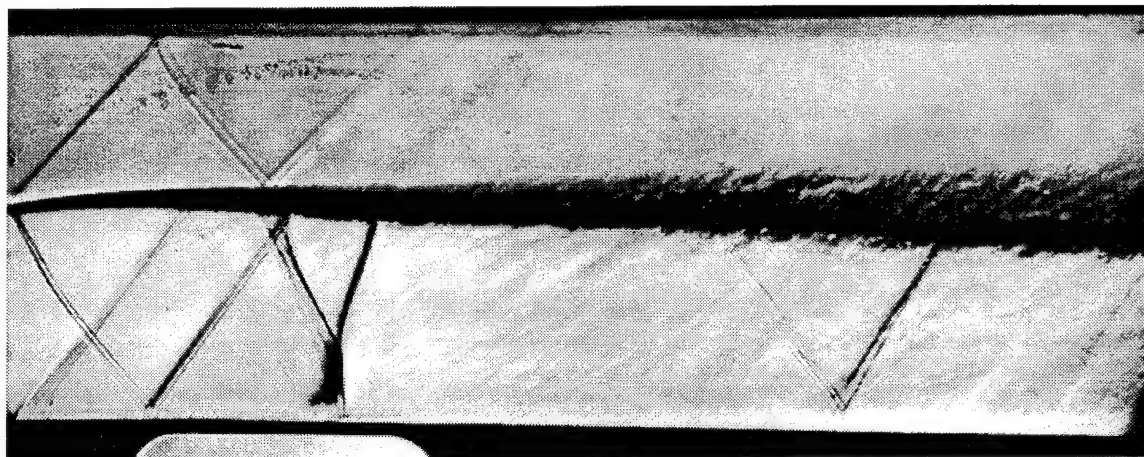

Fig. III.3. Schlieren (vertical knife edge) photograph of $M_1 = 1.5$ [He], $M_2 = 1.2$ [N$_2$] (nominal nozzle-exit conditions) mixing-layer flow.

This effort is part of the Ph.D. research of Michael Slessor.

II.2.2 Chemically-reacting, compressible-flow simulations

As part of our effort to accurately and efficiently compute chemically-reacting compressible flows, we have developed a new, unsplit, algorithm for the solution of the governing equations. Conventional, *i.e.*, split, algorithms employ separate numerical steps for the gas dynamics, ignoring the contribution of chemical reactions, and treat the chemically-reacting source terms in a separate step, artificially decoupling the dynamics. As a consequence, the application of such methods to chemically-reacting flows maybe questionable, depending on the details of the reacting flow, because of the extremely large range of (coupled) spatial and temporal scales encountered in such problems, as well as the very large number of unstable modes that characterize such systems, leading to a multiplicity of both linear and nonlinear instability paths. The new algorithm eliminates these difficulties by integrating the complete conservation equations, including the contributions by the chemical reactions, in a single, fully-coupled, step.

The new algorithm is an extension and generalization of the scheme developed at Caltech, under AFOSR sponsorship, for non-reacting flows (Lappas 1993, Lappas *et al.* 1994), finds surfaces in space-time where appropriate Riemann invariants hold, permitting the integration of the complete flow/chemistry evolution equations in an accurate, robust, and mathematically consistent manner. This method requires no flux-splitting, or other such artifice, as is usually required in conventional solutions of these equations.

In order to allow comparison to documented results, the first test runs with this unsplit algorithm were performed in one spatial dimension (plus time), for chemically-reacting systems where conventional methods are known to perform well, *e.g.*, for cases where the chemical-production

---

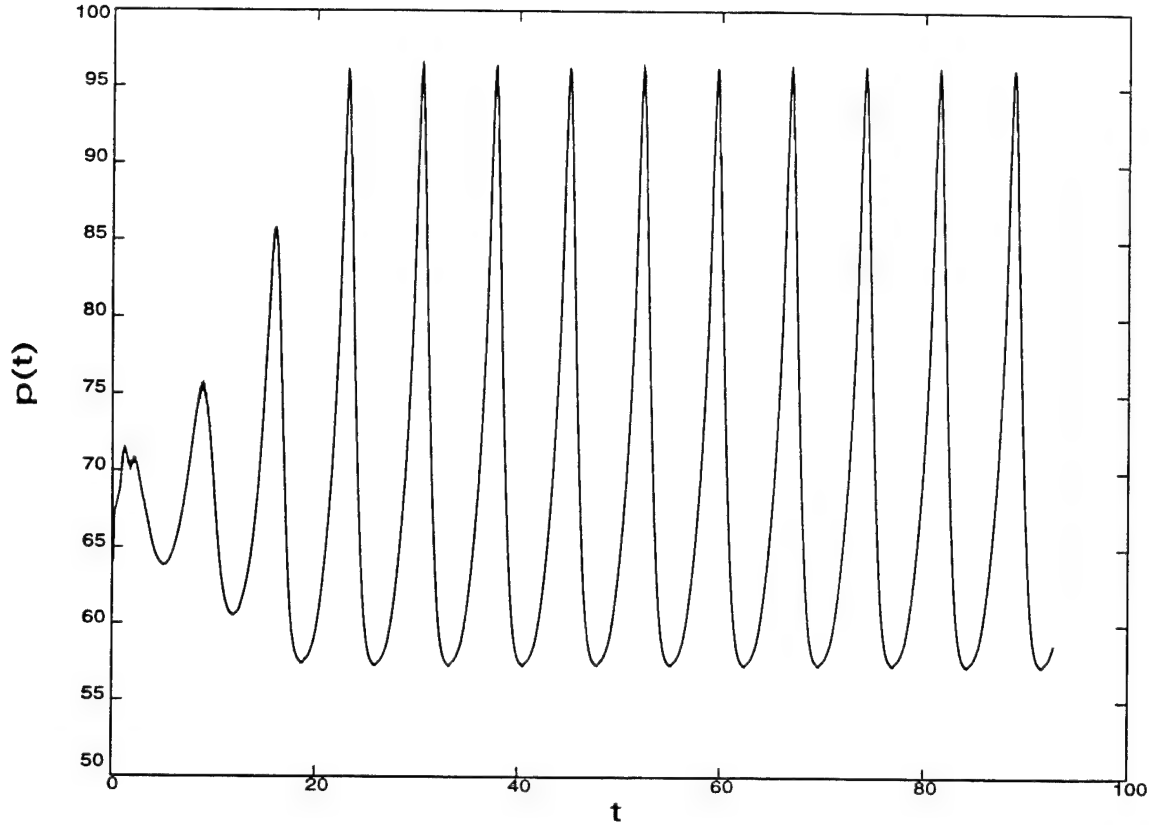** Case N31N17 of Papamoschou (1989).

Fig. III.4. Temporal profile of dimensionless shock pressure for an overdriven ZND detonation (over-drive factor 1.6). Note well-defined single temporal mode.

source term is not particularly stiff, and/or cases where the actual system is not characterized by multi-mode instabilities.[†] The algorithm, however, is genuinely multidimensional and, consequently, capable of computing up to full four-dimensional flows, *i.e.*, three spatial dimensions and one temporal dimension. Our test cases, of various steady and unsteady detonation waves, are in excellent agreement with well-known results in the literature, *e.g.*, Fickett & Wood 1966 and Bourlioux *et al.* 1991. A typical example of these test computations is shown in Fig. III.4. This case, an overdriven Zel'dovich-vonNeumann-Doering (ZND) detonation, with an overdrive factor of 1.6, is well-known to be linearly unstable, with one unstable mode (the overdrive factor is defined as the square of the ratio of the wave speed to the Chapman-Jouguet wave speed). As seen in Fig. III.4, our result is consistent with this analysis. In this simulation, the mesh resolution was set at 20 cells per reaction length.

We have also performed simulations of detonations near the Chapman-Jouguet (C-J) point, *i.e.*, with near-unity overdrive factors. These cases are typically very difficult to compute, because of the stiffness and other characteristics of the governing equations induced by the terms attributable

---

[†] We note that such systems are generally linearly and non-linearly unstable. In particular, it is imperative that the instability characteristics of the numerical-simulation model, used to mimic the actual system behavior, be characterized by as nearly similar a dynamical system behavior as the actual system. These systems, however, are also typically chaotic with a large number of (modal) degrees of freedom and extreme sensitivity to initial conditions and the details of the simulated evolution path. Unfortunately, general proofs for the requirements to satisfy this important criterion are not available at this time.
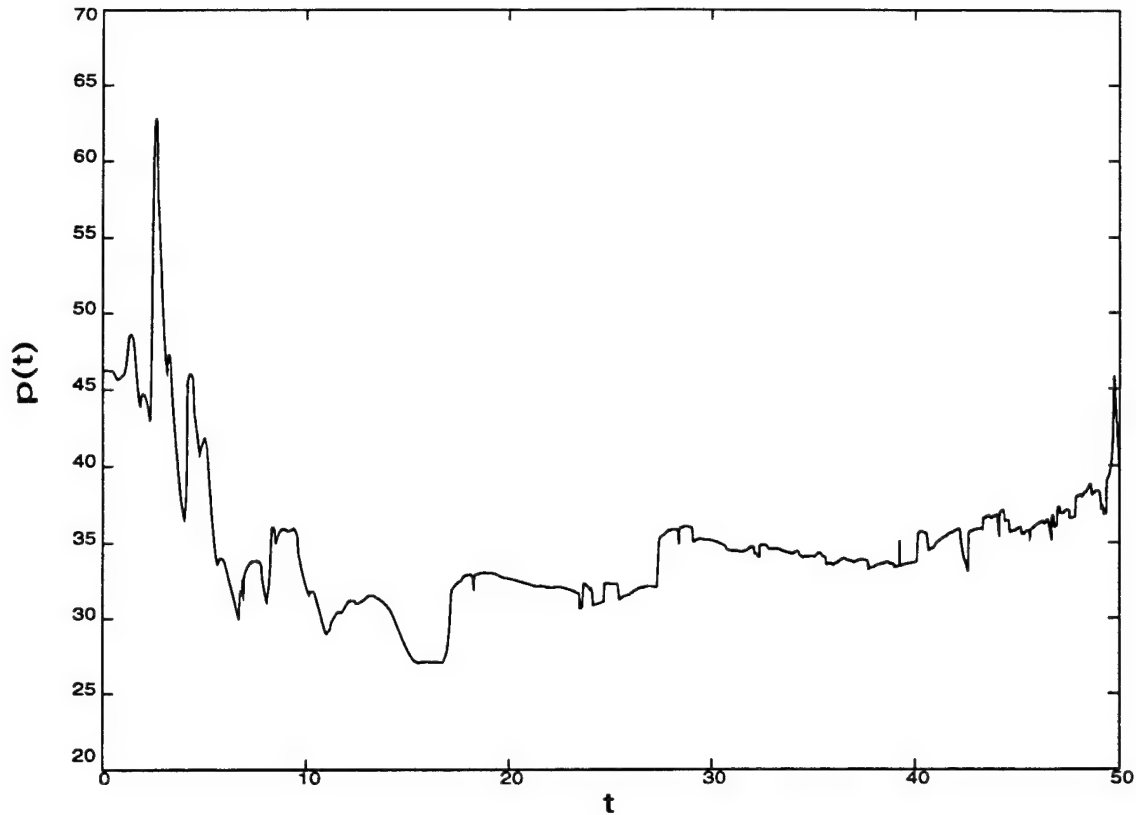
Fig. III.5. Temporal profile of dimensionless shock pressure for an overdriven ZND detonation (over-
drive factor 1.1). Note large range of temporal scales present in the solution.

to the chemical reactions (*cf.* footnote and related discussion above). Consequently, the necessary
resolution often exceeds available computational resources. The results of a stability analysis by Lee
& Stewart (1990) suggest that in one-dimensional detonations near the C-J point, we should expect
multi-mode instabilities, *i.e.*, multiple temporal scales, in contrast to the single mode behavior
exhibited in Fig. III.4. Our simulations reveal multi-mode, quasi-chaotic behavior, characterized
by the creation of pockets of reaction behind the leading shock front, accompanied by the formation
of secondary shock wave-systems with very large (local) heat release. An example of such behavior
is presented in Fig. III.5 as the temporal history of the shock pressure for a ZND detonation with
an overdrive factor of 1.1. For this case, a mesh resolution of 200 cells per reaction length was
required in order to overcome the stiffness difficulties.

We should note here that the problem of stiffness is real and not circumvented by the time-
explicit algorithms presently available, including the new one. This part of the problem must also
be addressed by the new algorithm by relying on adequate time/space resolution (with a coupling
through the CFL condition). The improvement here, however, is realized by the much higher
fidelity with which the system evolution can be tracked, through the use of (the proper) Riemann
invariants in each case. This feature of the new algorithm, at least, can address the sensitivity of
the chaotic-system behavior on the phase-space path.

Spatial profiles of pressure and density, at a dimensionless time of $t = 10$, are shown in Fig. III.6
and Fig. III.7, respectively. These data indicate the presence of secondary shock waves and asso-
ciated spatial non-uniformities, generated by combustion of previously-unreacted material, behind
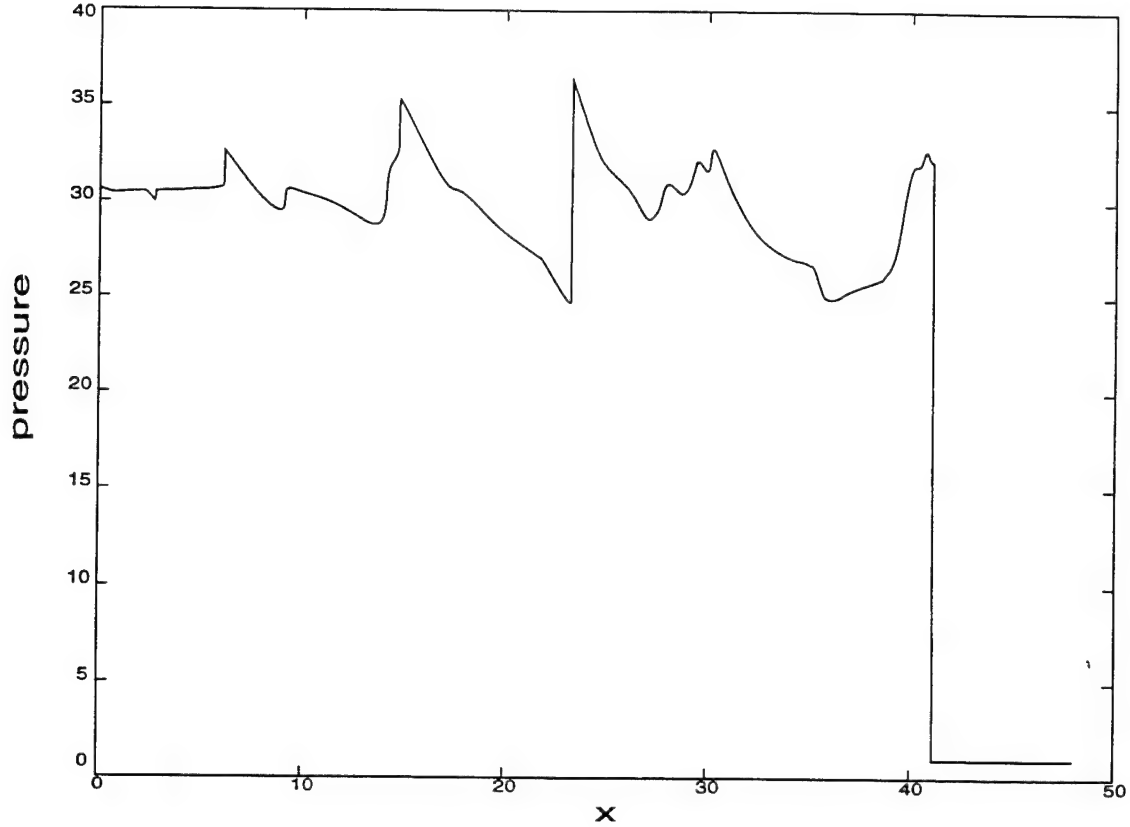
Fig. III.6. Spatial profile of dimensionless pressure, at a dimensionless time of $t = 10$, of an over-driven ZND detonation (overdrive factor 1.1).

the leading-wave region. Our results are in substantial variance and qualitative disagreement with the recently-published results by He & Lee (1995), who have attempted a simulation of this problem without regard to the considerations discussed above.

We are presently implementing the unsplit algorithm for multidimensional reacting flows, and expect numerical results in the near future.

This effort is part of the Ph.D. research of Miltos Papalexandris.

II.2.3   Image correlation velocimetry

Image Correlation Velocimetry (ICV) is a numerical method which estimates the velocity field of a flow from a sequence of images that are closely spaced in time. The method can analyze particle-image (PIV/DPIV) data, continuous-tone images of convected scalars, or any image sequence of a convected Lagrangian marker. See Tokumaru & Dimotakis (1993) for a more complete discussion and references. In the case of a pair of images, this is accomplished by iteratively minimizing the difference of a mapping of the first image and the second image. The minimization determines the mapping field, $\boldsymbol{\xi}(\mathbf{x})$, and is carried out in a least-squares sense (equation 3a).

$$\min_{q_0, q_1, \ldots, q_n} \int_A \{ E_0[\boldsymbol{\xi}(\mathbf{x})] - E_1[\mathbf{x}] \}^2 \, \mathrm{d}^2\mathbf{x} \; , \tag{3a}$$

where,

$$\boldsymbol{\xi} \; = \; \boldsymbol{\xi}\,[\,\mathbf{x}(t_0);\, q_0(t), q_1(t), \ldots, q_n(t)\,] \tag{3b}$$
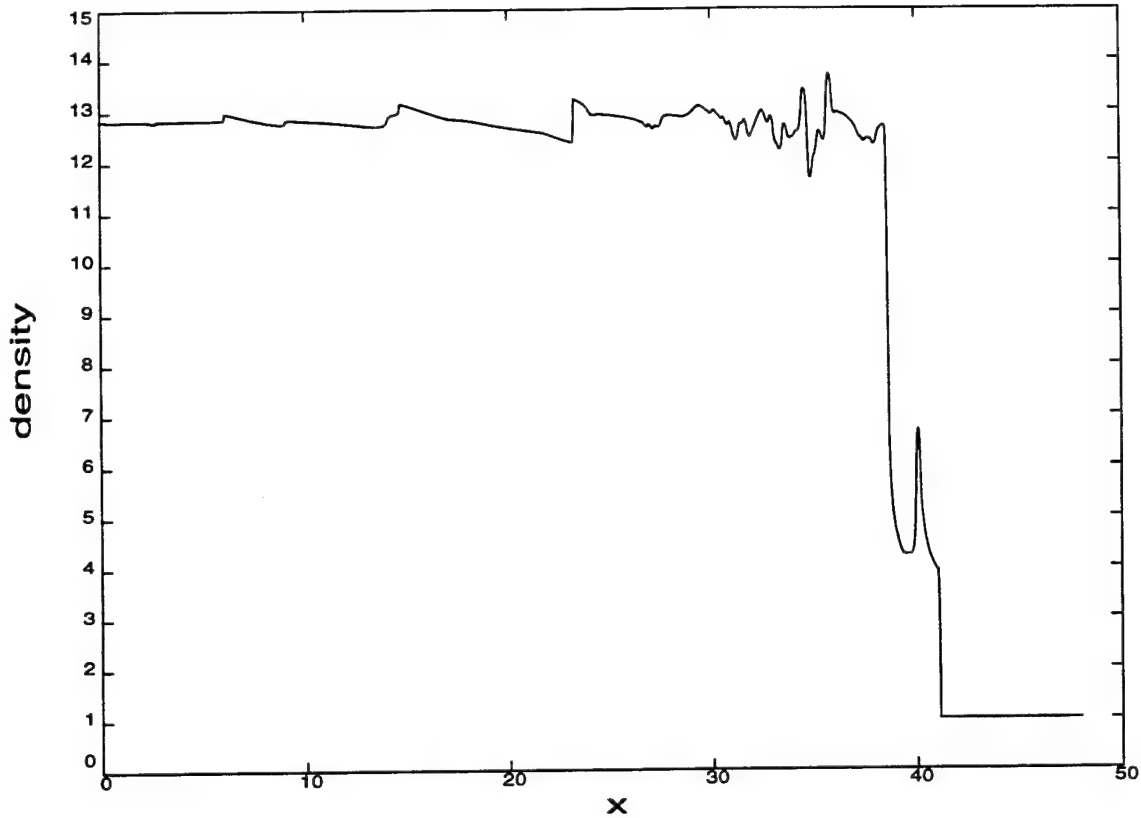
Fig. III.7. Spatial profile of dimensionless density, at a dimensionless time of $t = 10$, for an over-driven ZND detonation (overdrive factor 1.1).

A general mapping (displacement) field, $\boldsymbol{\xi}(\mathbf{x})$, is described parametrically (equation 3b), as will be illustrated below.

The velocity field is then derived as the time derivative of the displacement field, estimated, for a pair of images at $t = t_0, t_1$, in turn, as a first-order time difference, *i.e.*,

$$\mathbf{u}(\mathbf{x}) \simeq \frac{\boldsymbol{\xi}(\mathbf{x})}{t_1 - t_0} \;. \tag{4}$$

Higher-order estimates in time are possible if a sequence, rather than just a pair, of images is available.

The details of the velocity field representation have a significant impact on the accuracy of the results as well as the computational efficiency. The current effort has developed a spline representation of the velocity field, along with a new initialization scheme to increase computational efficiency and robustness of the method. These new methods have been used to successfully recover the velocity field of a simulated Oseen vortex from a pair of scalar images. A first use of this method is also in progress in a set of experiments that measure the velocity and vorticity fields generated by an impulsively-started NACA-0012 airfoil, at a high angle of attack, to provide feasibility tests of the new method. The latter effort will be described in subsequent reports and publications.

The first version of the ICV methodology represented the displacement (velocity) field by local Taylor expansions (Tokumaru and Dimotakis 1993). These were defined on a mosaic-like grid over the image. This representation was convenient in that only local regions of the two images were

considered when minimizing the parameters of the local displacement expansions. The resulting velocity field, however, was not continuous at the intersections of adjoining Taylor-expansion regions. An added term to minimize discontinuities in the displacement field and its lower derivatives was included in the overall cost function and was part of the global minimization.

The motivation for using splines in the current effort is to enforce continuity of the velocity field rigorously and by construction, to the desired order, so that computational effort is not expended on a degree of freedom that will be removed for other reasons. Spline choices include piecewise-interpolating polynomials. These are polynomials whose coefficients are defined over a given portion of the spline curve. The resulting curve (or surface) interpolates the data which define them. Another feature of these splines is that they are "global." Information from the entire domain is necessary to evaluate any local region. As with splines in general, they are constructed to have a specified degree of smoothness. For the natural cubic spline, up to second order derivatives are continuous, $i.e.$, they are C^2 functions. Boundary conditions must be imposed to evaluate these splines. In the case of the natural cubic spline, the procedure is closed by setting the second derivatives to zero at the boundaries.

While piecewise-interpolating polynomials have proven useful in many applications, they have serious shortcomings for use in ICV. The minimization scheme of ICV relies on repeated evaluations of the difference between the mapped first image and the second image, as the mapping (displacement/velocity) field parameters are varied. With global splines, information from the entire domain is required to evaluate even a small region. The many matrix inversions necessary to solve for the coefficients of the spline result in a substantial computational burden. Furthermore, splines which interpolate, $i.e.$, go through the actual data (control) points, are generally prone to large undulations between the data. This can in turn, lead to instabilities in the ICV algorithm.

These two problems are addressed in the current ICV implementation through the use of B-splines ($cf.$ Bartels $et\ al.$ 1987). These splines only approximate the data which define them. The relaxation of the requirement of strict interpolation eliminates the "overshoot/undershoot" tendencies of the piecewise interpolating natural bicubic splines discussed above. Furthermore, B-splines are "local," $i.e.$, only a small neighborhood of surrounding data is necessary to evaluate a local region. This feature results in substantial computational savings, especially when considering surfaces defined in terms of many points.

An important question that arises is what order spline is required to represent an actual velocity field. Consider the Navier-Stokes momentum and vorticity equations, $i.e.$,

$$
\begin{aligned}
\frac{\partial \mathbf{u}}{\partial t} + \mathbf{u} \cdot \frac{\partial \mathbf{u}}{\partial \mathbf{x}} &= -\frac{1}{\rho}\frac{\partial p}{\partial \mathbf{x}} + \nu\,\nabla^2 \mathbf{u} \\
\frac{\partial \boldsymbol{\omega}}{\partial t} + \mathbf{u} \cdot \frac{\partial \boldsymbol{\omega}}{\partial \mathbf{x}} &= -\left(\boldsymbol{\omega}\cdot\frac{\partial}{\partial \mathbf{x}}\right)\mathbf{u} + \nu\nabla^2\boldsymbol{\omega}\ ,
\end{aligned}
\tag{5}
$$

for incompressible flow. As can be seen from the vorticity equation, which imposes the stricter continuity requirements of the two, the vorticity field, $\boldsymbol{\omega}(\mathbf{x})$, must be $at\ least$ $C^2(\mathbf{x})$-continuous. In fact, a $C^2(\mathbf{x})$ ω-field would quickly acquire continuous, higher-order, spatial derivatives. To limit the continuity constraints to a manageable order we have elected to represent (incompressible) $\mathbf{u}$-fields as $C^4(\mathbf{x})$, resulting in vorticity fields that are $C^3(\mathbf{x})$. This provides a two-order continuity margin with respect to the momentum equation and one-order continuity margin with respect to the vorticity equation.

What follows is a brief description of univariate B-splines, *i.e.*, for curves that are functions of one independent variable. The univariate case is easily generalized into the bivariate case, as used in ICV, *i.e.*, surfaces that are functions of two independent variables, say, of x and y, as appropriate for two-dimensional fields. For a more complete description of B-splines, see (Bartels *et al.* 1987)
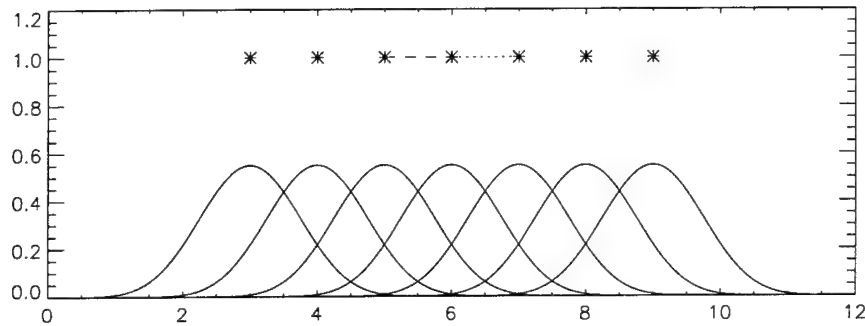

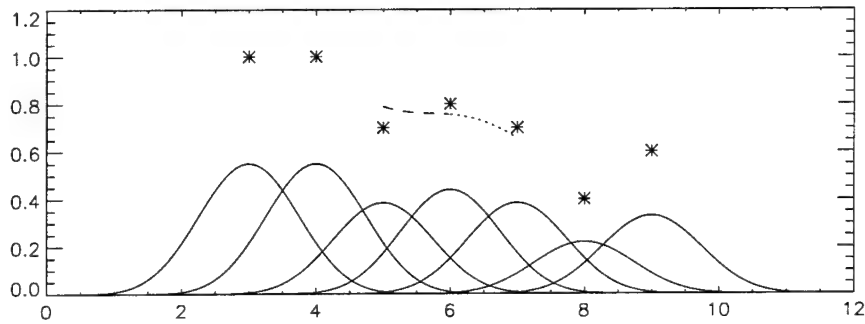Fig. III.8. Equally-weighted basis functions of the quintic B-spline.

Fig. III.9. Simple curve generated with quintic B-splines.

In the most general sense, a B-spline can be thought of as a summation of basis functions over a given region. Figures III.8 and equationIII.9 show the basis functions for the quintic-order spline as the bell-curve-shaped solid lines at the bottom. Basis functions are identically zero everywhere (compact support), except for the local region centered around their corresponding data (control) point. As illustrated in Fig. III.9, the basis functions are weighted by their corresponding data then summed over a region. The result of the summation is the desired spline curve, shown as the broken lines approximating the control points above the basis functions.

One should also note that the smoothness of the resulting curve is independent of the irregularity of the data. Furthermore, the curve will always lie in a region bounded by the data points. The ability of B-splines to produce smooth curves is a direct consequence of how the basis functions are constructed. While there are many ways to derive the B-spline basis functions, the following

recursion formula is a concise mathematical definition, for functions centered at the origin.

$$B^0(x) = \begin{cases} 1, & \text{for } -1/2 \le x \le 1/2 \text{ ,} \\ 0, & \text{otherwise;} \end{cases}$$

$$B^n(x) = B^0 * B^{n-1} \text{ ,} \tag{6}$$

where $B^n(x)$ is the nth-order basis function and "*" denotes convolution. The 1st-order function is found recursively by convolving the 0th-order function with itself. The 2nd-order is found by convolving the 0th-order with the 1st-order, *etc.* This produces basis functions that are centered at $x = 0$, which may be translated in x to position them as necessary. The spline curve, $S(x)$, is then given by,

$$S(x) = \sum_{i=0}^{k} q_i B_i^n(x) \text{ ,} \tag{7}$$

where the q_i are the weights of the ith control points and define the curve, parametrically, for a given set of basis functions.

In Figs. III.8 and III.9, the curve is only shown for the inner regions of the control points, *i.e.*, between 5 and 7 on the independent-variable axis. Quintic splines require the support of six basis functions to be completely defined. Various schemes exist to accommodate the limited support at the boundaries, which will not be covered here. One such scheme has been used in the current ICV method, allowing the surface to extend to the boundary data and/or accommodate appropriate boundary conditions, in each case.
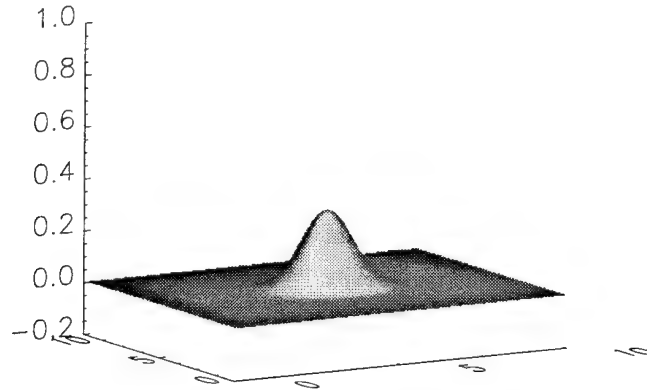
Fig. III.10. Single basis function of biquintic B-spline.

Generalization to two-dimensions can be realized using biquintic B-splines. The biquintic basis function in Fig. III.10 was defined by the tensor product of one-dimensional quintic basis (equation 6). Some lower-order tensor-product-defined bivariate B-spline bases are given in equation 8. The $B^{0,0}$ basis is the two-dimensional top-hat function and interpolation using B-splines of this order results in a "nearest neighbor" approximation.

$$B^{0,0}(x,y) = \begin{cases} 1, & \text{for } -1/2 \le x, y \le 1/2 \text{ ;} \\ 0, & \text{otherwise.} \end{cases} \tag{8a}$$

Bilinear B-splines interpolate four data points in a bilinear-sense. The equation for the basis function is given explicitly as follows,

$$B^{1,1}(x,y) = \begin{cases} (1+x)(1+y) & \text{for } -1 < x,y < 0, \\ (1-x)(1+y) & \text{for } 0 \le x < 1,\ -1 < y < 0, \\ (1-x)(1-y) & \text{for } 0 \le x,y < 1, \\ (1+x)(1-y) & \text{for } -1 < x < 0,\ 0 \le y < 1, \\ 0 & \text{otherwise.} \end{cases} \tag{8b}$$

Fig. III.11. Laser-induced fluorescence, 512 × 512-image data used for Oseen vortex test case. Data digitized at 11 bits/pixel.

The new ICV algorithm has been tested on a the model flow field of an Oseen vortex, which is an analytical solution for the temporal decay of a vortex filament. The analytical velocity field was used to map the image in Fig. III.11 into a simulated scalar image that would occur at a later time if the first-image scalar field was convected by the corresponding, two-dimensional field. The 512 × 512 test image in Fig. III.11 was formed using a fluorescent dye and a laser sheet in water, digitized at 11 bits/pixel. These two images were then used as the input to the ICV algorithm. The Oseen vortex, defined in equation 9, was centered in the image,

$$\begin{aligned} U_\theta(r,t) &= \frac{C}{2\pi r}\left[1 - e^{-r^2/4\nu t}\right] \\ U_r(r,t) &= 0\ , \end{aligned} \tag{9}$$

with the parameters C and νt chosen to produce an interesting velocity distribution. Figures III.12 and III.13 are surface plots of the vertical component of velocity, $v(x,y)$, and vorticity, $\omega(x,y)$, respectively.

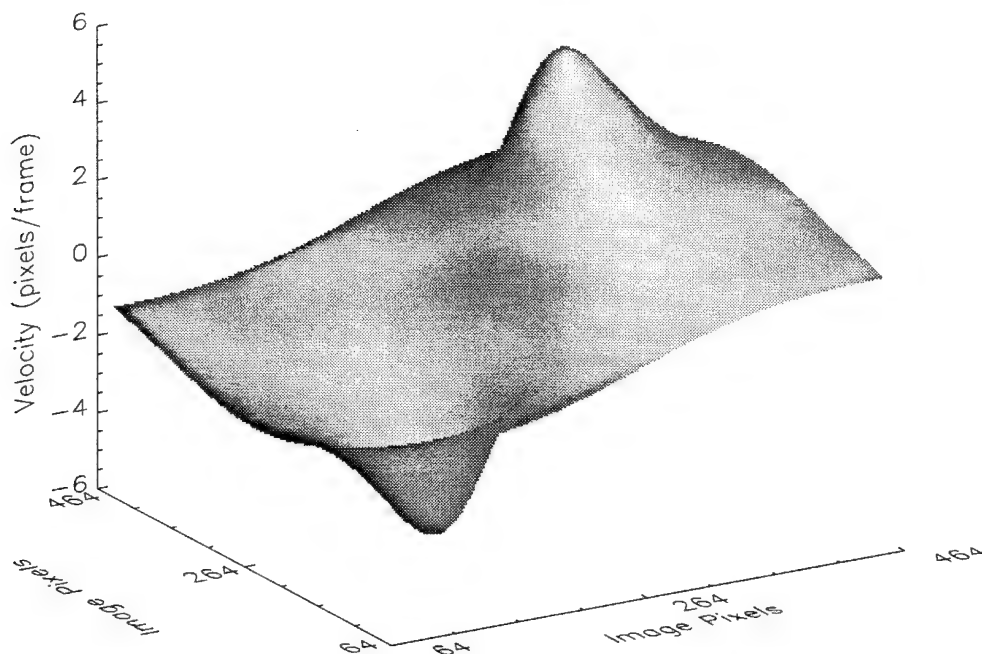
Fig. III.12. Surface plot of $v(x,y)$ for Oseen vortex used to map test image.

The ICV algorithm iteratively minimizes the difference between the mapped first image and the second image (equation 3a). A new initialization routine, based on Fourier cross-correlation methods, similar to DPIV techniques (*e.g.*, Willert and Gharib 1991), was developed to generate a first estimate of the velocity field, which is then used as the input to the main minimization routine. For DPIV (particle) images, cross-correlation region window sizes are of the order of 32×32 pixels. For the purpose of correlating images of scalars, window sizes on the order of 64×64, to 128×128, were required for a reliable initial estimation.

The new initialization routine goes a step beyond standard DPIV methods in that it generates a smooth displacement field by construction and is an iterative scheme. The velocity field from the initial Fourier cross correlation is represented using biquintic B-splines and then used to produce a mapping of the first image. One can iterate for a more accurate solution by performing the cross correlation again. In this iteration, the mapping of the first image is correlated with the second image. This second cross-correlation iteration is able to solve for translational errors in the initial mapping. In this manner, one arrives at a correction that is added to the previous mapping.

The initial estimation of the velocity field is then passed to the main ICV routine. The scheme is described in detail by Tokumaru and Dimotakis (1993), except that, in the present implementation, B-splines are used instead of local Taylor-expansions. Modifications in the implementation of the

– 48–
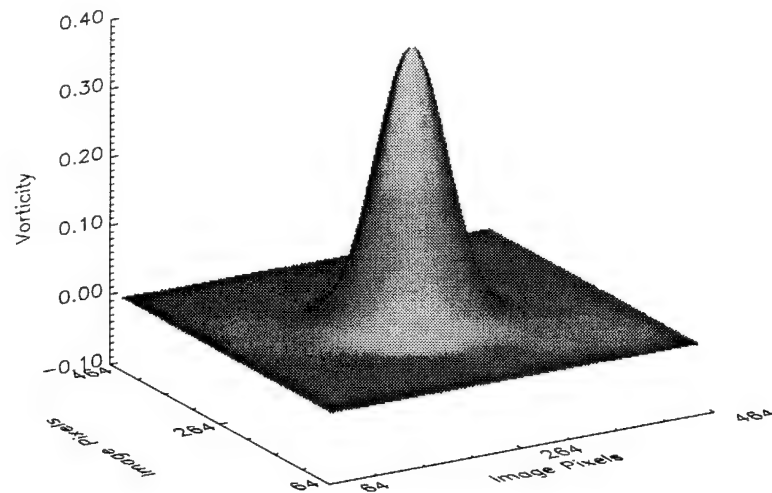
Fig. III.13. Surface plot of vorticity, $\omega(x,y)$ for Oseen vortex used to map test image.
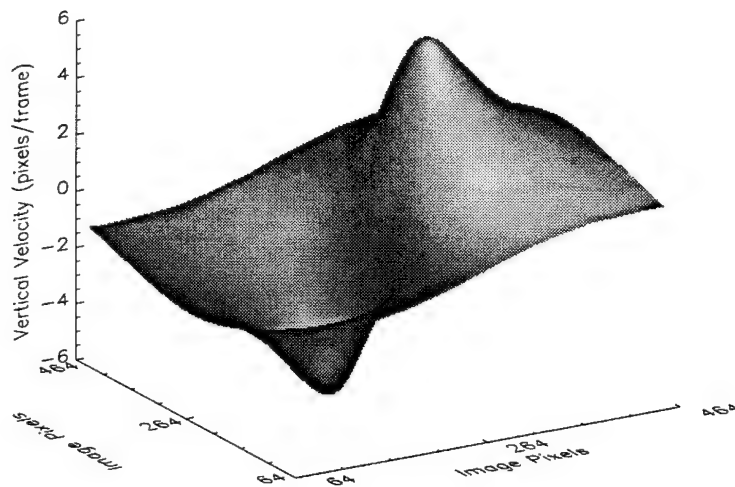
Fig. III.14. Surface plot of the vertical component of velocity, $v(x,y)$, deduced from ICV solution for the simulated Oseen vortex.

original algorithm have been performed to take advantage of the B-spline velocity-field representation. In particular, for a given region of the two images to be correlated, the minimization routine is not completely local in that it is allowed to vary the neighboring control points of the B-spline representation of the velocity field to achieve the best mapping. Results of the ICV minimization are shown in Fig. III.14 and Fig. III.15.
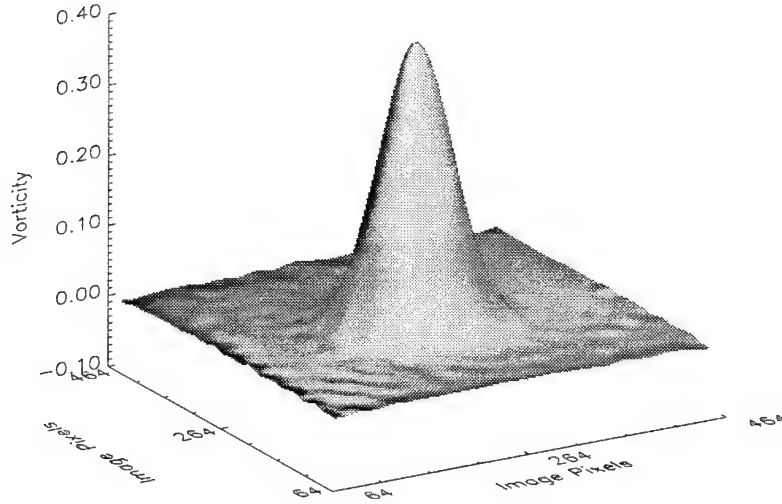
Fig. III.15. Surface plot of vorticity, $\omega(x, y)$, deduced from ICV solution for the simulated Oseen vortex.

The error surface for the experimentally-determined $v_{\exp}(x, y)$-velocity field, *i.e.*,

$$\epsilon_v(x, y) \equiv \frac{v_{\exp}(x, y) - v_{\mathrm{th}}(x, y)}{\max\{|v(x, y)|\}} \ . \tag{10}$$

is plotted in Fig. III.16, expressed as a percent of the maximum v-velocity in the field, *i.e.*, $z = 100 \, \epsilon_v(x, y)$. The error in the deduced v-velocity is 0.4% (rms) over the whole field and everywhere less than 1.2%.
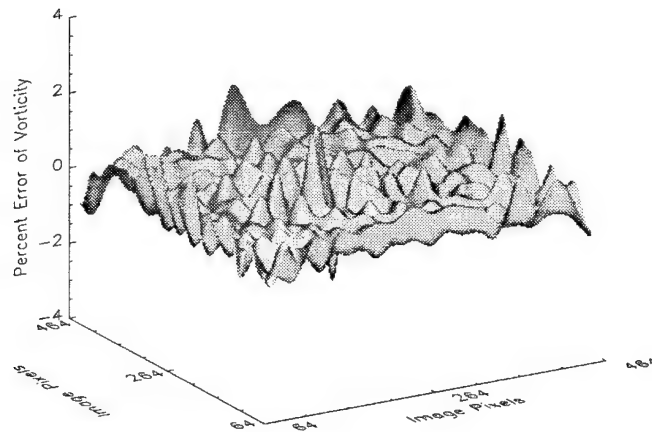
Fig. III.17. Surface plot of percent error in ICV solution for the vorticity, $\omega(x, y)$, of the simulated Oseen vortex (*cf.* equation 11 and related discussion).
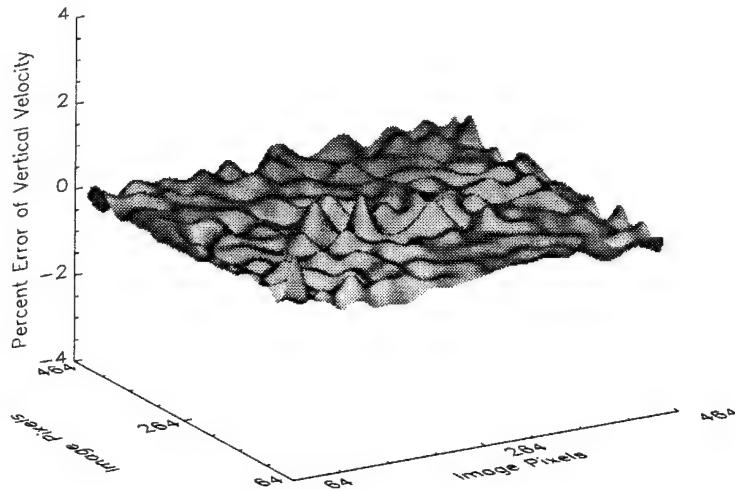
Fig. III.16. Surface plot of percent error in ICV solution for the vertical velocity, $v(x,y)$, of the simulated Oseen vortex (*cf.* equation 10 and related discussion).

The error surface for the experimentally-determined vorticity field, $\omega_{\exp}(x,y)$, *i.e.*,

$$\epsilon_\omega(x,y) \equiv \frac{\omega_{\exp}(x,y) - \omega_{\mathrm{th}}(x,y)}{\max\{\,|\omega(x,y)|\,\}} \ . \tag{11}$$

is similarly plotted in Fig. III.17, as a percent of the peak vorticity in the flow field, *i.e.*, $z = 100\,\epsilon_\omega(x,y)$. The error in the deduced vorticity over the whole field is 0.8% (rms) and everywhere less than 2.1%, for this test case, with much of it, as can be seen, traceable to the boundaries of the ICV flow domain.

In work in progress, we are processing the data from the experiment investigating the flow over the impulsively-started airfoil. This part of the effort will require further development of the B-spline flow-field surface description and the ICV method to allow more complex geometries as well as flow/body boundary conditions to be accommodated.

The important extension of this work to compressible flow fields that are not necessarily smooth, *e.g.*, flows with shocks, is also part of the overall effort. Envisaged algorithms will attempt to fit shocks first and then solve for piecewise-smooth velocity-field regions, as described above.

This effort is part of the Ph.D. research of Galen Gornowicz.

– 51–

References

Bartels, R.H., Beatty, J.C., and Barsky B.A. 1987 *An Introduction to Splines for Use in Computer Graphics and Geometric Modeling* (Morgan Kaufmann, Los Altos, CA).

Bourlioux, A., Majda, A., and Roytburd, V. 1991 "Nonlinear Development of Low Frequency One-Dimensional Instabilities for Reacting Shock Waves," *SIAM J. Appl. Math.* **51**, 303–343.

Candler, G. V., Dimotakis, P. E., Hornung, H. G., Leonard, A., Meiron, D. I., McKoy, B. V., Pullin, D. I., and Sturtevant, B. 1994 "Interaction of Chemistry, Turbulence, and Shock Waves in Hypervelocity Flow," AFOSR Annual Technical Report F49620–93–1–0338 (GALCIT Report FM 94–2).

Fickett, W., and Wood, W. 1966 "Flow calculation for pulsating one-dimensional detonation," *Phys. Fluids* **9**, 903–916.

Hall, J. L. 1991 *An Experimental Investigation of Structure, Mixing and Combustion in Compressible Turbulent Shear Layers*, Ph. D. thesis, California Institute of Technology.

Hall, J. L., Dimotakis, P. E., and Rosemann, H. 1993 "Experiments in non-reacting compressible shear layers," *AIAA J.* **31**(12), 2247–2254.

He, L., and Lee, J. H. S. 1995 "The dynamical limit of one-dimensional detonations," *Phys. Fluids* **7**(5), 1151–1158.

Lappas, T. 1993 *An Adaptive Lagrangian Method for Computing 1-D Reacting Flows and the Theory of Riemann Invariant manifolds for the Compressible Euler Equations*, Ph. D. thesis, California Institute of Technology.

Lappas, T., Leonard, A., and Dimotakis, P. E. 1994 "Riemann Invariant Manifolds for the Multidimensional Euler Equations. Part I: Theoretical Development. Part II: A Multidimensional Godunov Scheme," GALCIT FM94–6 report.

Lee, H.I., and Stewart, D.S. 1990 "Calculation of linear detonation instability: one-dimensional instability of plane detonation," *J. Fluid Mech.* **216**, 103–132.

Liepmann, H. W., and Roshko, A. 1957 *Elements of Gasdynamics* (John Wiley, New York).

Lowson, M. V., and Ollerhead, J. B. 1968 "Visualization of noise from cold supersonic jets," *J. Acoust. Soc. Am.* **44**, 624.

Martens, S., Kinzie, K. W., and McLaughlin, D. K. 1994 "Measurements of Kelvin-Helmholtz instabilities in a supersonic shear layer," *AIAA J.* **32**(8), 1633–1639.

Oertel, H. 1979 "Mach wave radiation of hot supersonic jets investigated by means of the shock tube and new optical techniques," 12th *Int. Symp. on Shock Tubes and Waves*, Jerusalem, 16–19 July 1979 (A. Lifshitz, J. Rom, eds., Magnes Press, Jerusalem), 266–275.

Papamoschou, D. 1989 "Structure of the compressible turbulent shear layer," *AIAA* 27th *Aerospace Sciences Meeting*, 9–12 January 1989 (Reno, Nevada), Paper 89–0126.

Shau, Y. R., Dolling, D. S., and Choi, K. Y. 1993 "Organized structure in a compressible turbulent shear layer," *AIAA J.* **31**(8), 1398–1405.

Tam, C. K. W. 1971 "Directional acoustic radiation from a supersonic jet," *J. Fluid Mech.* **46**, 757–768.

Tokumaru, P. T., and Dimotakis, P. E. 1993 "Image Correlation Velocimetry," GALCIT Report FM92–1a (accepted for publication in *Exp. in Fluids*).

Willert, C.E., and Gharib, M. 1991 "Digital particle image velocimetry," *Exp. in Fluids* **10**, 181–193.

Personnel associated with the research

C. L. Bond: Graduate Research Assistant, Aeronautics;

E. E. Dahl: Member of the Technical Staff, Aeronautics;

P. E. Dimotakis: John K. Northrop Professor of Aeronautics and Professor of Applied Physics;

D. C. Fourguette: Senior Research Fellow, Aeronautics;

G. G. Gornowicz: Graduate Research Assistant, Aeronautics;

D. B. Lang: Staff Engineer, Aeronautics;

A. Leonard: Professor, Aeronautics;

J. D. Melvin: Member of the Technical Staff, Div. of Engineering & Applied Science;

M. V. Papalexandris: Graduate Research Assistant, Aeronautics;

J. J. Quirk: Senior Research Fellow, Aeronautics;

M. D. Slessor: Graduate Research Assistant, Aeronautics;

P. Svitek: Staff Engineer, Aeronautics;

Degrees earned during reporting period

Galen G. Gornowicz, Master of Science in Aeronautics, June 1994.

Publications resulting from the research

Louis, H., Demiris, A., Budil, K. S., Miller, P. L., Peyser, T. A., Stry, P. E., Wojtowicz, D. A., and Dimotakis, P. E. 1995 "Miniature targets for hydrodynamic instability experiments on Nova," *Fusion Technology* (submitted).[‡]

Papalexandris, M. V., Leonard, A., and Dimotakis, P. E. 1995 "An unsplit scheme for 1-D unsteady chemically-reacting flows," *SIAM Annual Meeting* (Charlotte, NC), 23–26 October 1995 (submitted).

Slessor, M. D., Dimotakis, P. E. 1994 "Experiments on bi-supersonic turbulent shear layers," *Bull. Am. Phys. Soc.* **39**(9), 1880.

Tokumaru, P. T., Dimotakis, P. E. 1995 "Image Correlation Velocimetry," *Exp. in Fluids* (accepted for publication).

[‡] Collaborative effort with Lawrence Livermore National Laboratory.

Interactions and collaborations

A collaborative CCD-imaging technology development effort by P. E. Dimotakis and D. B. Lang, with J. R. Janesick and S. A. Collins of the Jet Propulsion Laboratory, to fabricate a two-image recording device (dubbed, the "Mach-II-CCD"). First fabrication lot presently in bench-testing phase.[♯]

Participation by P. E. Dimotakis of a workshop on laser fusion and high-energy laser applications, hosted by the Lawrence Livermore National Laboratory (LLNL), March 1995, Berkeley, CA.

An experimental and theoretical collaborative effort by P. E. Dimotakis, with LLNL personnel, on gasdynamics of high Mach-number shockwaves and mixing. Two week-long experiments using the Nova laser facility at LLNL in July 1995. Two visits at Caltech for discussions by LLNL personnel during reporting period.

CHAPTER IV

CHEMISTRY IN NONUNIFORM FLOW

IV.1 DISSOCIATION RATES WITH VIBRATIONAL NONEQUILIBRIUM

Objectives and Status of Research

One of the primary uncertainties in the modeling of hypersonic reacting flows is how the vibrational state of a molecule affects its dissociation rate. Therefore, the main objective of this research is to test chemical reaction rate models in the presence vibrational nonequilibrium. Our initial work showed that the flow of nitrogen over spheres at typical T5 conditions is not very sensitive to the choice of several popular vibration-dissociation coupling models. During the last year, we have been using computational fluid dynamics to design a new experiment that shows strong sensitivity to the coupling model. We have found several geometries and flow conditions that are good candidates; they will be tested in T5 during the summer. This experiment will provide the first data that can be used for the direct validation of vibration-dissociation coupling models, and it will provide new insight into how the vibrational state affects the dissociation rate.

The new experimental configuration is a double-wedge or double-cone geometry; the first cone or wedge causes an attached shock wave to form, and interact with the detached shock from the second wedge or cone. This creates a complicated flow field that is very sensitive to the vibration-dissociation coupling model. For example, Fig. IV.1 plots the pressure contours in the flow field of a double-cone geometry at typical T5 conditions. The shock wave-boundary layer interaction produces a region of separated flow at the intersection of the cones. Also, the shock-shock interaction produces a dramatic pressure rise, followed by an oscillating pressure distribution on the surface of the second cone. The only difference between these two calculations is the vibration-dissociation coupling model. The Park coupling model produces a flow field with a much smaller separation zone than the CVDV model. The difference in the separation zone causes a large change in the surface pressure distribution, as seen in Fig. IV.2. There is a similar change in the convective heating rate distribution. The experimental models will be instrumented with pressure and heat transfer gauges, and Mach-Zehnder interferograms will be made.

During the design of the double-wedge/cone experiments, we discovered some interesting flow features and what appears to be a new shock-shock interaction. For example, the Mach 6.9 flow of a perfect gas over a 15°-58° double-wedge creates a shock-shock interaction that is similar to, but different than, a Type IV interaction (Compare with the shock-shock interaction of section II.2). As seen in Fig. IV.3, the shock that is transmitted from the triple point undergoes a regular reflection from the first wedge surface, creating a supersonic flow along the surface of the body. This flow is similar to an underexpanded jet, making it undergo alternating expansions and recompressions.

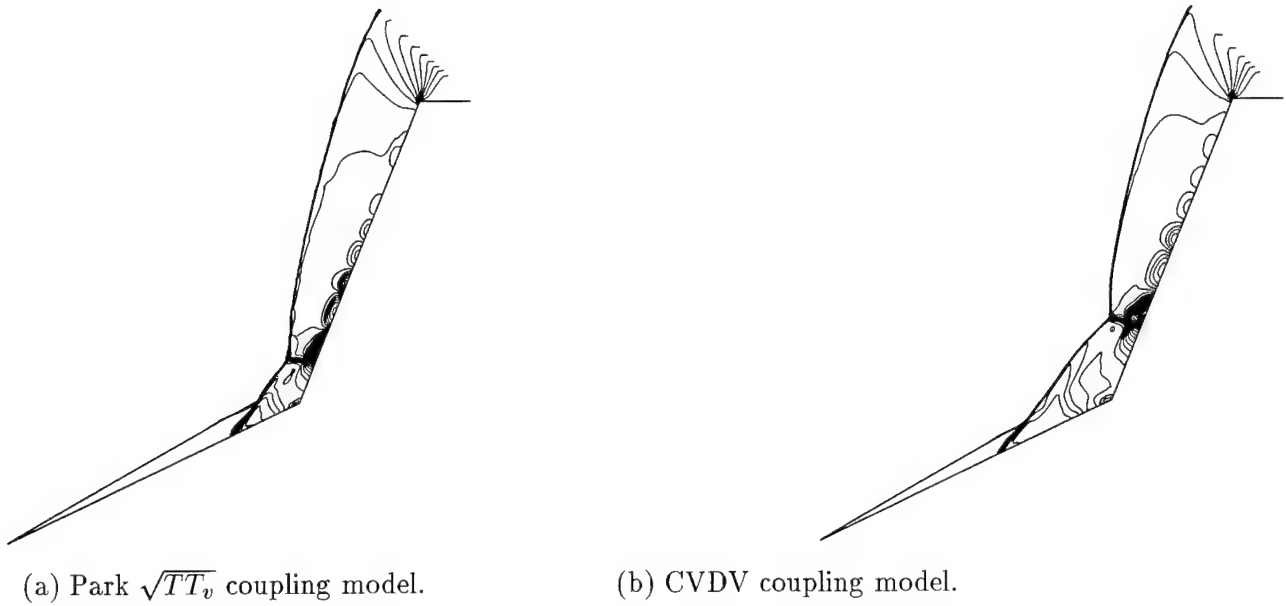(a) Park $\sqrt{TT_v}$ coupling model.   (b) CVDV coupling model.

Figure IV.1. Pressure contours for double-cone geometry at typical re-entry conditions ($\rho_\infty = 0.01\,\mathrm{kg/m^3}$, $T_\infty = 2260\,\mathrm{K}$, $u_\infty = 6690\,\mathrm{m/s}$, base height is 2 inches (5.08 cm)).
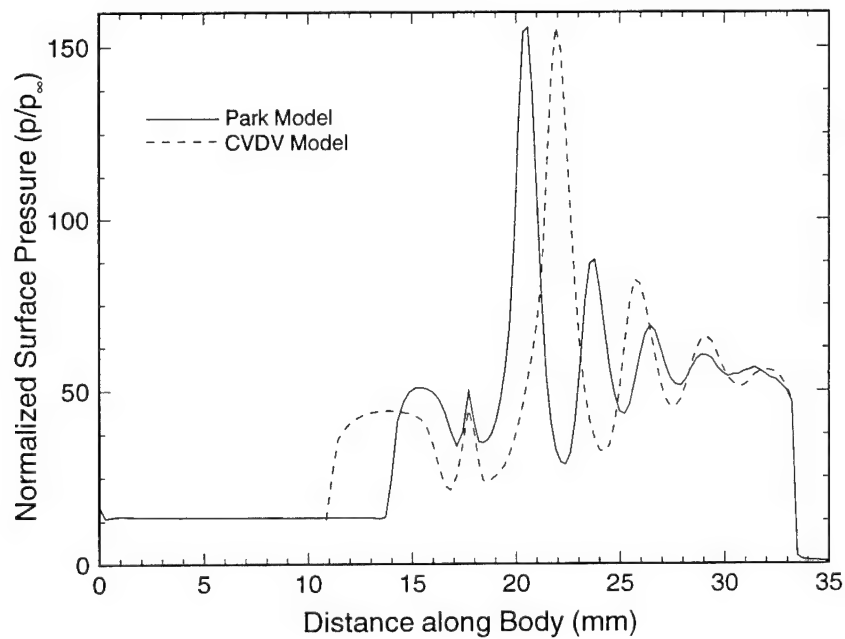

Figure IV.2. Surface pressure distribution on double-cone geometry shown in Fig. IV.1.

Figure IV.3. Mach number and pressure contours of the new shock interaction. The flow is inviscid with $M_\infty = 6.9$ and $\gamma = 1.4$; computation performed on a 512×512 grid.

Personnel Associated with Research

Graham V. Candler, Associate Professor of Aerospace Engineering and Mechanics, University of Minnesota.

Joseph Olejniczak, Graduate Research Assistant, Department of Aerospace Engineering and Mechanics, University of Minnesota.

Publications Resulting from Research

J. Olejniczak, "Experimental Evaluation of Vibration-Dissociation Coupling Models," M.S. in Aerospace Engineering, University of Minnesota, May 1994.

Olejniczak, J., G.V. Candler, H.G. Hornung, and C. Wen, "Experimental Evaluation of Vibration-Dissociation Coupling Models," *AIAA Paper No. 94-1983,* June 1994, also University of Minnesota Supercomputer Institute Research Report 94/127R.

Olejniczak, J., and G.V. Candler, "Vibrational Energy Conservation with Vibration-Dissociation Coupling: General Theory and Numerical Studies," forthcoming in *Physics of Fluids,* July 1995. Also University of Minnesota Supercomputer Institute Research Report 94/210, Nov. 1994.

Olejniczak J., and G.V. Candler, "A Study of Experiments Sensitive to Vibration-Dissociation Coupling Models," *20th International Symposium on Shock Waves,* July 1995.

Olejniczak, J., G.V. Candler, and M.J. Wright, "Numerical Study of Shock Interactions on Double-Wedge Geometries," extended abstract submitted for presentation at the 34th AIAA Aerospace Sciences Meeting, Jan. 1996.

Interactions

Presentation of a paper at the 6th AIAA/ASME Joint Thermophysics and Heat Transfer Conference, Colorado Springs, CO, June 20-23, 1994.

Invited speaker at the Second European Symposium on Aerothermodynamics for Space Vehicles, held in ESTEC, Noordwijk, The Netherlands, Nov. 21-25 1994.

Invited lecturer at the Von Karman Institute for Fluid Dynamics short course on Hypersonic Aerothermodynamics, Rhode-St. Genèse, Belgium, April 24-28, 1995.

Invited lecturer at the NATO Advanced Study Institute on Molecular Physics and Hypersonic Flows, held in Maratea, Italy, May 22-June 2, 1994.

Presentation of a paper at the 20th International Symposium on Shock Waves, July 23-28, 1995.

IV.2 ELECTRON-DRIVEN REACTIONS IN HYPERSONIC FLOW

Background and Objective

Electrons resulting from ionization due to bow-shock heating play an important role in determining the physical and chemical properties of hypersonic flows.

Processes of interest include vibrational excitation, formation of negative ions (which may then fragment), and electron impact excitation and deexcitation of excited metastable states. Furthermore, with temperatures as high as 10,000 Kelvin due to non-equilibrium overshoots, electrons in the tail of the energy distribution function can lead to electronic excitation of ground state species, particularly those that are vibrationally excited. The available data base for these electron-molecule collision processes which can occur in flowfields is generally fragmentary, and, in many cases, inconsistent. Furthermore, cross sections for electronic excitation of molecules by electrons with barely enough energy to drive the excitation and for electron collisions with electronically excited molecules and with radicals such as OH are essentially *non-existent* and *experimentally inaccessible*. Finally, the experimental effort to measure electron-molecule collision cross sections is very limited and shrinking in the United States.

An obvious strategy for obtaining these electron collision cross sections is to calculate them. However, the significant computational demands of such calculations have made such an approach impractical to date with conventional (sequential) computers. *The objective of our work is to exploit the high-performance computing provided by parallel computers, consisting of arrays of commercially available microprocessors, to calculate the cross sections for electron-molecule collisions needed in modelling the chemical and physical properties of hypervelocity flows.* With appropriate computational strategies, the high aggregate speeds and large memory of these parallel computers make such an approach feasible.

Progress and Highlights

At the relatively low impact energies of interest in hypersonic flowfields, the accurate treatment of the electron-molecule collision process is a computationally challenging problem. In these studies we employ a multichannel extension of the variational principle for scattering amplitudes originally introduced by Schwinger.[1] This formulation, known as the Schwinger multichannel method,[2] was specifically designed to address low-energy electron-molecule collisions.

As in most variational approaches, there are two major computational tasks in these studies: (*i*) calculation of the primitive matrix elements of the operators arising in the variational expression for a given expansion basis, and (*ii*) transformation of these primitive matrix elements to generate the physical matrix elements of the linear equations defining the variational solution. In the Schwinger multichannel method, as in the original Schwinger method, the trial wave function need not satisfy scattering boundary conditions; *square-integrable functions such as Cartesian Gaussians may be employed.* In this basis all matrix elements in the variational expression can be evaluated analytically, except those involving the Green's function. These Green's function matrix elements have no known analytic form and must be done by quadrature. In fact, evaluation of these matrix elements becomes the computationally intensive step of our calculations. The occurrence of these difficult matrix elements in variational principles based on integral equations has discouraged their use to date, in spite of highly desirable features of these approaches such as the flexibility of em-

ploying trial functions which do not satisfy scattering boundary conditions and their very favorable convergence.

Though initially implemented on conventional (sequential) computers, the computationally intensive step of these calculations is ideally suited to computers of distributed-memory parallel architectures. Its most compute-intensive tasks are (i) the evaluation of a very large number (typically 10^{10} or more) of elementary integrals describing the interaction of pairs of electrons, a step requiring a code of about 2000 lines of Fortran, and (ii) the transformation of these elementary quantities into the matrix elements appearing in the variational expression. The evaluation of the two-electron integrals is readily parallelized: one simply has each processor independently calculate a different subset of the integrals. Step (ii), the transformation of the integrals, can be organized as a series of large distributed matrix multiplications between the global array of integrals and a distributed transformation matrix that is easy to construct.[3]

The overall performance of our program on the *Intel Paragon* (512 *i*860 processor) or *CRAY T3D* (256 DEC alphas) cannot be characterized by a single number. Although evaluating and subsequently combining the integrals are by far the dominant steps in the calculation, the relative importance of these two steps is strongly dependent on the specific calculation. Depending on the nature of the calculation at hand, then, and taking into account load balance, communication, I/O, and other overhead, we typically see throughout speeds in the range from 3 to 10 GFLOP. To put these numbers in perspective, our original sequential program, which is only partially vectorizable, averages about 30 MFLOP on a CRAY Y-MP processor. This increase of over two orders-of-magnitude in computational performance significantly enhances our ability to fill the large gaps in the electron collision data base needed for modelling reactive flows of interest.

We have exploited this computational procedure and parallel computer resources at the Institute and Wright-Patterson and Eglin Air Force Bases to carry out the following calculations:

• We have studied the cross sections for near-threshold excitation of the lowest lying excited state of OH ($A^2\Sigma^+$) by low-energy electrons. OH fragments are produced in flows of interest via dissociation of water vapor. No measured data is available for electron impact on the OH fragment.

• We have completed calculations of the cross sections for electron impact excitation of the A $^2\Sigma^+$ state of NO. This upper state is responsible for the γ-band emission which is prominent in the bow shock of flows over hardbodies. There have also been no measurements of these cross sections.

• We have completed extensive calculations of the cross sections for electron impact excitation of five excited electronic states of CO_2. There is again essentially no measured data for any of these cross sections.

References

1. J. Schwinger, Phys. Rev. **72**, 742 (1947)

2. K. Takatsuka and V. McKoy, Phys. Rev. A **30**, 1734 (1984); C. Winstead and V. McKoy, Phys. Rev. A **5**, 648 (1972)

3. C. Winstead, P.G. Hipes, M. A. P. Lima, and V. McKoy, J. Chem. Phys. **94**, 5455 (1991)

Publications

The following publications have resulted from the research outlined above:

1. Lee, C-H, Winstead, C., Pritchard, H.P., and McKoy, V. *Studies of Collisions of Low-Energy Electrons with CO_2*, Phys Rev. A (submitted).

2. Zobel, J., Mayer, U., Jung, K., Ehrhardt, H., and Pritchard, H., Winstead, C., and McKoy, V., *Absolute Cross Sections for Electron-Impact Excitation of CO Near-Threshold*, J. Phys. B. (submitted).

3. Winstead, C. and McKoy, V., *Studies of Electron-Molecule Collisions on Massively Parallel Computers*, Modern Electronic Structure Theory, Edited by D. Yarkony (World Scientific, 1995).

4. Winstead, C., Pritchard, H.P., and McKoy, V., *Electron-Molecule Collisions for Plasma Modelling Experiences on the CRAY T3D* CRAY CHANNELS (Cray Research, Inc., 1995).

5. Winstead, C., Pritchard, H.P., and McKoy, V., *Parallel Computations of Electron-Molecule Collisions*, Invited Article in Computational Science and Engineering, IEEE Computer Society (1995).

Personnel Associated with Research

Principal Investigator: Vincent McKoy, Professor of Theoretical Chemistry

One graduate student (C-H. Lee) and a Senior Research Fellow (C. Winstead, part-time) are involved in this effort.

Presentations

The research outlined above has been presented in the following talks:

- *Electron-Molecule Collisions for Modelling Plasmas*, Invited Talk at the Mardi Gras '94 Conference "Toward Teraflop Computing and New Grand Challenge Applications", Baton Rouge, 1994.

- *Electron-Molecule Collisions for Modelling Plasmas*, Invited Talk at the High-Performance Computing Symposium, 1994, Simulation MultiConference, La Jolla, 1994.

- *Studies of Electron-Molecule Collisions on Highly Parallel Computers*, Joint Chemical Physics-Mechanical Engineering Seminar, Ohio State University, May 1994.

- *Data for Modelling Materials-Processing Plasmas: The Impact of Parallel Computers*, Invited Talk at the Defense Science Study Group Symposium on Applications of Advanced and Innovative Computational Methods to Defense Science and Engineering, Institute for Defense Analyses, October 1994.

- *Data for Modelling Materials-Processing Plasmas: The Impact of Parallel Computers*, Invited Talk in the High-Performance Computing Seminar Series, National Institute for Standards and Technology, April 1995.

• *Studies of Electron-Molecule Collisions on Highly Parallel Computers*, Bucy Lecture, Texas Tech University, February 1995.

• *Studies of Electron-Molecule Collisions on Parallel Computers*, Invited Talk at the 1995 Annual Meeting of the Division of Atomic, Molecular and Optical Physics, American Physical Society, May 1995, Toronto, Canada.

IV.3 NONEQUILIBRIUM LEEWARD SHOCK-VORTEX AERODYNAMICS

Objectives and Status of Research

The objectives of this research are to study the hypervelocity flow at enthalpy sufficient to activate dissociation/recombination chemistry about cones and blunt-nosed delta-wings at large incidence, with particular reference to the effect of chemistry on the structure of the leeward flow shock/vortex system. Significant progress has been made in two relevant areas. These are

(1) A new kinetic scheme based on the equilibrium flux method (*EFM*) and modified using Osher intermediate states has been developed. This new scheme, called *EFMO*, is designed to retain the robustness of the original Boltzmann-type method in capturing intense shock waves and at the same time substantially reduce the numerical diffusivity of the original *EFM* method for resolution of boundary layers.

(2) A fully implicit version of the viscous three-dimensional (3D) flow code, *PGP3D* has been made developed with *EFMO* incorporated. The code has been tested extensively on viscous laminar cone flow at zero and at finite incidence.

(3) The Lighthill-Freeman ideal-dissociating gas chemistry model has been incorporated into both the explicit and implicit versions of *PGP3D* and is currently undergoing testing.

A comprehensive statement of accomplishments in the areas (1-3) above is outlined below. These statements constitute the current status of the research effort. They are followed by a brief statement of the expected progress within the next year.

IV.3.1 The EFMO Scheme

The *EFMO* scheme (*EFM* and Osher) is based on a formal similarity between the mathematical expressions of the *EFM* numerical flux and the Osher numerical flux. In Osher's method (Osher & Solomon 1982), the numerical flux is given by

$$F_O(U_L, U_R) = \frac{1}{2}\left(F_L + F_R - \int_{LN} |A|dw - \int_{NL} |A|dw\right), \qquad (1)$$

where LN refers to the linearly degenerated subpath which corresponds physically to a contact discontinuity, and NL refers to the genuinely nonlinear subpaths which correspond to either compression or rarefaction waves. The matrix $|A|$ is the absolute value of the Jacobian matrix of the exact flux F and is defined in the following sense:

$$|A| = R|\Lambda|R^{-1} \qquad |\Lambda| = \mathrm{Diag}(|\lambda_p|)_{p=1,\dots m}, \qquad (2)$$

where λ_p is an eigenvalue of A.

The *EFM* numerical flux (Pullin 1980) defined traditionally as

$$F_{EFM}(U_L, U_R) = F^+(U_L) + F^-(U_R), \qquad (3)$$

can be put under a form similar to Osher's numerical flux

$$F_{EFM}(U_L, U_R) = \frac{1}{2}\left(F_L + F_R - \int_{LN} |B|dw - \int_{NL} |B|dw\right), \qquad (4)$$

where $|B|$ is now defined as $|B| = B^+ - B^-$ where $B^\pm$ is the Jacobian matrix of the fluxes $F^\pm$.

The idea of *EFMO* is to observe that for the nonlinear paths (i.e. shock waves, in particular) *EFM* performs extremely well while it tends to artificially broad contact discontinuities owing to its large numerical diffusivity. On the other hand, Osher scheme is known to present some inconsistencies in the vicinity of sonic lines or of strong shocks while giving excellent resolution of contact discontinuities. The present idea is to retains that part of the integral corresponding to the nonlinear path (shock wave) in the *EFM* numerical flux while replacing the integral corresponding to the linear path (contact discontinuity) by the expression from Osher's numerical flux. The resulting numerical flux is then

$$F_{EFMO}(U_L, U_R) = \tfrac{1}{2}\left(F_L + F_R - \int_{LN} |A|dw - \int_{NL} |B|dw\right), \tag{5}$$

or equivalently

$$F_{EFMO}(U_L, U_R) = F_{EFM}(U_L, U_R) + \tfrac{1}{2}\int_{LN}(|B| - |A|)dw, \tag{6}$$

where the integral represents an anti-diffusive flux which almost vanishes in the vicinity of shocks and removes the excessive numerical dissipation near contact discontinuities. In practice, the previous relation can be further simplified by defining two intermediate states U_1 and U_2 defined by using Riemann invariants in the sense of Lax as implied in the original Osher's method.

These two intermediate states are then used to calculate the anti-diffusive flux so that eventually the *EFMO* numerical flux reads

$$F_{EFMO}(U_L, U_R) = F_{EFM}(U_L, U_R) + \begin{cases} -F^-(U_2) + F^-(U_1) & \text{if } v_n > 0 \\ F^+(U_2) - F^+(U_1) & \text{if } v_n < 0 \end{cases}, \tag{7}$$

where v_n is the common value of the normal velocity component for both intermediate states and $F^\pm$ are the regular *EFM* fluxes which appear in Eq. (3).

IV.3.2 PGP3D and Implicit EFMO

An implicit version of *PGP3D* incorporating *EFMO* (*PGP3D.2*) has been developed based on a linearization of the fluxes using an approximate analytical evaluation of the Jacobian in which only the regular *EFM* part of the numerical flux is retained. This technique provided a rate of convergence with *EFMO* comparable to that obtained with *EFM*, for which the Jacobian is exact. For three-dimensional flow this procedure results in a block hepta-diagonal system of linear equations which must be solved at each time-step, and this is done by factorization into tridiagonal systems which are solved by standard methods. The extension of *EFMO* to high order of accuracy is achieved using the usual MUSCL technique which consists of reconstructing the primitive variables on each side of a given interface where the flux is calculated.

The PG3D/*EFMO* code has been subject to extensive testing for a variety of supersonic and hypervelocity frozen flows. These include viscous flow over a flat plate at zero incidence at at various Mach numbers, the flow over a flat-plate ramp combination at $M = 14.2$ and at a ramp angle of 24^0, and hypersonic viscous cone-flow at zero and at finite incidence. The aim is to produce a reliable method which will accurately reproduce compressible laminar boundary-layer behavior and strong
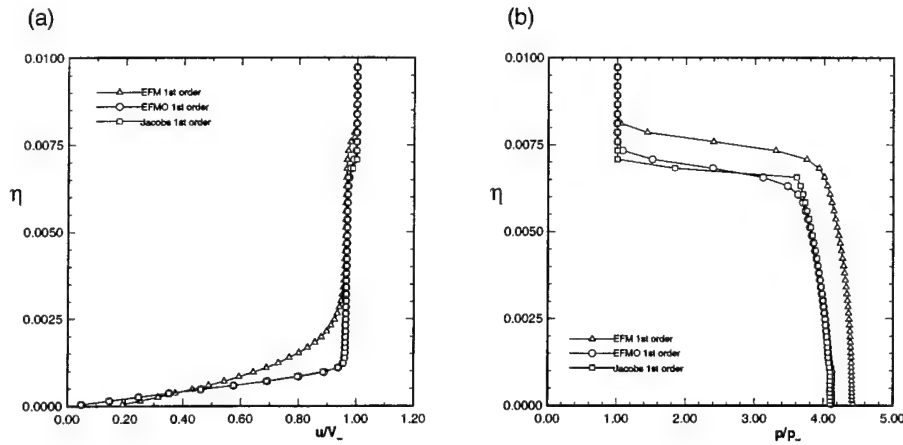
Figure IV.4. Flow property profiles at $x/L = 0.1$ on a cone of half-angle 10^0 at zero incidence in a hypersonic stream at $M = 7.95$. Frozen flow, $R_e = 4.2 \times 10^5$ based on distance L from apex and $Pr = 1$. Adiabatic wall. (a) u/V_∞ versus $\eta = y/L$ where y is normal to the wall. (b) p/p_∞ versus η.
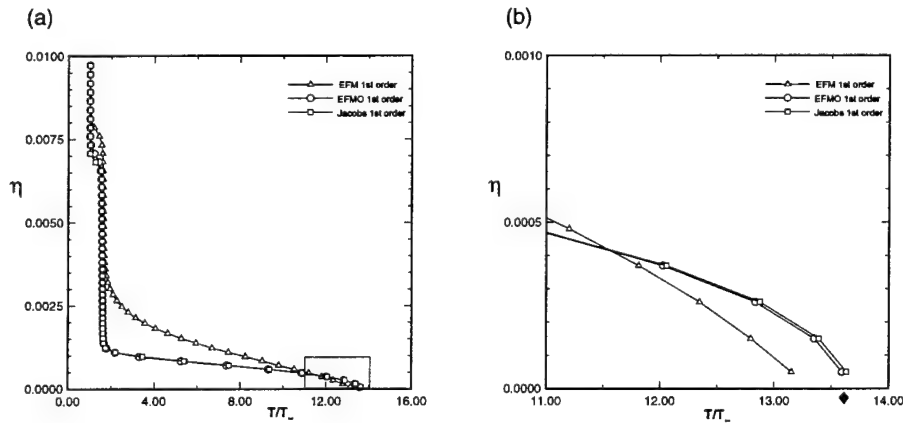

Figure IV.5. For key, see Figure IV.4. (a) T/T_∞ versus $\eta = y/L$. (b) Detail of (a). Diamond gives wall temperature. using recovery factor $r = 1$.

detached or attached shocks. Figures IV.4 and IV.5 show profiles of tangential velocity u/V_∞, static pressure p/p_∞ and temperature profiles T/T_∞, normalized against free-stream conditions, at a station $x/L = 0.1$ along a cone of half-angle 10^0 at zero incidence in hypersonic viscous laminar frozen flow at $M_\infty = 7.95$, where x is measured along the cone axis and L is the cone length. The Reynolds number based on free-stream conditions and L was 4.2×10^5. The Prandtl number was $Pr = 1$ and an adiabatic wall boundary condition was used. Results for viscous first-order *EFM*, *EFMO* and a Riemann solver due to Jacobs (1991) are compared. The first-order *EFM* method tends to thicken the boundary layer and underestimates the value of the wall-temperature as calculated with a recovery factor $r = 1$. There is general good agreement between *EFMO* and Jacob's method (which does not handle strong normal shocks well). Figure IV.6 shows results for laminar flow past a cone at incidence 24^0. The other flow conditions are as above. This case was chosen to match the experimental conditions of Tracy (1969). The parts of Figure IV.6 show the Mach-number distribution and the sectional streamlines. The Mach-number contours clearly show
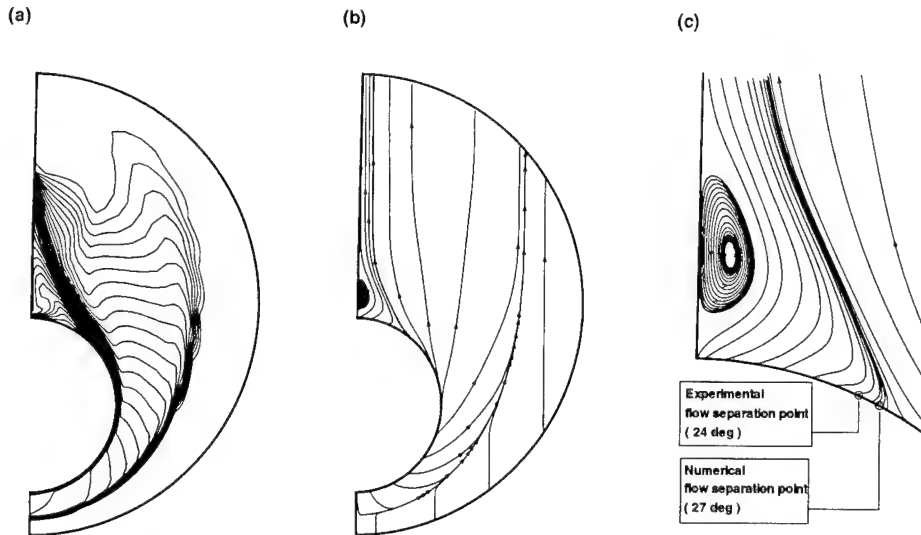
Figure IV.6. Cone of half-angle 10^0 at incidence 24^0 in a hypersonic stream at $M = 7.95$. Frozen flow, $R_e = 4.2 \times 10^5$ based on distance from apex. (a) Contours of Mach number. (b) Sectional streamlines in a plane normal to the cone axis. (c) Detail of streamline pattern near the leeward plane of symmetry.

the separating shear layer and the formation of a weak shock just outboard of this layer on the leeward side of the body. Between the shear-layer and the body a compact vortex forms near the leeward plane of symmetry. The angular position of separation can be estimated from the sectional stream-line pattern and is found to be at 27^0 from the leeward symmetry plane compared to 24^0 found by Tracy (1969) from surface stream-line patterns.

IV.3.3   EFMO and the IDG Chemistry model

Two versions of *PGP3D* incorporating the Lighthill-Freeman ideal-dissociating gas (IDG) chemistry model exist and are currently undergoing testing. This strategy has been developed with the aim of comparing the predictions of the two codes against each other, and against experiment and other computation, for the purpose of code validation The first of these (*PGP3D.3*; Shaun Shariff) is based on an operator-splitting approach in which the hydrodynamic and the chemistry terms in the equations of motion are split, and each is implemented separately at each time step. The result is an explicit time-marching method for both the gas-dynamics and the chemistry.

In the second approach, the implicit *PGP3D/EFMO* code discussed above (*PGP3D.2*) has been extended to include IDG chemistry in a partially implicit way (*PGP3D.4*; Jean-Marc Moshetta). This is done, as opposed to a fully-implicit strongly-coupled approach, because owing to the presence of source terms in the chemical rate equations, the Riemann invariants in the sense of Lax are no longer defined, and it is again necessary to decouple the gas dynamics part from the chemistry equation. In the context of *EFMO* this then gives an approximate Riemann problem which must be solved with different values of the specific heat ratio γ for the left state and for the right state. This leads to a local iterative procedure in order to obtain the intermediate states. This procedure
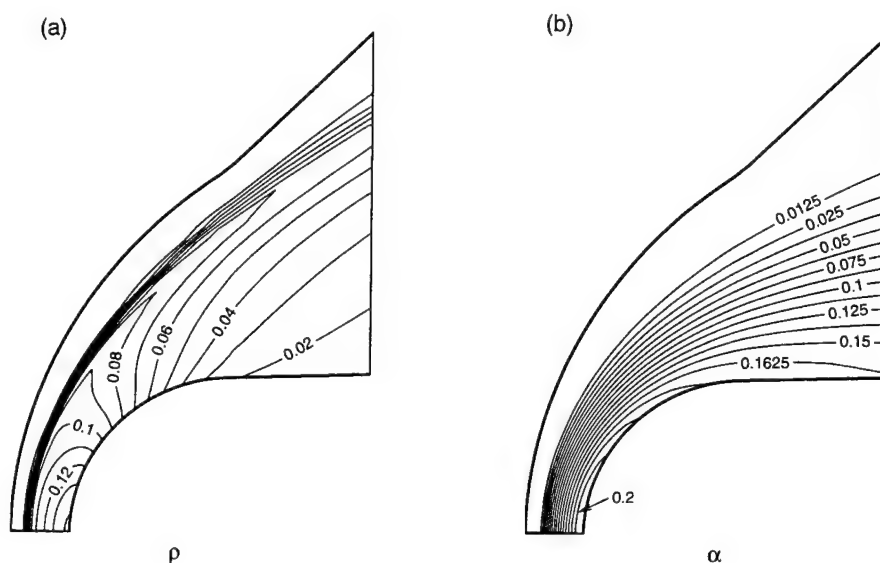
Figure IV.7. Two-dimensional inviscid flow of dissociating oxygen past a cylinder. $M_\infty = 15.0$. Dimensionless reaction-rate parameter $\Omega = 0.218$. (a) contours of density. (b) contours of dissociation fraction α.

has been modified to guarantee convergence in 2 or 3 iterations by the method of Abgrall & Montagné (1989). The IDG rate equation is solved implicitly by second-order Runge-Kutta, while the gas-dynamics is handled implicitly as described above.

Both *PGP3D.3* and *PGP3D.4* are currently undergoing testing for a variety of one-dimensional and two-dimensional cases. These include the simple one-dimensional steady propagating shock wave and two-dimensional chemically non-equilibrium flows about cylinders and spheres. In Figure IV.7 we show results from a test calculation of the inviscid two-dimensional flow of dissociating oxygen at $M_\infty = 15$ past a cylinder using *PGP3D.3*. The dimensionless reaction-rate parameter is $\Omega = 0.218$ based on the dissociation rate $d\alpha/dt$ on the downstream side of a stationary normal shock at the free-stream conditions. For the viscous hypervelocity flow about spheres, detailed comparisons with the computations and experiments of Chihyung Wen (Phd, Caltech 1994) are planned for the near future.

IV.3.4   Future Work

Fully three-dimensional tests of *(PGP3D.2)* on the hypersonic flow about the a blunt nosed delta wing of 70° sweep, at an angle of attack of 30° and at $M_\infty = 8.7$ are currently underway with the aim of comparing these with the calculations of Mallet *et al* 1994, done using the viscous *EFM* method. For the laminar viscous flow two Reynolds numbers, of $Re = 2.25 \times 10^5$ and 2.25×10^6 will be used. When the one- and two-dimensional tests on *PGP3D.3* and *PGP3D.4* have been completed, it is planned to undertake computations of the blunt delta-wing flow with active non-equilibrium gas chemistry. It is planned that Shaun Shariff will use both *PGP3D.3-4* to perform a sequence of computations on viscous reacting cone flow with a view to investigation of the chemical scaling of both the windward and the leeward flow characteristics. In the longer term it is planned

to incorporate a more complex partial equilibrium model of air (Rein 1992) into *PGP3D*.

References

Abgrall, R., Montagné J.–L., 1989 Generalization of the Osher Scheme for Calculating Flows of Mixed Gases of Variable Concentrations and of Real Gases, *La Recherche Aérospatiale*, No. 1989-4, 1–13.

Coquel, F., Liou M.–S., 1992 Stable and Low Diffusive Hybrid Upwind Splitting Methods, *Proceedings of the First European Computational Fluid Dynamics*, Vol. 1, Elsevier,

Jacobs, P.A., 1991 An Approximate Riemann Solver for Hypervelocity Flows, ICASE Report 91-75.

Osher, S., Solomon, F., 1982, Upwind Difference Schemes for Hyperbolic Systems of Conservation Laws, *Mathematics of Computation*, **38**, 339-374.

Pullin, D.I., 1980 Direct Simulation Methods for Compressible Inviscid Ideal-Gas Flow, *Journal of Computational Physics*, **34**, 231-244.

Rein, M. 1992 The partial-equilibrium approximation in reacting flows. *Phys. Fluids* , **A**, 4, 873-886

Tracy, R.R., 1963 Hypersonic Flow Over a Yawed Circular Cone, Hypersonic Research Project Memorandum No. 69, Graduate Aeronautical Laboratories, California Institute of Technology, Pasadena, California

Publications Resulting from Research

Macrossan, M.N and Pullin, D.I., A computational investigation of inviscid, hypervelocity flow of a dissociating gas past a cone at incidence. *J.F.M.* **266** 69-92 (1994).

Mallett, E.R. A numerical study of hypersonic flow over a blunt-nosed delta wing at incidence. Phd Thesis, University of Queensland, Jan 1994.

Mallett, E.R. Pullin, D.I. and Macrossan, M.N., A numerical study of hypersonic leeward flow over a blunt nosed delta wing. Accepted for publication in *AIAA J.* In Press, 1995.

Personnel Associated with Research

(1) D. Pullin, Professor of Aeronautics

(2) Dr Jean-Marc Moshetta, Associate Professor of Aeronautics, SUP'AERO, Toulouse France. Visiting Associate Professor of Aeronautics at Caltech.

(3) Jean-Cristian Bordier, Special Graduate student.

(4) Shaun Shariff, Postgraduate student.

Interactions

Invited participant, Centeer for Turbulence Research Summer Research School NASA Ames Research Center, July, 1994.

CHAPTER V
DIAGNOSTICS

Introduction

Since the major part of the research in this program is experimental, much of our work is also oriented toward development of better diagnostic methods. In some instances the techniques being developed are very closely coupled to particular projects and the progress in their development can be more effectively presented together with the progress in the sub-project in which they are being applied. This is the case for the development of the new holographic interferometer described in section II.2, and the image-correlation velocimetry technique described in section III.

In the case of the following section on laser-induced thermal acoustics, the presentation is separated from a specific application, because it is a project in its own right. The method is now established as a powerful diagnostic tool, however, and is ready to be applied to the other sub-projects.

V.1 DIAGNOSTICS WITH LASER-INDUCED THERMAL ACOUSTICS

Objectives and Status of Research

The objectives of the research described in this subsection are to develop laser-induced thermal acoustics (LITA), a nonlinear optical technique for single-shot measurement of gas and flow properties, including species concentration, temperature, transport properties, and velocity, and to apply LITA to hypersonic flows in T5.

This year, LITA has been transformed from a promising technique into an accurate and well-understood tool for the study of gas properties. This transformation has been accomplished through improvements in LITA signal modeling and a successful series of LITA experiments. The experiments demonstrate the accuracy of the improved model and the ability to extract accurate values of the sound speed and thermal diffusivity from LITA signals. The experiments also demonstrate the ability to obtain LITA signals in gases over a wide pressure range ($\sim$3 Pa–14 MPa at room temperature) and in challenging environments, e.g., CO_2 near its liquid-vapor critical point, and in flowing, turbulent gases.

V.1.1 Hardware

A high-pressure bomb was built with optical access that allows the study of LITA signals and gas behavior at various pressures, temperatures, and flow conditions. The bomb and its gas-handling system cover a pressure range from $\sim$3 Pa (absolute) to >20 MPa. The design of the gas handling system eliminates sources of contamination and exposure to the test gases. The bomb was used for all but the initial LITA experiments. Most of the experiments were conducted using stationary gases, although the effects of turbulence and flow were studied using an interior stirring fan. The bomb is currently being outfitted as a test section of a combustion-driven shock tube (described in Bélanger, 1993). This shock tube will permit LITA studies of high-speed and high temperature gases using the current LITA apparatus, thereby easing the transition of LITA from static cell to the T5 free-piston shock tunnel.

V.1.2 Theoretical model

Progress has also been made on the theoretical modeling of LITA signals. An expression for the LITA signal had previously been derived including some of the effects of the use of spatially finite laser beams (Cummings, 1992). This expression successfully predicted the nature and amplitude of LITA signals from the first round of LITA experiments. However, there were discrepancies in some cases between the measured and theoretical signals that arose from neglected beam-size effects (Cummings, 1994b). Therefore, an expression for the LITA signal that includes complete beam-size effects was derived. Through this derivation, phenomenological interpretations of LITA scattering were elucidated.

The analysis showed how two compelling but contradictory physical pictures of LITA scattering were correct in the limits of small and large detection angle (Cummings et al., 1995a). The dependence of LITA spectra on molecular gas properties was treated theoretically. The effects of finite laser noise and flow velocity were also explored. This expression accurately models LITA signals over the range of experimental conditions, except at the lowest pressures, where the theory needs to be modified to include rarefied gas effects.

V.1.3   Comparison with experiment

Examples of the agreement between theoretical and measured signals appear in Fig. V.1 and Fig. V.2. Fig. V.1 shows experimental and theoretical time-histories of LITA signals formed by the opto-acoustic effect of thermalization (Cummings, 1995b) at relatively low pressure in air at ~300 K, seeded with trace (< 10 parts-per-million) NO_2. The experimental apparatus used to obtain these signals is discussed in Cummings, 1994b and Cummings, 1995b. Signal averaging (3–100 shots) was typically employed in these experiments so that systematic deviations between experimental and theoretical signals would be unambiguously exposed. However, at relatively high seed-gas concentration or high buffer gas pressure, signal averaging was not strictly needed even for the stringent task of model verification.
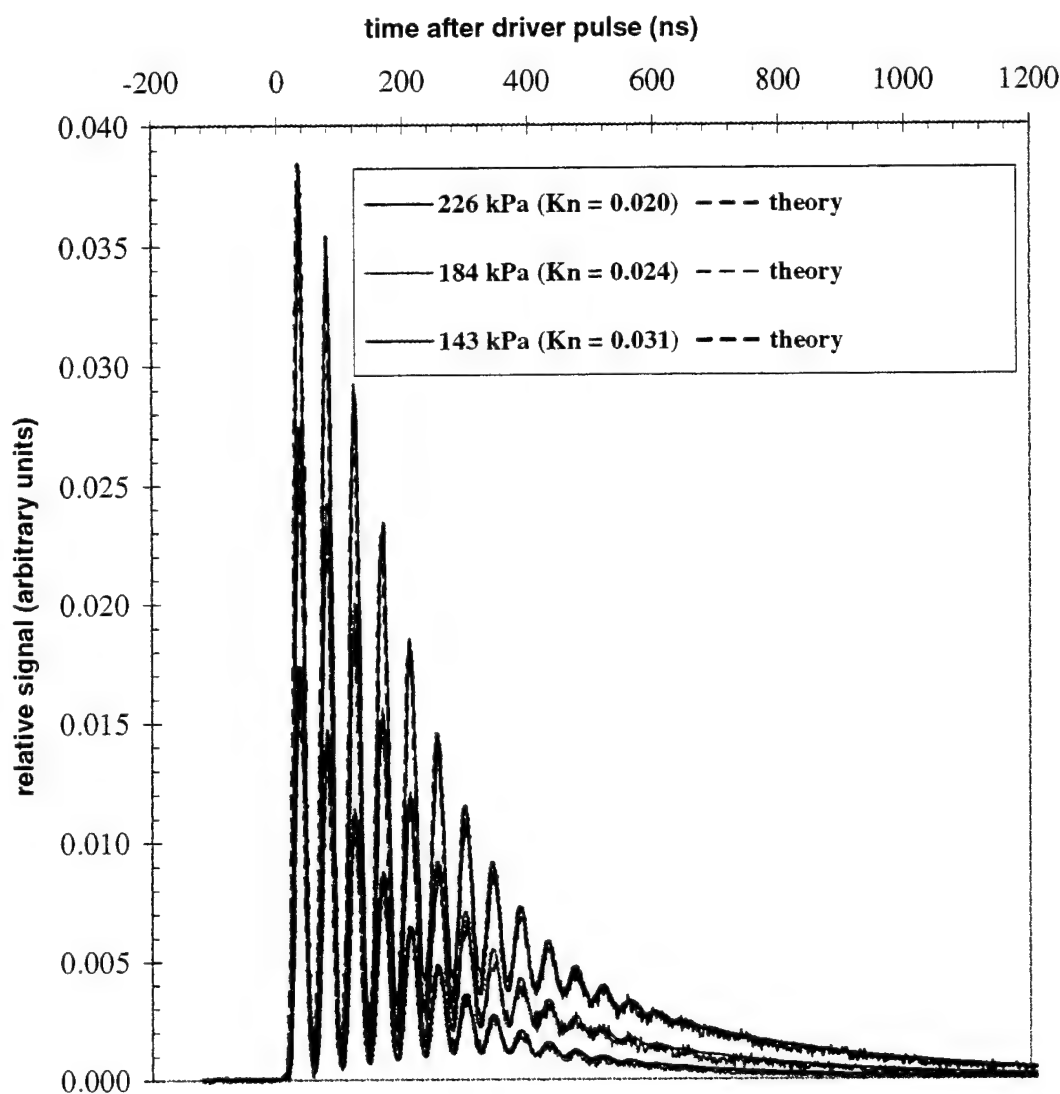

Fig. V.1. Experimental and theoretical LITA signals from thermalization in NO_2-seeded air near-atmospheric pressure and 300 K.

The grating Knudsen number—the ratio of the molecular mean-free path in the sample volume to the laser-induced grating wavelength—is the most important parameter in LITA scattering. LITA

typically excels when this parameter is much less than unity. Fig. V.2 shows a LITA signal taken in seeded air at 3.45 MPa and 300 K. The long oscillation-free tail of the signal is caused by the motion of the laser-induced acoustic traveling waves away from the source beam. A detailed discussion of the physics from which these signal patterns arise appears in Cummings, 1995b, along with plots of the experimental and theoretical signals over a wider range of grating Knudsen numbers.
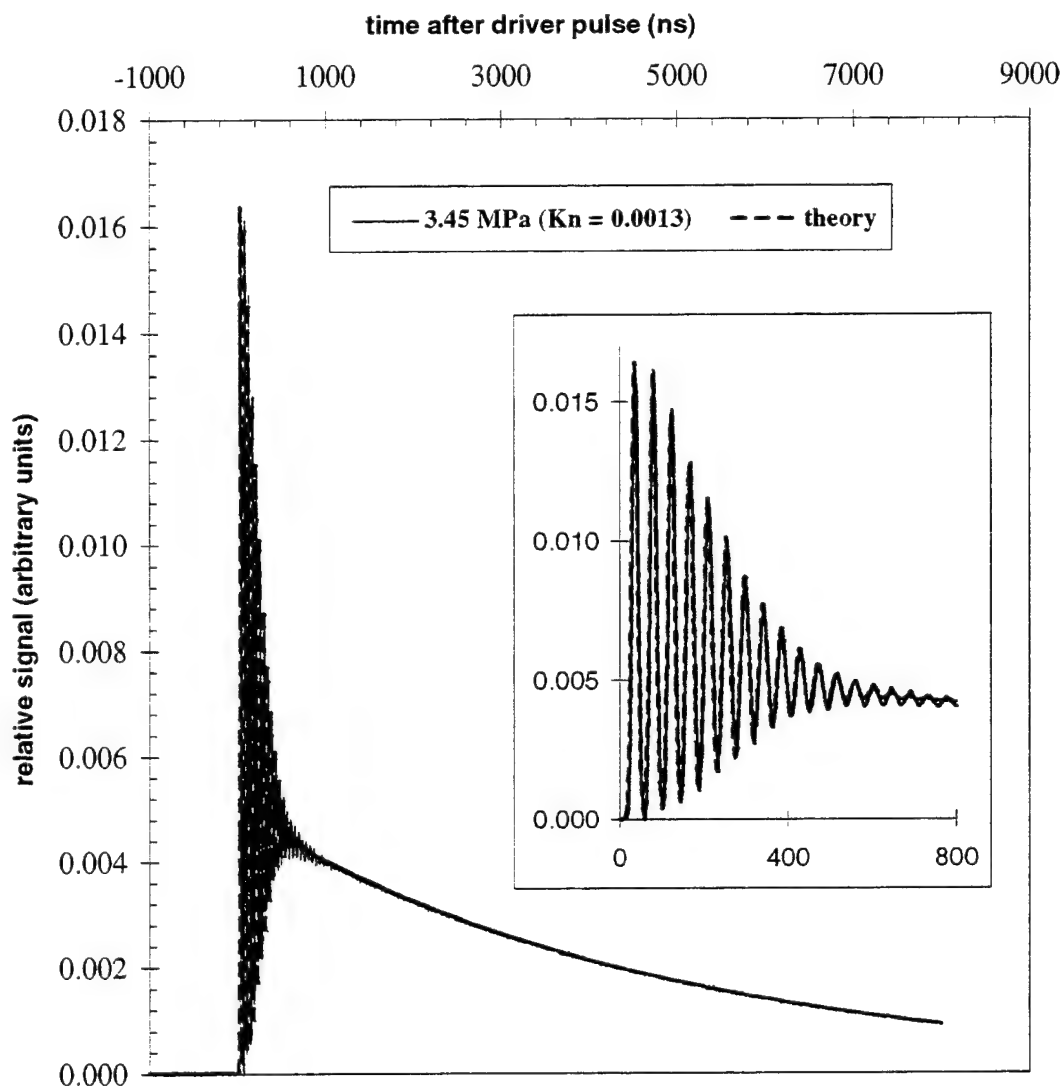

Fig. V.2. Experimental and theoretical LITA signal from thermalization in NO_2-seeded air at 3.45 MPa and 300 K.

In gases with low levels of seeding or strong nonresonant susceptibility, the opto-acoustic effect of electrostriction (Cummings et al., 1995c) contributes to the LITA signal. A combination of electrostriction and thermalization produced the signal that appears with a fit theoretical signal in Fig. V.3, taken in unseeded atmospheric-pressure CO_2 at 300 K.

Automated fitting of theoretical and experimental curves was performed using a nonlinear least-squares numerical technique. This fitting is a type of optimal nonlinear filtering which permits accurate measurements of signal parameters, e.g., sound speed and thermal diffusivity, from noisy
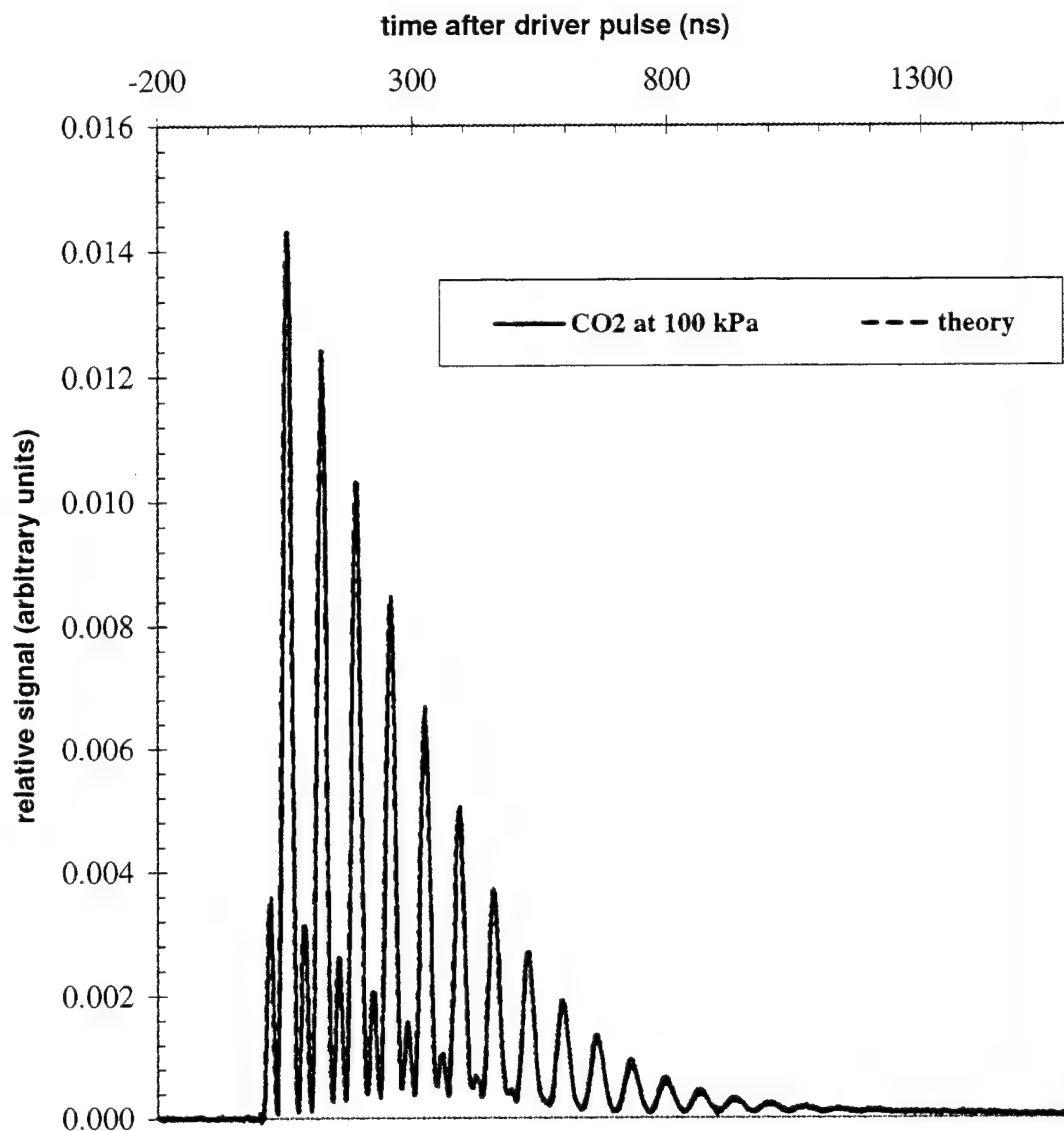
Fig. V.3. Experimental and theoretical LITA signals from electrostriction and thermalization in unseeded CO_2 at atmospheric pressure and 300 K. The secondary peaks in this signal arise from electrostriction.

signals. Currently, the automated filtering of a 2000-point LITA-signal time history requires typically one minute on a Sun Sparc 5. An example of sound-speeds extracted from LITA signals taken in NO_2-seeded air at different pressures and $\sim$300 K appears in Fig. V.4.

The sound speeds are corrected for small temperature excursions by scaling them with $\sqrt{300K/T}$, where T is the measured temperature of the gas in the test cell, and normalizing by their proper value at atmospheric pressure. The data of Hilsenrath et al., (1955), appear as solid circles. The agreement between the measured and published values is $\sim$0.1% when the pressure is above $\sim$200 kPa. At lower pressures, finite-Knudsen-number effects and rotational nonequilibrium effects arise, limiting the accuracy of the current model, which is based upon the equations of hydrodynamics.

Fig. V.5, a plot of the thermal conductivity (derived from the thermal diffusivity extracted from LITA signals) vs. pressure, demonstrates several shortcomings of the current theoretical model.
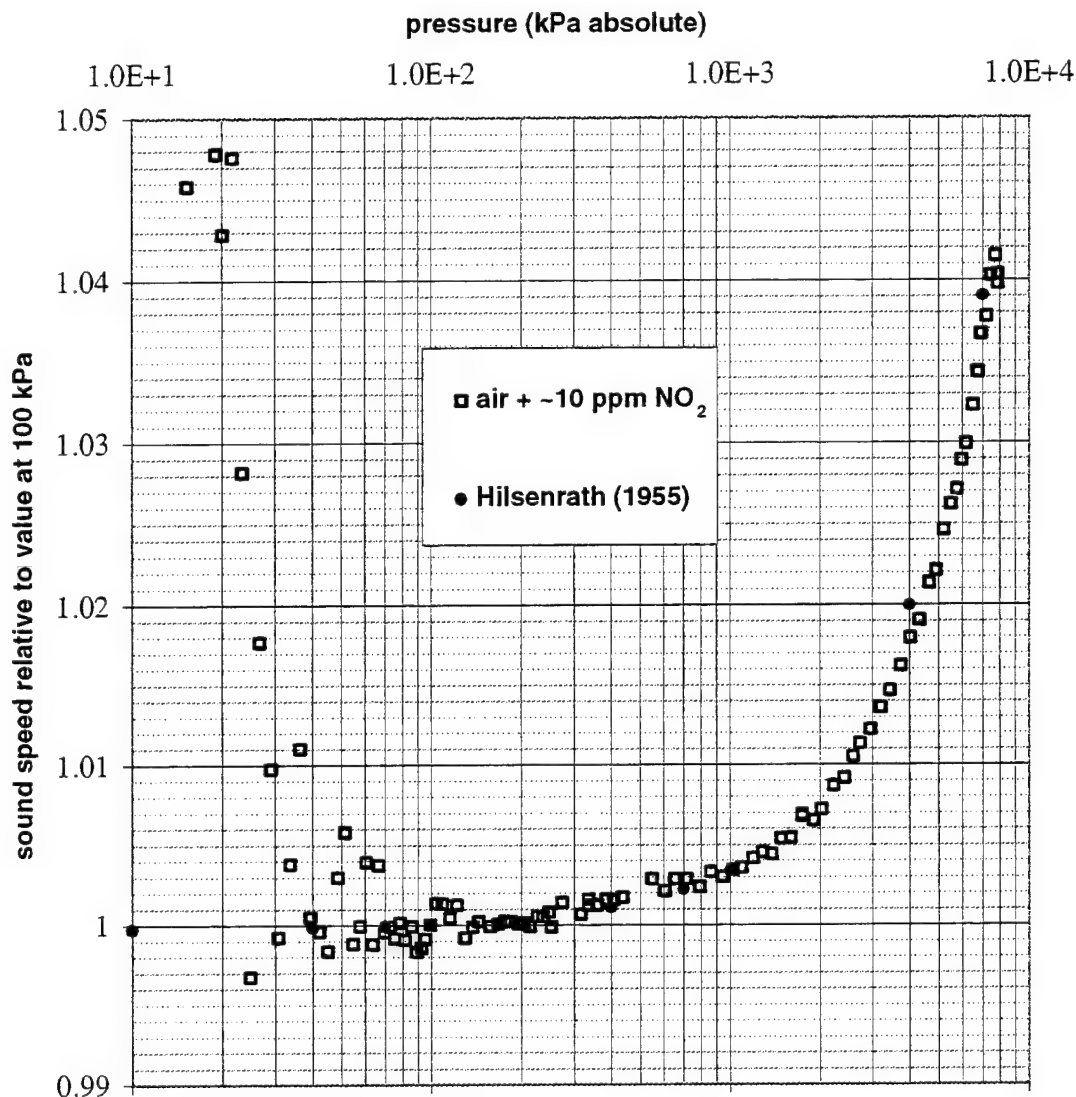
pressure (kPa absolute)

Fig. V.4. Sound speed of air vs. pressure corrected for 300 K and normalized to the value at atmospheric pressure. The solid circles are independent measurements from the National Bureau of Standards.

Two data sets taken with slightly different beam geometries are compared with the data of Vargaftik. et al., (1994). At low pressures, the model's treatment of the thermalization process is oversimplified, ignoring long-time-scale deposition of excited-state energy into thermal energy of the gas. In experiments this slow deposition prolongs the life of the thermal grating. The automated filter reacts by artificially lowering the extracted thermal diffusivity. An improved treatment of thermalization dynamics in the LITA signal model can practically eliminate this effect, although such a treatment could require extensive study of the quenching behavior of the seed species in the buffer gas.

At moderate pressures, the effects of slight beam misalignment skew the shape of the signal in a manner that is consistent with an decreased thermal diffusivity. In one data series, the data rise rapidly at high pressure to within ~1% of the published value after fine adjustments were made in the beams in order to optimize their overlap. As the pressure was reduced, differential refraction
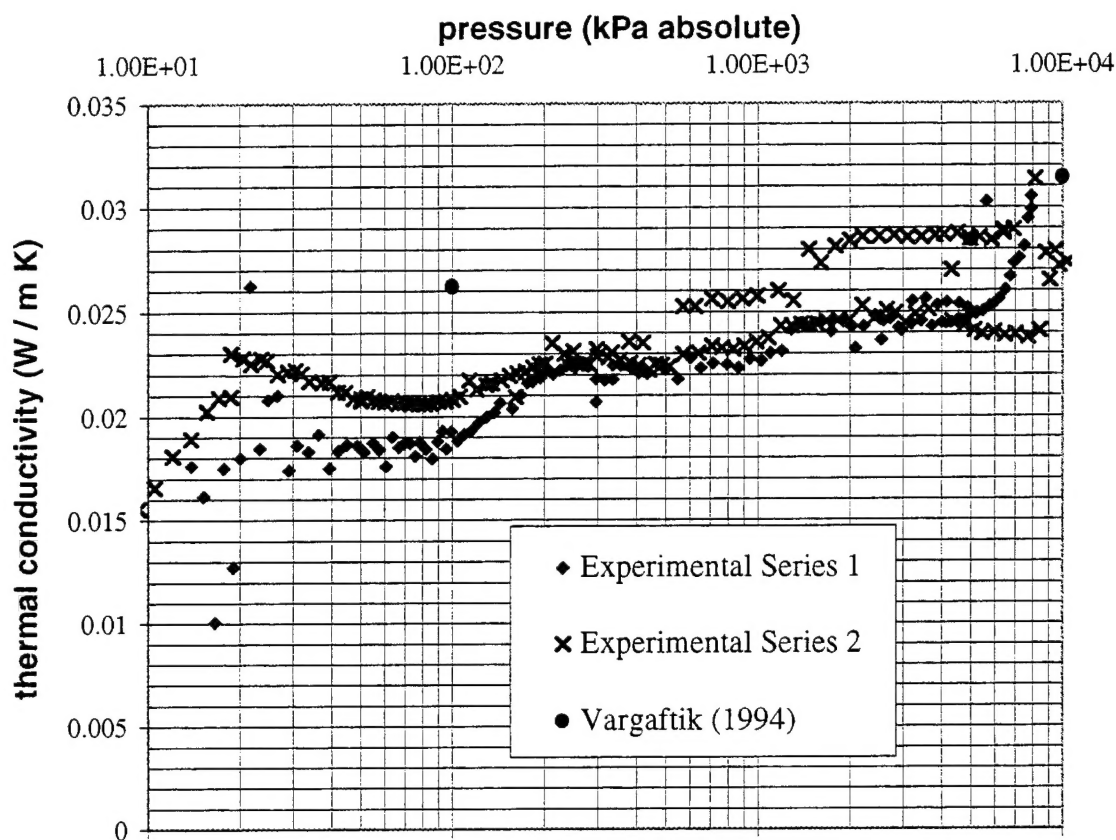
Fig. V.5. Thermal conductivity of air from LITA measurements and data of Vargaftik *et al.*.

again caused the beam alignment to degrade. While beam misalignment effects could be trivially inserted into the current model, a better solution to this modeling error in future experiments could be to employ unfocused beams, which would dramatically ease alignment requirements.

The LITA model predicts and experiments verify that the peak LITA signal intensity scales as the square of the buffer-gas pressure at constant seed-gas concentration, provided the seed-gas absorption spectrum is relatively constant with pressure. The integrated signal intensity scales as the cube of the buffer-gas pressure. Fig. V.6 shows the pressure dependence of peak and integrated signal intensities from experiments. The approximate regimes over which various complications may arise in taking and interpreting LITA signals are indicated.

The effects of convection and turbulence in the sample volume on LITA signals were observed and analyzed. The magnitude of these effects now may be predicted from general flow properties, such as the Mach and Reynolds numbers and beam parameters, such as the frequencies, crossing angles, and diameters (Cummings, 1995b). Flow-related difficulties may be mitigated in advance of experiments by adjusting experimental parameters such as the beam geometry.

V.1.4   Plans

A new series of LITA tests will employ the combustion-driven shock tube throughout the summer and into the fall. In these and a continued series of static tests, new approaches to LITA will be explored, including the use of

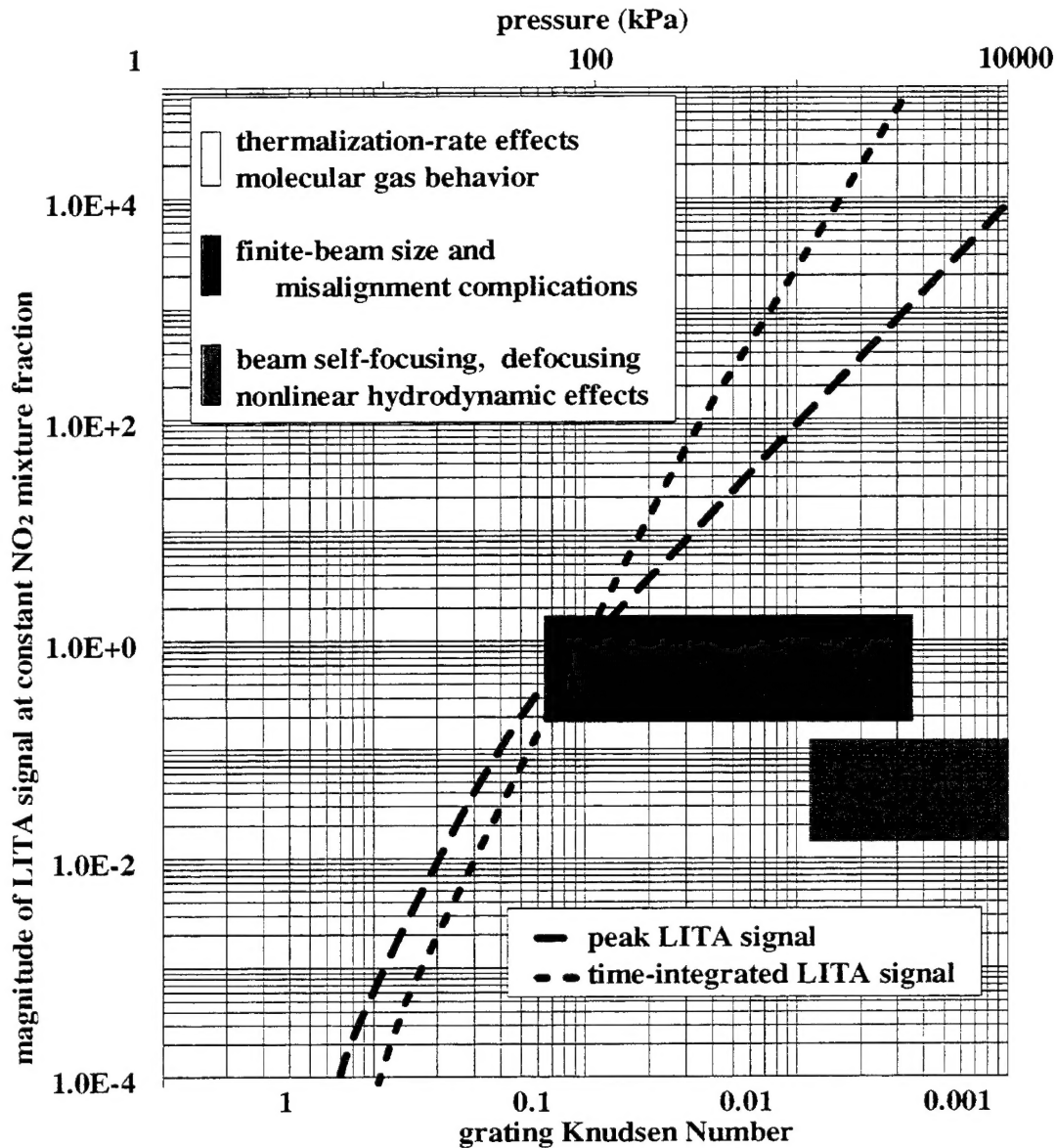- advanced techniques to ease beam-alignment,

Fig. V.6. Variation of LITA signal intensity with pressure (grating Knudsen number). Region of the complicating effects that were noticed during experiments and data analysis are indicated.

- ultra-violet light to study LITA using the target species NO, a gas indigenous to T5,

- a flashlamp-pumped dye laser as a source laser to boost signal levels,

- heterodyne detection to recover the Doppler shift of the signal beam scattered by convecting gratings. thus measuring the gas velocity

and a variety of other approaches designed to reduce the risk and increase the rewards of LITA measurements in T5.

Personnel associated with the research

1. Hans G. Hornung, Kelly Johnson Professor of Aeronautics, GALCIT Director.

2. Eric B. Cummings, Graduate Research Assistant.

3. Bahram Valiferdowsi, Staff Engineer.

4. Bonifacio Calayag, Graduate Student.

5. Ivett Leyva, Graduate Student.

6. Geoffrey Mach, Senior Student.

7. Michael Brown, MetroLaser.

Degrees earned in reporting period

E. B. Cummings, Ph. D., 1995.
Ivett Leyva, M. S., 1995.

Publications resulting from the reserch

Cummings, E. B. (1994a) "Laser-induced Thermal Acoustics (LITA): Simple, Accurate Single-shot Gas Measurements," 1994 Technical Digest Series, Vol 5, Optical Society of America, Washington, DC.

Cummings, E. B. (1994b) "Laser-induced Thermal Acoustics (LITA): Simple Accurate Gas Measurements," *Opt. Lett.* **19**, pp 1361–1363.

Cummings, E. B., Leyva, I. A. and Hornung, H. G. (1995a) "An expression for laser-induced thermal acoustic signals from finite beams," *Appl. Opt.*, to be published in May 1995.

Cummings, E. B., (1995b) *Laser-Induced Thermal Acoustics*, Ph.D. Thesis, Calif. Inst. of Technology, Pasadena, CA.

Cummings, E. B., Hornung, H. G., Brown, M. S., and DeBarber, P. A. (1995c) "Measurement of Gas-Phase Sound Speed and Thermal Diffusivity Over a Broad Pressure Range Using LITA," to be published in *Opt. Lett.*

References

Bélanger, J. (1993) *Studies of Mixing and Combustion in Hypervelocity Flows with Hot Hydrogen Injection*, Ph.D. Thesis, Calif. Inst. of Technology, Pasadena, CA.

Cummings, E. (1992) "Techniques of single-shot thermometry by degenerate four-wave mixing," GALCIT Report FM 92-2, Calif. Inst. of Technology, Pasadena, CA.

Cummings, E. B. (1993) "Laser-induced Thermal Acoustics (LITA): Four-wave Mixing Measurement of Sound Speed, Thermal Diffusivity, and Viscosity," Proceedings of the International Conference on Lasers 1993, SOQUE, McLean, VA, 441–450.

Interactions

The success of this project has led to intensive interest from the company MetroLaser. Two contracts with MetroLaser have resulted. Under these contracts MetroLaser bring equipment and instrumentation to the T5 laboratory, and use T5-lab equipment and instrumentation to further develop LITA, and to apply resonant holographic interferometric spectroscopy (RHIS) in the T5 environment.

Presentations at GALCIT Fluid Mechanics Seminar, and at GALCIT Research Conference. Seminar presentation at Princeton University. Discussions with the group of Stepanek at AEDC. Consultant to AEDC, (H. Hornung).